Statistical Estimation of Loads from Gas Explosions

Stian Høiset

Telemark College
Department of Technology
Institute of Process Technology
Kjølnes Ring, N-3914 Porsgrunn
Norway

Thesis for the Dr. Ing. Degree

Skien, February 20, 1998

Abstract

In the design of structures in the offshore and process industries, the possibility of a gas explosion must always be considered. This is usually incorporated by performing explosion simulations. However, estimations based on such calculations introduce uncertainties in the design process.

The main uncertainties in explosion simulations are the assumption of the gas cloud, the location of the ignition point and the properties of the explosion simulator itself.

In this thesis, we try to investigate the level of these uncertainties and quantify them. This is done by performing a large number of simulations on three offshore modules; the Piper Alpha C module and the CMR M24 and M25 modules in full scale, and one onshore plant; the Nypro UK plant at Flixborough.

The simulations of the offshore modules show that

- there is an approximate linear relation between pressure and gas volume
- it seems possible to find a linear relation between pressure and impulse
- an inverse relation between pressure and duration is observed
- the response of offshore structures exposed to gas explosion are rarely in the impulsive regime
- loading rates vary widely in magnitude
- an assumption of a triangular explosion pulse is often correct
- louvres increase pressure, impulse and duration of an explosion

The effect of ignition point location is studied in detail. The location of the ignition point may result in explosion pressure variation with a factor of 20. While explosion impulse as function of ignition point location seems to follow a normal distribution, explosion pressure has to be treated with non-parametric statistics.

It is possible to derive an *ignition point uncertainty load factor* that shows predictable behaviour by generalising the non-parametric properties of the explosion pressure. The load factor will vary with the chosen level of safety. Values of this factor for the offshore modules with different gas volumes, gas types and different levels of safety are provided. Based on the mean of a few simulations, a factor of 2 will in general be sufficient to achieve the 90% quantile in any explosion distribution investigated.

A model for taking into account the uncertainties regarding gas volume, ignition point location and simulator imperfectness is proposed. Several levels of safety may be chosen. The model is intended to produce a characteristic load for structural design.

Preface

This thesis is the result of the Dr.ing. programme I entered in August 1993. It seems a long time ago. I've learned a lot and have the feeling I've gained thorough insight to various aspects of gas explosions. The contrasts have been tremendous; during the same period of theoretical studies and extensive computer simulations, I've spent a half year at home with my daughter. There's a lot insight to gain by that, too, and it was an experience I wouldn't have been without.

My work has been sponsored by the Norwegian University of Science and Technology (NTNU) in an interacademic program with Telemark College (HiT/TF), who let my research work be done at Telemark Technological R & D Centre (Tel-Tek).

One of the intentions with my research work has been to integrate the fields of structural design and numerical flow simulations. The usefulness of this thesis will prove whether this goal has been achieved or not.

I would like to thank

- Prof. Bjørn Helge Hjertager and Ass. Prof. Kjell Arne Malo for their guidance and support throughout this doctoral work.
- Senior Scientist Dr Tron Solberg, Prof. Dag Bjerketvedt and Ass. Prof. Sigmund Kalvenes for their suggestions, constructive comments and reading my manuscript.
- Aalborg University Esbjerg, Denmark, for allowing me use their parallel computer during the last year of the Dr. ing. study.
- Fellow collegues at GISP, Tel-Tek, for interesting discussions, exchange of views and humourous spirits.
- My wife Hildegunn and our lovely daughter Torunn for their patience regarding my work.

Skien, February 20, 1998

Stian Høiset

Contents

Chapter 1

Introduction

1.1 The problem

Modern structural design codes still base their philosophy, to a large degree, on empirical knowledge. Hundreds of years with successful building history form a vast range of experiences of what kinds of structures that can be considered as "safe". Common practice, partly modified with modern reliability theory, is today quantified and used in structural design. This practice is often referred to as *semi-probabilistic design*, i.e. traditional design modified with modern knowledge of load and structural probabilistic properties.

However, in some design situations, our empirical knowledge is limited. Examples are modern, large, multi-stories buildings in areas prone to earthquakes, offshore installations in the oil and gas industry and nuclear reactor buildings. We build more complex structures placed in environments where we have no previous experience of the behaviour of these structures under extreme loading situations. Modern materials are introduced, and our knowledge of the long-time behaviour of these may also be limited.

In addition to increasing structural complexity, economical demands are put on the designers and the constructors. Larger built-in structure safety against failure implies larger initial cost. This motivates the use of less costly, but new and untested solutions to constructional problems. This is a natural evolution of building practice, but introduces constructional details in which we have little or lacking experience.

On the other hand, our probabilistic knowledge of structural behaviour and load distributions are increasing, thus helping us in finding new and creative ways in design and construction. Modern computer codes make it possible to take into account a wider range of probabilistic information during planning and production.

A better understanding of the probabilistic behaviour of load and structures is in any way advantageous. With access to probabilistic information about e.g. a load, we can be able either to produce a code to take advantage of this knowledge or calibrate our present empirical models to gain a better economical yield within an acceptable risk.

This thesis has acknowledged the importance in producing and publishing probabilistic data. The thesis deals with the loads from gas explosions, both maximum explosion pressure and impulse load. Based on simulations, explosion loads are tested versus several known, parametric distributions and also classified by non-parametric statistics. The effect of geometry, gas cloud size and ignition point location are discussed and visualised. A model for taking into account the uncertainties arising from gas cloud size, ignition point location and explosion simulator imperfectness is proposed.

1.2 Related work

According to Madsen et al. [1], it was in the period from 1967 to 1974 an increasing growth in academic interest in structural reliability theory and a growing acceptance of probability-based structural design. Influential work was published by Freudenthal [2], Johnson [3], Pugsley [4] and Ferry Borges and Castanheta [5]. Later, both Thoft-Christensen and Baker [6] and Ditlefsen and Madsen [7] has elaborated the theory of structural safety.

1.2.1 Load distributions

There seems to be little research work done in the field of the probabilistic nature of explosion loads and the use of statistics applied to these.

On the general level, European standards [8] divides actions on structures into *permanent actions*, *variable actions* and *accidental actions*. *Permanent actions* are commonly regarded as normally distributed [8]. According to Borges [9] and The American National Bureau of Standards [10], *variable actions*, including snow and wind, can often be classified by some Gumbel distribution. Aune and Larsen [11] mention that Norwegian wind strength tables often are presented as frequency tables, and that the extremal statistics (as described by Gumbel) are prone to uncertainties. For snow, Aune and Larsen [11] put forward the *return period* as the main key, disregarding any distribution.

For *accidental actions*, there is a large amount of literature on earthquake loads, but a modest number of works describing the effect of gas explosions loads on structures. Bjerketvedt et al. [12] published the Gas Explosion Handbook that describes the physical and dynamic aspects of a gas explosion. The European prestandard Eurocode 1, part 2–7 [13] has a separate chapter describing actions from gas explosions, but the usefulness of the described method is limited. Høiset et al. [14] have presented a model for incorporation of uncertainties regarding explosion simulator code, gas volume and ignition point location.

1.2.2 Structural safety

In reliability theory, the *risk of failure* is the main subject. While European structural design standards [8] mostly are based on historical methods, modern structural safety theory is based on probabilistic data, as described by Thoft-Christensen and Baker [6]. Both Thoft-Christensen and Baker and Ditlefsen and Madsen [7] acknowledge a *safety index* in structure reliability. However, both the empirical methods and the probabilistic methods supplement each other, and merge together in the *partial coefficient method.* The partial coefficient method is adopted both in European standards [8], national standards (e.g. Norwegian, NS3479 [15]) and American design guides such as API RP 2A LRFD [16].

This *semi-probabilistic design*, that takes into account both empirical and probabilistic dimensioning criteria, is described by Aune and Larsen [11]. A discussion of general model uncertainties in structural reliability and how to include elements for subjective assessment of model uncertainties in the reliability model has been published by Ditlefsen [17].

1.2.3 Structural resistance

The field of structural resistance and material strength exposed to explosion loads is extensive. Dynamic design of structures, modes of failure and material strength issues must be taken into view. These areas are not covered here. The background documentation to the Eurocode 1 [18] suggests a time-step analysis on the basis of the pressure-time history for the consideration of dynamic effects and a non-linear modelling of materials and geometry in the structure.

1.2.4 Explosion simulators

There are several explosion simulation codes available, such as EXSIM [19], FLACS [20] and REAGAS [21]. These computer codes generally use the control volume method as described by Patankar [22], and solve the conservation equations for mass, momentum and energy together with a turbulence and combustion model as described by Hjertager [23]. Validation data are important in estimation of model uncertainty. Sæter et al. [24] have presented a validation of the EXSIM code, later updated by Solberg and Hjertager [25], while van Wingerden et al. [26] have presented a validation of the FLACS code.

1.2.5 Statistics

Fitting of experimental data to known parametric distributions is covered in several textbooks. In this thesis, the test of experimental data versus normal and lognormal distributions are done as described by Ang and Tang [27]. The test of observations versus extremal distributions are done as proposed by Gumbel [28, 29] and described by Ang and Tang [30]. This includes the curve fitting procedure described by Lieblein [31].

1.3 Overview of thesis

The scope of this thesis is to foresee a characteristic value of the magnitude of a gas explosion, either explosion pressure or impulse by means of a proposed load model. The model is based on the existence of two or more explosion simulation results.

In the load estimation process, areas of uncertainty are located and quantified. The quantification of uncertainties are done by applying statistics to the observed data.

In order to get large enough data sets to apply statistical tests with some reasonable confidence spans, nearly 10 000 explosion simulations have been done. As a side effect of having so many explosion simulator results available, the effect of varying several parameters are visualised and discussed.

Chapter 2 seeks to elaborate the uncertainty aspects of structural design with respect to gas explosion loads. A delimitation of the work is done. The text discusses the influence of various parameters affecting the resulting explosion load and how to deal with them, statistically, in structural design. The statistical methods are chosen, and application to a load model is described.

The proposed explosion load model uses partial coefficients as load factors to produce a characteristic load. In order to understand and use load factors correctly, we start with looking at failure philosophy in chapter 3. There the current risk philosophy is discussed. A short overview of reliability analysis is given, and probabilistic properties of various variable loads are presented.

In chapter 4, a load model that takes into account the uncertainties arising from gas cloud size, ignition point location and computer simulation imperfectness is proposed. This model concludes with a characteristic value for explosion loads. The characteristic value is achieved from a nominal value from explosion simulations combined with partial factors to reach the desired level of safety.

Chapter 5 presents the summary of nearly 10 000 simulations of explosions in offshore geometries. The effect of several parameters are visualised and discussed.

In chapter 6, the probabilistic properties of gas explosions with respect to the location of the ignition point are investigated. Tests versus normal, lognormal and Gumbel distributions are carried out. A non-parametric approach to the analysis of the observations is shown to be insightful.

A lesser number of simulations on a land-based process plant are presented in chapter 7. The subject of the simulations is a reconstruction of the Flixborough accident. A overview of literature is presented along with simulated values.

Chapter 8 presents appropriate partial coefficients for the characteristic load model presented in chapter 4. Values for ignition point location and explosion simulator code uncertainties are given.

Chapter 9 presents the conclusions of this work and recommendation for further work.

Abbreviations and a nomenclature are presented after the conclusion. Most figures are presented in appendix A.

Chapter 2

Scope of thesis

2.1 Quantitative Risk Assessment

2.1.1 Overview

Quantitative risk assessment (QRA) is based on the premise that one must evaluate both the consequences *and* the expected frequency of potential hazardous events [32]. Such an evaluation will hopefully lead to a logical decision on whether the installation of a particular safety measure can be justified on safety and loss control grounds. There are 4 basic concepts in QRA [32]:

- Identification of likely accidental events.
- Consequences of events if they occur.
- Frequency of accidental events.
- Acceptable criteria.

Combinations of consequence and frequency can be combined to produce a measure of *risk*.

The QRA technique can be used to identify, assess and establish which of a range of potential accident scenarios should be considered in design.

According to the Steel Construction Institute [32], a probabilistic assessment of structural resistance will not normally be added into the QRA process. At the present time, QRA is used to identify appropriate design events.

2.1.2 The application of QRA in this thesis

This thesis adapt the QRA principle and tries to describe the procedure to achieve an appropriate characteristic gas explosion load, A_k for the use in an accidental design sit-

uations. It does not cover all the fields of the subject, but is limited to the following scenario.

The likely accident investigated is taken to be a *gas explosion* within an offshore module or at an onshore plant. An existing, combustible gas mixture and the presence of an ignition source are assumed. Thus, the accidental event is limited to a gas explosion.

The consequence of the gas explosion consists of two elements:

1. The magnitude of the explosion (load effect)
2. The strength of the structure (resistance)

While the relationship between these are discussed in chapter 3, the main issue is the first point; if there exists a combustible gas mixture and the presence of an ignition point, *how powerful will the explosion be* in the cases of offshore and onshore installations?

The answer depends on a number of factors. Some of these factors are easily (roughly) quantified, whereas others have larger uncertainties.

2.2 Sources to uncertainty

2.2.1 Overview

Probabilistic data have been collected for several types of variable loads. However, the distribution properties of *gas explosion loads* seem to be absent in the literature. In estimation of gas explosion loads, explosion simulations done with computers are commonly used. Gas explosion loads are functions of many variables [12, 33]. The most important are:

- Geometric layout, e.g. confinement, equipment and pipes.
- The gas type(s) involved.
- The size and location of the exploding gas cloud.
- The equivalence, or fuel-oxygen ratio.
- The ignition point source and location.
- The initial turbulence field.

To gain a characteristic load in the structural design phase, each of these variables must be estimated in some way. In this estimation process, we introduce *uncertainties* that affect our characteristic explosion value.

Geometric model or module layout has a significant effect on the explosion pressure. There has to be an interaction in the planning process between the layout planning and the

explosion risk evaluation to minimize the effect of missing pipes etc. in the calculations. The geometry of the explosion hazard area is one of the most important factors influencing the explosion. A correct specification of the layout is of major importance.

The gas type likely to explode is usually known. If there are several possible explosive gas types in the area, parallel simulations have to be done to conclude which gas type has the most destructive effect in an explosion. Validation of explosion simulator results with respect to the explosive gas under investigation should be available. If this procedure is followed, the errors from misinterpretation of the gas type are expected to be negligible.

The size and location of the exploding gas cloud will significantly affect the explosion pressures. These factors have a great uncertainty associated with them, and they have to be evaluated thoroughly in the risk assessment. Flow simulators can be used to produce input data for the explosion simulators. If possible, the use of statistical methods to quantify the level of uncertainty is desirable. In some cases, e.g. offshore modules, an assumption of the module completely filled with explosive fuel/oxygen mix can be viewed as the "worst case".

The equivalence, or fuel-oxygen ratio in the exploding cloud is also of great significance. The ratio will be a function of space and time, and will generally not be available. Experiments done by Hjertager et al. [34] show that the explosion peak pressure maximizes at stoichiometric or slightly fuel-rich mixtures. A stoichiometric mixture in the simulations is therefore assumed to be a conservative assumption.

The ignition point location has great influence on the resulting explosion pressure and impulse. Informal calculations show that the maximum overpressure may vary with a factor of order 10 according to choice of ignition point location [14, 12]. This fact shows that the location of the ignition point is of great importance in explosion simulations. Therefore, a user of explosion simulators in the design phase can hardly be expected to pick a "worst case" with respect to ignition point when performing calculations of explosion values.

The initial turbulence field can affect the explosion progress. The existence of turbulence will enhance the combustion, and thus produce higher explosion pressure. This is a parameter difficult to estimate. Wind will on one hand generate turbulence, but on the other hand tend to dilute the fuel/oxygen mixture, and thus may lower the risk of an explosion. A jet leakage of flammable gas can be more dangerous, causing turbulence without diluting the explosive mix. The scenario is extremely case-dependent and hard to generalise.

The EMERGE report [35] concluded that there was no difference in maximum explosion pressure with respect to the initial turbulence field. However, in the experiments where an initial turbulence field was introduced, the geometry was very congested. An early occurrence of high turbulent velocity could have been expected without the extra initial turbulence. We may at least assume that in congested areas, the existence of a turbulence field at the time of ignition will not necessarily produce a higher explosion pressure.

The transition from deflagration to detonation may be of interest for either highly congested geometries or very reactive gases. In this thesis, all explosions are taken to be deflagrations. If a detonation is taken to be a possible outcome of an explosion, the values in this thesis will not be representative. All explosion simulations in this thesis are deflagrations.

As a last point, during the structural design phase, explosion simulators are commonly used to predict the characteristic explosion load. Thus we introduce another variable prone to uncertainty:

- Imperfectness in physical model and mathematical implementation in the explosion simulator.

The latter can be handled by correct specification of the explosion simulator validation data.

2.2.2 How to deal with uncertainties

With the limitations of the problem as described section 2.1.2, we can deal with the occurring uncertainties in the following way.

The geometric model of the structure is taken to be in the final stage of planning, i.e. the representation of the structure and the internal equipment is close to the final result. In this way, the possible errors in explosion pressure estimation that arises from incorrect layout specification is taken to be negligible.

The size and location of the exploding cloud has obviously great influence on the resulting explosion pressure. There exists a number of fluid flow simulators that are capable of determining the dispersion of a gas as a function of time, given a leakage point, leakage rate and a realistic layout of obstacles.

Pappas [36] showed that in the case of an explosion within an offshore module, a filling ratio of 30–50% may cause the same explosion pressure as a 100% filled compartment. This is due to the exploding, expanding gas pushing the uncombusted fuel-oxygen mixture away from the explosion. This observation can argue for a module filled completely with gas as the design case. A such assumption may cover the actual explosion explosion pressure for a wide range of filling ratios.

Thus, while the gas volume has great influence in the case of onshore plants, a reasonable assumption on the "safe side" in offshore modules may be the whole module filled with an explosive mixture, if there is enough leakable gas to provide a such volume. However, we do not specify any probability distribution properties for gas volume and placement in this thesis. Several exploding gas volumes are investigated, but no statements are done on which to prefer in the design process.

The equivalence ratio rarely produces any source to uncertainty. An assumption of a stoichiometric mixture is reasonable and probably a slightly conservative precaution. The fuel-oxygen mix will be most explosive at the stoichiometric ratio. Leaner or richer mixtures will produce lower explosion pressures [34], and too lean or too rich mixtures will not ignite. However, a rich mixture may always become stoichiometric. All the explosion cases investigated in this thesis are taken to be stoichiometric.

The ignition point location is of great importance to the resulting explosion pressure. The actual ignition source is rarely known. It can be a hot surface or a spark, either by equipment, switches or an electrical discharge of static voltage. In the inquiry into the Piper Alpha disaster [37], the conclusion was

> "The location and nature of the source of the ignition are unknown, but the location was probably such as to favour high over-pressures."

Likewise, the report of the Court of Inquiry after the Flixborough disaster [38] did not conclude with respect to where the ignition source were located, but pointed out that there were several hot surfaces at the nearby hydrogen plant, and that one of these may have ignited the explosive cloud.

These statements show that the ignition source is hard to locate, even in retrospect, and can be described as impossible to prescribe in the planning phase. The ignition point may occur almost anywhere near a hot surface or equipment supplied with electrical power.

In this thesis, we assume the ignition point to be a simple spark. The spark may be generated anywhere in free fuel/air mixture. This is hardly the real situation, where sparks generally will occur in the close vicinity of a hot surface or close to electrical equipment. Thus, the real set of ignition point can be presented as a subset of the ignition point applied in this thesis. Given that the real ignition points may be located such that an early turbulence may occur, while the simulated ignition point generally will have a "late" turbulence generation, consequently the real ignition points will most likely produce slightly higher overpressure than the assumed ones.

The generation of random ignition points in free air, both close and far from surfaces, is not the ideal solution in estimating the most likely explosion progress. However, the temperature of surfaces and planned and future electrical cabling and switching can hardly be incorporated into our planning model. Thus, a realistic level of specifying possible ignition source areas seems unreachable.

One solution can be to specify the model to only look for possible ignition points "close to" any surface. However, the available geometrical details of the simulated cases (Piper Alpha [39, 37], CMR M24 and CMR M25 [40] and Flixborough [38, 41]) does not allow such specification. These sources specify the geometrical layout to an acceptable degree for flow simulations, but minor details, such as placement of electrical cabling bridges, are not available.

Furthermore, it is hardly the *vicinity* of an ignition point to a surface that influences on the maximum pressure, but rather the *degree of confinement* around the ignition point. A procedure to pick out possible ignition points with a certain degree of confinement to generate early turbulence seems complex to establish.

Thus, the approach to the ignition point location problem during simulations is the arbitrary choice. A possible solution to maintain the most realistic scenario is to read the probabilistic information gained in this thesis "as is", and keep in mind that the actual explosion pressure may tend to be somewhat higher than the results from the estimation model presented. The distribution quantile (i.e. safety level) sought by the user may be influenced by this fact.

The initial turbulence field is taken to be negligible, i.e. the fuel/air mixture is taken to be quiscent. This is taken to be the most probable situation if the fuel/air ratio is within the explosive limits, although this assumption may be on the non-conservative side. The effect of this assumption remains unknown.

The choice of simulator may influence on the uncertainty level when estimating the explosion pressure. In fluid flow equations, there are several constants, such as the Courant number Co and several turbulence parameters that relies on the results from experiments [23]. These can be "tuned" to solve the equations such that the calculated value of the explosion pressure, p_{cal}, is close to the observed explosion pressure, p_{obs}, *in the mean.* This, along with previous experience of the above constants, is a common way to calibrate an explosion simulator code. Other methods to gain a mostly correct code is to implement better numerical schemes, specify correct drag coefficients for different obstructions and to use up-to-date models for laminar and turbulent combustion.

Correct coding of the flow problem together with the above precautions to calibrate the code make the simulators predict the explosion pressure pretty well. Validations of the codes are published [24, 25, 26].

However, the validation results still emerge with a dispersion within the data sets. Quantification of this dispersion is, as far as the author know, only done for EXSIM [24, 25]. The dispersion of the results from the FLACS code [26] are described in more general terms. Following the calculations done by Sæter et al. [24] and Solberg and Hjertager [25], the quantile values that are necessary to achieve a certain safety level is possible to quantify .

2.3 Statistical aspects

2.3.1 Overview

Reliability theory uses the probability of failure as the main parameter. Design regulations and standards who use this approach often prescribes a *probability of failure per year.* With respect to explosions, this probability is usually of the order 10^{-4}. With this approach, it follows that the *return period* of the design explosion is 10 000 years. Explosions can occur more frequently, but they will not have such high overpressures. Given that the probability of an explosion occurring and the magnitude of the explosion are independent, the probability of failure will be the product of the probability of an explosion occurring and the probability of explosion pressure (given an explosion occurring) exceeding the characteristic value.

By separating the failure probability into these basic probabilities, we can isolate the effects of an explosion. In this thesis we prescribe methods to determine whether the explosion pressure and impulse will exceed some characteristic values, but not the probability of an explosion occurring.

2.3.2 Applied statistics

Variable loads can usually be classified into either the lognormal, the gamma (rarely) or the Gumbel Type I or II extremal distributions.

The data sets gained by the present simulations are, as a result of the above observation and selective choice, tested versus the *normal, lognormal* and *Gumbel Type I and II extremal distributions.* Since the gamma function is rather rare, the data sets are not tested versus against this distribution. The normal distribution test are done as a reference.

Furthermore, in view of the possibility of not finding an appropriate parametric distribution, the data sets are also classified with means of *non-parametric statistics.* In this way it is possible to quantify safety levels without knowing the exact distribution or make assumptions to make a fit of the data into a known parametric distibution.

The quantification of the safety level is done by choosing an explosion load quantile that satisfies some criterion, and producing load coefficients to obtain this characteristic load from the nominal, calculated load.

Chapter 3

Probabilistic design of structures

3.1 Reliability analysis

The term *reliability* covers safety, serviceability and durability of a structure [8]. The level of reliability varies regarding structural safety and structural serviceability. We can accept periods where the structure is unusable as long as structural failure is not achieved.

Further, the level of reliability versus failure may depend on [8]:

- Cause of failure.
- Possible consequences in terms of risk to life, injury, potential economic losses and the level of social inconvenience.
- Expenses necessary to reduce the risk of failure.
- National, regional or local circumstances.

An overview of reliability methods is given in figure 3.1. Let $g(x_1, \ldots, x_n) = 0$ be the equation for the distinction between failure and non-failure of a structure. The equation will form a surface in the n-dimensional space. If this equation is solved exactly, the procedure is called a *level III* method as shown in figure 3.1. The level III methods require a knowledge of the joint distribution of all uncertainty parameters [1]. They take into account the true nature of the failure domain [6].

If the solution is approximated, the procedure is called a *level II* method [8]. The level II methods involve certain approximate iterative calculation procedures to obtain an approximation to the failure probability of a structure or structural system. They generally require an idealisation of failure domain and are often associated with a simplified representation of the joint probability distribution of the variables [6]. Such methods generally operates with a *safety index,* β. The level II methods can be divided into first order reliability methods (FORM) or second order reliability methods (SORM). The former

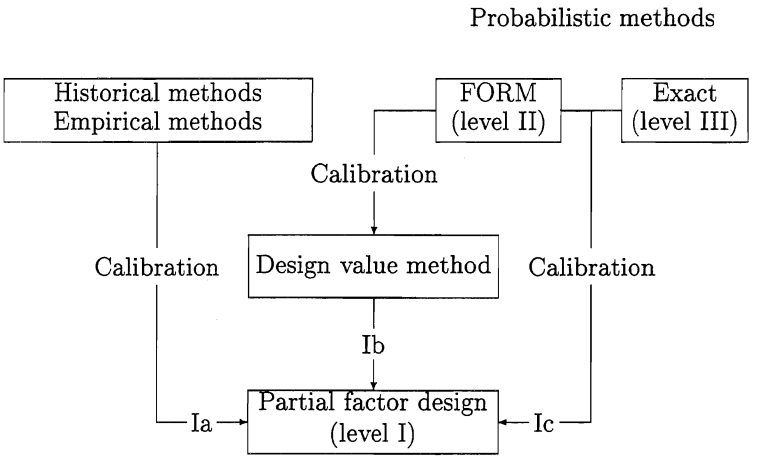

Figure 3.1: An overview of reliability methods [8]

approximates the surface described by the g function as small, piecewise planes, while the latter takes into account the curvature of the surface [7]. They employ two values of each uncertain parameter (commonly mean and variance), supplemented with a measure of the correlation between the parameters (usually covariance) [1].

The present generation of Eurocodes are mostly based on method Ia in figure 3.1, i.e. historical and empirical methods. The *level I* methods employ only one "characteristic" value of each uncertain parameter [1].

Madsen et. al [1] also proposed a *level IV* method. This will compare a structural prospect with a reference prospect according to the principles of engineering economic analysis under uncertainty, considering costs and benefits, of construction, maintenance, repair, consequences of failure and interest on capital, etc.

3.1.1 Probability of failure

Modern structure philosophy tends to emphasise the probability of structural failure in structural design. Failure is a consequence of *structure resistance* being less than *load*

effects. If we denote structure resistance as R and load effects as L, the *risk* of failure is

$$\text{risk} = P(R < L) \tag{3.1}$$

with $P(R < L)$ being the probability of load effects exceeding the resistance.

Allowable risk is less for structures with greater failure consequences than for structures with minor failure consequences. e.g. temporary structures or storehouses with small risk of loss of human lives. Norwegian construction regulations [42] give values for the maximum yearly probability for failure as presented in table 3.1.

Table 3.1: Maximum nominal yearly probability of failure [42].

Reliability class	Failure consequence[a]	Largest yearly probability of failure, ultimate limit state	Largest yearly probability of failure, accidental limit state
1	Minor	10^{-2}	—
2	Meduim	10^{-3}	—
3	Serious	10^{-4}	10^{-5}
4	Very serious	10^{-5}	10^{-6}

[a]The translations of the "failure consequence" terms are done by the present author on basis of on-line information by the Norwegian National Office of Building Technology and Administration[43]. They are not authorative.

In the proposal to the new Norwegian structural design standard [44], offshore installations are classified in reliability class 3, i.e. with an acceptable largest yearly probability of failure in the accidental limit state of 10^{-5}. According to the guidelines to the Norwegian construction regulations [42], this safety level is in agreement with other national regulations, e.g. Canadian.

Other design guides, e.g. American [16], also emphasise the importance of employing probabilistic methods in structural design. According to American design guides, a specification based on reliability analysis should consider three components—uncertainties, risk and economics. The main goal is to minimise the *total cost*, as given by [16]

$$\text{total cost} = \text{initial cost} + \text{risk} \times \text{failure cost} \tag{3.2}$$

A sketch of the total cost is given in figure 3.2.

The procedure is complicated by the estimation of the failure cost, which has to include human, social and political factors as well as the actual structure cost. The model does not include failure due to human errors or wrong usage of the structure. Nevertheless, the model serves as an important guide for structural design, and can be improved by taking into account existing design practice and experience.

Bjerketvedt et al. [12] use the common definition of *risk* as the product of frequency and consequence. The authors cite a flow scheme for risk analysis made by Ramsay [45], reprinted in figure 3.3.

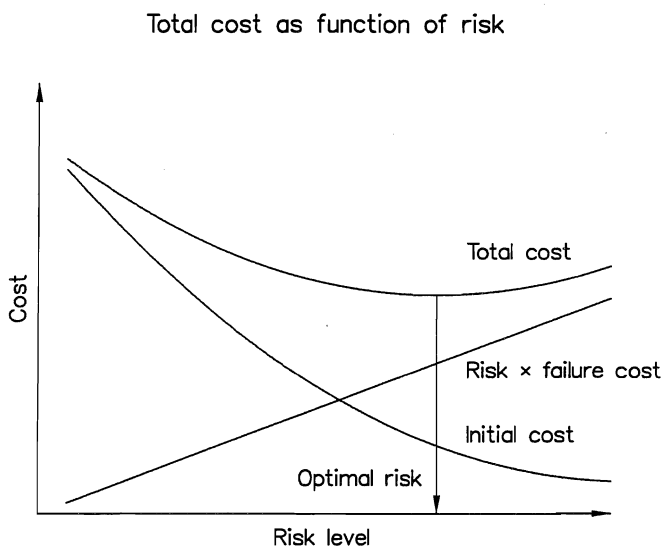

Figure 3.2: Total cost as function of risk level.

3.1.2 Structure failure equations

Structural resistance can be measured by testing. Any set of similar structures will show up with some *resistance distribution* due to variances in yield stresses and geometric properties.

Load effects can be observed. Measurements of load effects from e.g. snow or wind will produce *load effects distributions.*

Both resistance and load effect distributions can be described in statistical terms. We present the observations as *accumulated probability functions* or *cumulative distribution function*, F, or *probability density functions*, f [27].

If X is a random variable of interest to us, an observed property, i.e. resistance or load effect, the cumulative distribution function is given by

$$F_X(x) = P(X \leq x) \qquad \forall \quad x \tag{3.3}$$

where x is any value X can take. For our purposes, X can be assumed to be a continuous variable. In this case, the probability density function in the interval $\langle a, b]$ is given by

$$P(a < X \leq b) = \int_a^b f_X(x)\, dx \tag{3.4}$$

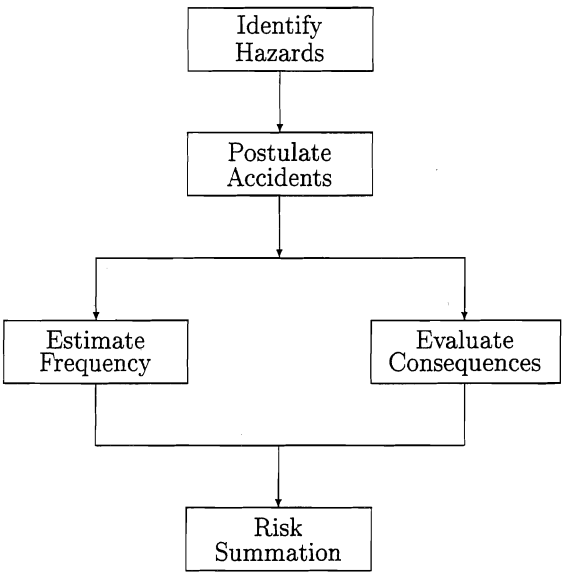

Figure 3.3: Risk analysis [45]

The corresponding cumulative distribution function is

$$F_X(x) = P(X \leq x) = \int_{-\infty}^{x} f_X(\xi)\, d\xi \tag{3.5}$$

and, accordingly

$$f_X(x) = \frac{dF_X(x)}{dx} \tag{3.6}$$

The probability of non-failure of a structure can be found based on the distribution properties [11]. We denote the resistance R and the load effect L. For any load value x, non-failure will occur when $R > x$. The probability of L occurring in an infinitesimal interval dx around x is $P(x - \frac{1}{2}dx < L < x + \frac{1}{2}dx) \approx f_L(x)\, dx$. Thus, the probability of non-failure within dx is

$$dP_N = \underbrace{(1 - F_R(x))}_{P(R>x)} \cdot \underbrace{f_L(x)\, dx}_{P(L \text{ close to } x)} \tag{3.7}$$

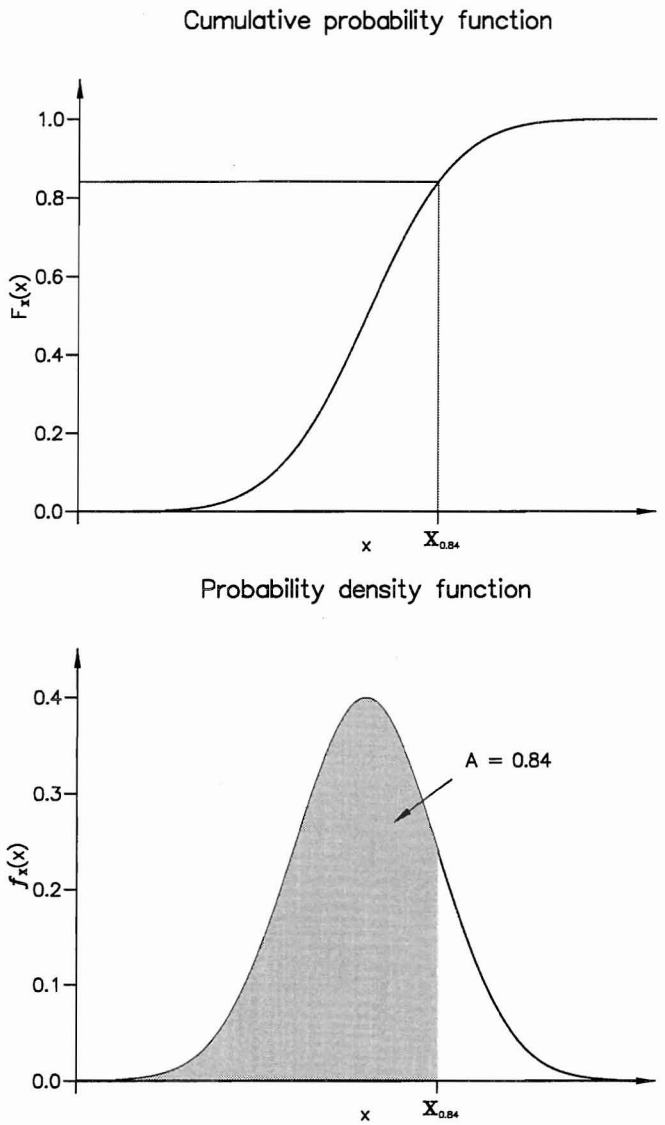

Figure 3.4: The cumulative probability function $F_X(x)$ and probability density function $f_X(x)$.

$$P_N = \int_0^\infty dP_N = \int_0^\infty (1 - F_R(x)) f_L(x)\, dx \tag{3.8}$$

which, with partial integration leads to

$$P_N = [(1 - F_R(x))F_L(x)]_0^\infty + \int_0^\infty f_R(x)F_L(x)\, dx \tag{3.9}$$

The boundary conditions are given by

$$F_R(\infty) = F_L(\infty) = 1 \tag{3.10a}$$
$$F_R(0) = F_L(0) = 0 \tag{3.10b}$$

and leads to the equation for structural non-failure

$$\boxed{P_N = \int_0^\infty f_R(x)F_L(x)\, dx} \tag{3.11}$$

that might be more convenient than eqaution 3.8. The probability of structural failure can likewise be deduced.

$$P_F = P(L > R) \tag{3.12}$$

$$dP_F = \underbrace{F_R(x)}_{P(R<x)} \cdot \underbrace{f_L(x)\, dx}_{P(L \text{ close to } x)} \tag{3.13}$$

$$\boxed{P_F = \int_0^\infty F_R(x) f_L(x)\, dx} \tag{3.14}$$

3.1.3 Safety index

The introduction of a *safety index* was done by Cornell [46] according to Thoft-Christensen and Baker [6].

Let $g = g(x_1, \ldots, x_n)$ be the *state limit function* where $x_1, \ldots, x_n$ are stochastic values describing geometry, material properties and load effects for a structure [7]. The values $x_i, i = 1, \ldots, n$ have their respective variables $X_i, i = 1, \ldots, n$.

We introduce the *safety margin* M as a stochastic variable when we replace the values $\boldsymbol{x}$ with their respective variables $\boldsymbol{X}$.

$$M = g(X_1, \ldots, X_n) \tag{3.15}$$

where $M < 0$ denotes structural failure, $M > 0$ non-failure and $M = 0$ the limit state. The *safety index* β is defined by the coefficient of variation

$$\boxed{\beta = \frac{E[M]}{D[M]}} \tag{3.16}$$

where $E[\cdot]$ is the expected value and $D[\cdot]$ is the standard deviation.

If M is linear in $\boldsymbol{X}$, i.e. $M = a_1 X_1 + \cdots + a_n X_n + b = \boldsymbol{a}'\boldsymbol{X} + b$, we will achieve the *linear safety index* from equation 3.16. However, such a linear relation is uncommon, and may generally only be used as an approximation. A better result is achieved if we replace the state limit function $g(\boldsymbol{X})$ with it's first order Taylor series in the mean value $\boldsymbol{\mu} = E[\boldsymbol{X}]$ [7]. This improvement also allows for introduction of probability assumptions of the components in $\boldsymbol{X}$:

$$g(\boldsymbol{X}) \overset{\boldsymbol{\mu}}{=} g(\boldsymbol{\mu}) + \sum_{i=1}^{n} \left.\frac{\partial g}{\partial X_i}\right|_{\boldsymbol{X}=\boldsymbol{\mu}} (X_i - E[X_i]) \tag{3.17}$$

From this formula, it is possible to calculate the safety index $\beta_{\boldsymbol{\mu}}$ by using the second order moment representation of $\boldsymbol{X}$, i.e. both mean and standard deviation can be taken into account.

Our definition of β (eq. 3.16) has one drawback. As we represent β by means of $g(\boldsymbol{\mu})$, β will depend on the formulation of g. The state limit function g is in principle arbitrary except at the limit surface, i.e. $g = 0$.

The definition $\beta = E[M]/D[M]$ has a formulation invariant property, it represents the distance from origo to the state limit surface in the normalised, n-dimensional space. This property forms the foundation for a generalisation of β to include non-plane limit state surfaces [7].

A formulation of β that takes into account non-plane formulation and curvature of the limit state surface is the *generalised safety index* as presented by Ditlefsen and Madsen [7]. They introduce a weight function ψ_n on the volume in n-dimensional space enclosed by the limit state surface $\mathcal{S}$, and by applying a set of rules on the weight function ψ_n derives the relation

$$\beta = \Phi^{-1}(p) \tag{3.18}$$

where Φ is the normal distribution function (i.e. Φ^{-1} is the inverse normal distribution function) and p the probability of non-failure. The elements in the stochastic vector $\boldsymbol{X}$ does not need to follow the normal distribution, but must be known by their second-order moments. By making demands on the weighting function ψ, we can treat the safety index β as normally distributed.

API RP 2A LRFD [16] defines the safety index β as

$$\boxed{\beta = \frac{\text{Mean safety margin}}{\text{Uncertainty level}}} \tag{3.19}$$

where legal, social, economic and psychological factors are not taken into account. There are no preassigned β levels, as β values in general depend on the model(s) describing the mean safety and uncertainty levels. Equation 3.19 is noted to be a rephrasing of equation 3.16.

3.2 Probabilistic properties

For both loads and strengths it is common to denote a *characteristic value* as a quantile within the load or strength distribution. The quantile can be prescribed in design standards. It is noticeworthy that the characteristic value is allowed to be exceeded (for loads) or gone below (for strengths) with some prescribed probability.

3.2.1 Structural strength—resistance

Characteristic material strength in terms of stress, σ_k is determined by testing as [11]

$$\sigma_k = \sigma_m - k \cdot s \tag{3.20}$$

where σ_m is the mean value and s is the standard deviation of the stress distribution. The parameter k determines σ_k as a quantile in the distribution of σ. In the case of Gaussian distribution, a choice of $k = 1$ leads to $\sigma_k = \sigma_{0.16}$, i.e. the 16%-quantile in the distribution of σ. Likewise, $k = 2$ gives $\sigma_k = \sigma_{0.02}$; 2% of the measured σ's will have lower values than σ_k.

European standards [8] describes the properties of materials or products by characteristic values which correspond to the value of the property having a prescribed probability of not being attained in a hypothetical unlimited test series. Furthermore, unless otherwise stated, the characteristic values should be defined as the 5% quantile for strength parameters and as the mean value for stiffness parameters, according to Eurocodes [8, 18].

NBS Special Publication 577 [10] used Monte Carlo simulations to calculate the ratio R_n/R and its coefficient of variation, V_R. R_n is the nominal strength and R the calculated strength based on material distribution properties.

The NBS Publication [10] assumed the probability distributions for the materials in reinforced concrete to be the normal distribution, and for metal (e.g. steel) members the lognormal distribution. Masonry structures appeared to be modeled satisfactory with lognormal distribution, while glue-laminated structures could be modeled either by the Weibull or lognormal distribution.

3.2.2 Load distributions

Loads are either permanent or variable (magnitude over time), fixed or free (position over time) and static or dynamic (nature of induced structure) [6].

Permanent loads can often be assumed to take Gaussian distribution [8, 18]. This is due to the fact that the sum of n identically distributed random variable, such as the self-weights of many individual structure parts, takes the form of a normal probability function [6, 27].

Variable loads can be defined by a variety of probability distribution functions. If the failure occurs when and only when the variable, time-dependent load exceeds some threshold, the form of the load distribution as a function of time will not be of any specific interest, but the maximum value will. It is the largest value during a specified reference period T of the variable load that is of interest.

Borges [9] supplied some probabilistic definitions of actions from permanent and variable loads, shown in table 3.2. The American National Bureau of Standards [10] provided a classification of the distribution of load effect as shown in table 3.3.

Table 3.2: Probabilistic definitions of actions after Borges [9]

Type of actions	**Type of distribution function**
Self-weight of concrete structures	Normal
Self-weight of steel structures	Normal
Superimposed loading in dwellings	Extreme I
Superimposed loading in office buildings	Extreme I
Superimposed loading in retail premises	Extreme I
Superimposed loading in parkings	Extreme I
Snow loads on roofs	Extreme I
Wind pressures in Western Europe	Extreme I
Bedrock and surface seismic vibrations	Extreme I[a]

[a]It is assumed that yearly extremes fit Type II Extreme distribution below the 0.98 quantile

The *extreme* or *extremal I*, resp. *II* distribution functions as mentioned in these tables were originally described by Gumbel [29].

The Gumbel extremal probability concept can be described as follows: Variable loads are a function of time. Let us sample the distribution of a variable load for a reference period. We will then be able to produce a probability density function $f_X(x)$. The maximum value of the sample is denoted X. If the sampling is done for a new reference period, we will achieve a new maximum X. Thus, a set of i repeated load histories with their respective maximum values X_i will form a population of their own. If we observe n load histories, the stochastic variable describing the maximum value is denoted X_n.

The probability density function for the maximum values, $f_{X_n}(x)$, relies on the probability function of the initial variable, $f_X(x)$ [29, 30]. Furthermore, $f_{X_n}(x)$ will vary with the sample size n. As n approaches infinity (e.g. sampled maximum values of snow loads on

Table 3.3: Load effect distribution according to NBS [10].

Load effect type	Distribution type
dead load	Normal
live load	Extremal I
live load, apt.[a]	Gamma
wind load	Extremal I
wind load, ann.[b]	Extremal I
wind load, apt.	Extremal I
snow load	Extremal II
snow load, ann.	Lognormal
earthquake	Extremal II

[a]apt. = arbitrary point in time
[b]ann. = annual

roofs over many years), the probability density function f_{X_n} will asymptotically approach some limit. This is known as the *asymptotic theory of statistical extremes* [47].

Thus, the load effect distributions mentioned in the literature are either normal, lognormal, gamma or the Gumbel extremal type I or II. There seems to be no proposal of load distribution for explosion loads.

Another load classification can be done by regarding the *return period* of a characteristic load. In that way we can disregard the load distribution and focus on the probability of exceeding the characteristic load. The European prestandard for accidental loads, prENV 1991–2–7:1996 [13], mentions no probability form of the explosion pressure from gas explosions. A structural failure probability of 10^{-4} per year is described as appropriate in the informative annex, i.e. the probability of an explosion occurring *and* the resulting explosion pressure being greater than the structure's design resistance in the accidental situation. This value is proposed in the absence of quantification of consequences and economical optimisation.

With this approach, it follows that the return period of the design explosion is 10 000 years. Explosions can occur more frequently, but they will not have such high overpressures. Given that the probability of an explosion occurring and the magnitude of the explosion are independent, we can write the probability of exceeding the design load as

$$\begin{aligned}\text{probability of failure} &= \text{probability of an explosion occurring} \\ &\times \text{probability of explosion pressure exceeding design value} \end{aligned} \quad (3.21)$$

The prestandard prescribes a design accidental equivalent static explosion pressure p_d for use in buildings. The quasi-static explosion pressure p_d is in general a function of the venting areas in the confinement.

3.3 Semi-probabilistic design

3.3.1 General

The equations in section 3.1.2 are valid for any section in any member in a structure. However, to calculate the probability functions for every section in a structure, for both resistance and load effects, is unpractical and usually fails from lack of sufficient data [8]. Simpler design methods must be used.

The most common design method today is the *partial coefficient method* [11], which tries to implement the effects of varying resistances and load effects and achieve a reasonable safety index. The partial coefficient method is based on the characteristic values of load effects and resistance, L_k and R_k, and their respective partial coefficients, γ_F and γ_M [48].

It's framework is based on the combination of building tradition and probabilistic methods and calibrated against past experience and measured data. Thus the partial coefficient method can be classified as a *semi-probabilistic design method.* Several design guides, such as Eurocode 1 [8], API RP 2A LRFD [16] and NS 3479 [15] use this approach.

3.3.2 Limit states

Limit states are often defined as states of the structure beyond which the structure no longer satisfies the design performance requirements [8, 11, 15]. Common limit states are the ultimate limit state and the serviceability state. Accompanying the limit states are a set of *partial factors* that are intended to use with different kinds of actions.

Accidents are handled in European and Norwegian standards [8, 44] by prescribing an *accidental design situation* in the *ultimate limit state.* Furthermore, Norwegian standard [44] provides a set of load factors for offshore installations in the pertroleum industry.

The accidental design situation covers e.g. explosions, collisions, fires and earthquakes. Because of the wide spectrum of possible load types, a case-invariant, general design situation is hard to prescribe. Literature describing material behaviour and load effects in the particular situation must be studied to establish an appropriate model.

3.3.3 The method of partial coefficients

The partial coefficient method is based on the characteristic values of load effect and resistance, L_k and R_k and their respective partial coefficients γ_F and γ_M. The design load effect and strength are generally calculated as $L_d = L_k\gamma_F$ and $R_d = R_k/\gamma_M$.

For design action or load effect, we denote the *characteristic value* as L_k. The characteristic value will generally correspond to a prescribed probability of not being exceeded on the unfavourable side during a "reference period" [8, 11]. The *design value* of the action

can be obtained by multiplying the characteristic value by a partial factor γ_F:

$$L_d = L_k \gamma_F \tag{3.22}$$

where γ_F is the partial factor for the action considered taking account of [8]:

- the possibility of unfavourable deviations in the actions
- the possibility of inaccurate modeling of the actions
- uncertainties in the assessment of effects of action

For material strength, we denote the *characteristic value* as R_k. The characteristic value will generally correspond to a specified quantile of the assumed statistical distribution of the particular property of the material [8]. The *design value* of the material is obtained by dividing the characteristic value by a partial factor γ_M:

$$R_d = R_k / \gamma_M \tag{3.23}$$

where γ_M is the partial factor for the material property taking account of [8]:

- unfavourable deviations from the characteristic values
- inaccuracies in the conversion factors
- uncertainties in the geometric properties in the resistance model

Equations

The equations to achieve the paritial coefficients are derived by e.g. Larsen [49]. We start with the definitions of the characteristic values

$$R_k = \bar{x}_R - k_R s_R \tag{3.24a}$$
$$L_k = \bar{x}_L + k_L s_L \tag{3.24b}$$

where the $\bar{x}$'s and s's are the respective estimates of mean and standard deviation. The k factors are constants defining prescribed quantiles within the respective distributions. They are visualised in figure 3.5.

The safety index β was defined earlier in equation 3.16 by the safety margin M as $\beta = E[M]/D[M]$. If we let M be the distance from resistance R to action, or load effect L, we get

$$M = R - L \tag{3.25}$$

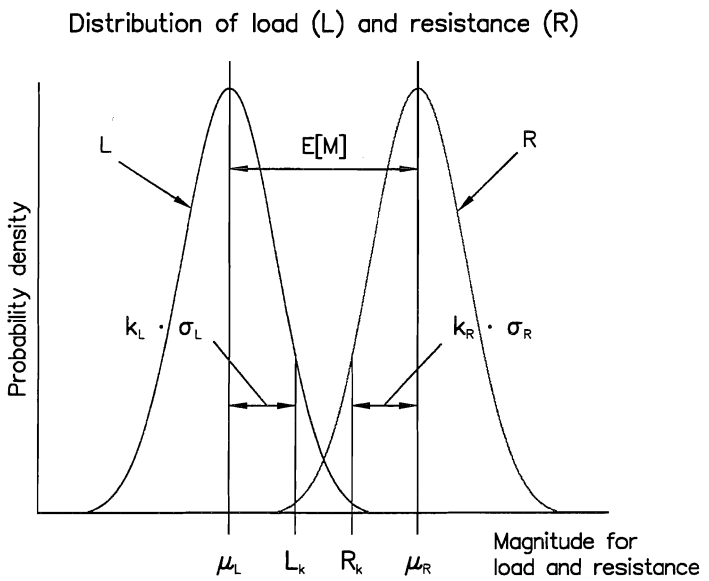

Figure 3.5: An idealisation of the distributions of load and resistance.

and, if R and L are independent and we neglect the covariance

$$E[M] = E[R] - E[L] = \mu_R - \mu_L \tag{3.26}$$

$$D[M] = \sqrt{\mathrm{Var}[R] + \mathrm{Var}[L]} = \sqrt{\sigma_R^2 + \sigma_L^2} \tag{3.27}$$

and we get

$$E[M] = \beta D[M] = \beta\sqrt{\sigma_R^2 + \sigma_L 2} \tag{3.28}$$

We let the *safety factor*, denoted as γ, be defined as

$$\gamma = \frac{R_k}{L_k} = \frac{\mu_R - k_R\sigma_R}{\mu_L + k_L\sigma_L} = \frac{\mu_R}{\mu_L}\underbrace{\frac{1 - k_R V_R}{1 + k_L V_L}}_{\gamma_R} \tag{3.29}$$

where we have used the coefficient of variation, $V_L = \sigma_L/\mu_L$ and $V_R = \sigma_R/\mu_R$. The fraction μ_R/μ_L can be rewritten with $\mu_R = \mu_L + E[M]$ as

$$\gamma_0 = \frac{\mu_R}{\mu_L} = \frac{\mu_L + E[M]}{\mu_L} = \frac{\mu_L + \beta\sqrt{\sigma_R^2 + \sigma_L^2}}{\mu_L}$$

$$\gamma_0 = 1 + \beta\sqrt{\gamma_0^2 V_R^2 + V_L^2} \tag{3.30}$$

Equation 3.30 is an ordinary second-order polynomal equation in γ_0. The result has a somewhat complex form. We can get a more handy result if we introduce the approximate linearisation

$$\sqrt{\sigma_R^2 + \sigma_L^2} \approx \alpha_R\sigma_R + \alpha_L\sigma_L \tag{3.31}$$

into the previous step in the deduction

$$\gamma_0 = \frac{\mu_L + \beta(\alpha_R\sigma_R + \alpha_L\sigma_L)}{\mu_L} = 1 + \beta(\alpha_R V_R\gamma_0 + \alpha_L V_L) \tag{3.32}$$

where we again have used the definition $V = \sigma/\mu$. Equation 3.32 can be solved for γ_0, and we get

$$\gamma_0 = \frac{\mu_R}{\mu_L} = \frac{1 + \beta\alpha_L V_L}{1 - \beta\alpha_R V_R} \tag{3.33}$$

Thus, the *safety factor* γ can be written as

$$\gamma = \frac{\mu_R}{\mu_L}\frac{1 - k_R V_R}{1 + k_L V_L} = \frac{1 + \beta\alpha_L V_L}{1 - \beta\alpha_R V_R}\frac{1 - k_R V_R}{1 + k_L V_L} = \gamma_L\gamma_R \tag{3.34}$$

where γ_R and γ_L are "safety factors" for resistance and load, respectively.

In Norwegian standards [15], γ_R is denoted γ_m (m for *m*aterial) and γ_L is denoted γ_f (f for *f*orce). In the proposal to the new structural reliablilty standard NS-ENV 1991-1 [44], γ_R is denoted γ_m or γ_M and γ_L is denoted γ_G (permanent actions), γ_Q (variable actions) or γ_A (accidental actions).

Nordic regulations

According to the NKB-report [48], the partial coefficient γ_F can be considered as a function $\gamma_F = \gamma_F(\gamma_{F1}, \gamma_{F2})$, where

- γ_{F1} takes account of the possibility of unfavourable deviations of the actions from the characteristic values, uncertainty in the loading model and of possible accurate assessment of the action effect as far as it may be assumed to be independent of the structural material.
- γ_{F2} takes account of the reduced probability of combinations of actions all at their characteristic value.

The material resistance factor γ_M can be considered as a function of five factors; $\gamma_M = \gamma_M(\gamma_{M1}, \gamma_{M2}, \gamma_{M3}, \gamma_{N1}, \gamma_{N1})$, where

- γ_{M1} takes account of the possibility of unfavourable deviations of the strengths of materials and other properties from the characteristic values.
- γ_{M2} takes account of possible inaccurate assessments of the resistance, uncertainty of geometrical parameters, as well as that part of the action effect which may be dependent upon the structural material.
- γ_{M3} takes account of possible deviations from the strength of material properties in the structure or structural element involved, as compared to that derived from control test specimens.
- γ_{N1} takes account of the consequences and types of failure.
- γ_{N2} takes account of the degree of control on site (besides the statistical quality control of the material properties).

The load model proposed in chapter 4 uses this approach, but presents an alternative to the γ_{M1} coefficient, thus resulting in a different partial coefficient for load effect, γ_M.

American design guides

Another approach to the partial coefficient method is referred to as Load and Resistance Factor Design (LRFD). The LRFD principle is described in American design guides [16] as

$$\text{resistance factor} \times \text{nominal strength} > \text{load effect due to sum of factored external loads}$$

where each term is multiplied with its respective strength or load factor that takes into account the uncertainties associated with the value, i.e.

$$\phi R_n \geq \sum \gamma_i L_i \tag{3.35}$$

where

ϕ = component resistance factor,
R_n = nominal strength equation,
γ_i = load factor for load type i,
L_i = nominal load effect on component due to load type i

The LRFD approach is applied to a set of limit states. i.e. states beyond which the structure no longer satisfies the design performance requirements [8].

European standards

For accidental situations such as gas explosions, European standard [8] prescribes design values of actions for accidental design situations for use in the combination of actions

$$\sum_{j\geq 1} \gamma_{GAj} G_{kj} + \gamma_{PA} P_k + A_d + \psi_{11} Q_{k1} + \sum_{i\geq 1} \psi_{2i} Q_{ki} \tag{3.36}$$

where

γ_{GAj} is the partial factor for permanent action j for accidental design situations
G_{kj} is the characteristic value of permanent action
γ_{PA} is the partial factor for prestressing actions for accidental design situations
P_k is the characteristic value of a prestressing action
A_d is the design value of the accidental action
ψ_{11} is the frequent combination coefficient for Q_{k1}
Q_{k1} is the dominant variable action
ψ_{2i} is the quasi-permanent combination coefficient for Q_{ki}
Q_{ki} are the characteristic values of the non-dominant variable actions
$+$ implies "to be combined with"

The design value of the accidental action, A_d is given by $A_d = \gamma_A A_k$, where γ_A is the partial factor for accidental load and A_k is the characteristic value of the accidental load.

Norwegian standard

There exists a proposal to a Norwegian standard for structural design [44], it's title informaly translated to «Basis for design of structures — demands on reliability». It is almost identical with the Eurocode 1 standard [8] in nomenclature, design practice and load factors, but includes a separate appendix for load factors for offshore installations in the petroleum industry.

Chapter 4

Characteristic action model for gas explosions

4.1 General

European and Norwegian standards [8, 44] use the *characteristic accidental action*, A_k as their input to the accidental design situation in the ultimate limit state. Here we will try to establish this characteristic value based on values from explosion simulations.

A characteristic load model applicable to gas explosions must take into account the uncertainties that arise from

- Gas cloud size and location
- Ignition point source location
- Explosion modeling idealisation

Other variables affecting the uncertainty level can either be taken care of by conservative assumptions or are of minor significance compared to the above mentioned. A possible exception can be the initial turbulence field.

4.2 Load model corrected for uncertainties

The explosion pressure is a dynamic quantity, $p = p(t)$. Since the response of structures due to gas explosions however rarely will be in the impulsive regime [32], the impulse of the loading will be a parameter of minor interest. The response in the dynamic and quasi-static regime are dominated by the maximum overpressure, and therefore emphasis will here be put on the maximum pressure, denoted $p_{\max} = \max\{p(t)\}$. This value will serve as our *sample action*, i.e. $p = p_{\max}$.

A *characteristic action*, A_k, which takes into account the given uncertainties can be presented as

$$A_k = p\gamma_G\gamma_I\gamma_M \tag{4.1}$$

where $p = p_{\max}$ is the maximum explosion pressure load obtained from the explosion simulator, γ_G is a factor compensating for uncertainty in estimating size and location of the gas cloud, γ_I is a factor taking account for variance of ignition point location and γ_M is a factor compensating for mathematical and physical inaccuracy in the explosion simulator.

4.3 Gas cloud size and location

The factor γ_G represents uncertainties regarding gas cloud size and location. The type of gas is taken to be known.

The effect of varying gas cloud size is illustrated in section 5.3. The survey is limited to three gas volumes:

1. Gas in a low quarter of a module
2. Gas in lower half of module
3. Module filled completely with gas

Partial factor γ_G for these limited set of cases are presented in section 8.2.

4.4 Ignition point location

The factor γ_I represents uncertainties regarding the assumption of the location of the ignition point.

The effect of varying the ignition point location is thoroughly discussed in chapter 6. Derived factors for γ_I are presented in section 8.3.

4.5 Computer simulations

The factor γ_M represents the uncertainties regarding the accuracy of explosion simulators.

For calculations of this factor, extensive explosion validations must be available. As reported in section 2.2.2, such validation data are rare. The only validation data available that can be used for deduction of γ_M are for the EXSIM program [24, 25].

Sæter et al. [24] presented a validation of the EXSIM-94 gas explosion simulator based on 40 cases. The validation was only performed on the maximum overpressures. The paper

proposed to use a method that calculated a "relative error", e_i, to investigate the quality of the results;

$$e_i = \frac{y_i - x_i}{y_i} \tag{4.2}$$

where y_i is the predicted result and x_i is the observed, experimental result of the ith observation.

The paper further assumed that the relative error e_i followed a Gaussian distribution and that 4 of the 40 cases that showed extreme behaviour could be discarded. The authors also discussed the simulator results if 8 of 40 cases could be classified as "abnormal" and consequently be discarded. The last case is not taken into account here.

Within these limits (i.e. assumption of Gaussian distribution and 4 cases discarded by "common sense"), and using the most recent version of EXSIM [25], we estimate the mean e_i as -0.05, i.e. the EXSIM model underpredicts the maximum explosion overpressure with about 5%. Further, we can estimate the 95%-confidence interval of the relative error to lie within $\pm 70\%$ of the mean value and the 99%-confidence interval to lie within $\pm 104\%$ of the mean value.

The data in the EXSIM validation is based on the maximum explosion pressure. The code is not validated versus explosion impulse. However, the authors' impression is that the coefficients derived with care also may be used with respect to impulse values.

Factors that take into account the imperfectness of the EXSIM program are presented in section 8.4. Data from other explosion simulator software are not available.

4.6 Correlation

The form of the proposed model is valid if the events leading up to the three γ factors are independent. If this is the case, the multiplying prescription is allowed.

On the other hand, if the parameters "gas cloud size and location", "ignition source location" and "choice of simulator" are in some way dependent of each other, the multiplying form can not be used without some kind of correlation coefficient.

There has not been found any general dependency between gas cloud size or ignition point and simulator in the literature. This would be the case if an explosion simulator calculated e.g. ignition point placed in corners especially well or bad, or that an explosion simulator predicted explosion from small gas volumes better than large ones. There is no evident reason for such a behaviour to occur, either.

For some explosions, e.g. the Flixborough disaster [38, 50], the ignition point is reported to presumably lie at the border of the gas cloud. It is imaginable that the ignition point will have an affinity with the border of the flammable cloud. If there is a constant ignition source, i.e. an open flame, the gas cloud will ignite at it's border at arrival.

Reports have also claimed the ignition point to lie well within the gas cloud, e.g. the Port Hudson explosion [50]. That may well be the case if the ignition source is an electrical switch. Hot surfaces also may need some time to heat up the surrounding gas cloud.

The conclusion is that the general, case-nonspesific ignition point can not be assumed to occur at any prescribed place relative to the gas cloud. Thus we may make the presumption that the ignition point location and gas cloud are independent.

Chapter 5

Results from simulations

5.1 Simulated cases of offshore platform modules

In search of probabilistic explosion data, explosions in three different offshore modules and one onshore plant are simulated. The onshore plant simulations was a reconstruction of the Flixborough accident, see chapter 7.

One of the offshore modules is the Piper Alpha C module, as implemented by Førrisdahl [39] with some minor modifications done with origin in drawings and photos from the report by Lord Cullen [37]. A visualisation of the computer model is shown in figure 5.1.

The two other modules are the CMR M24 and M25 full scale modules, based on the experiments reported by Hjertager et al. [40] and simulator implemented by Sæter et al. [24] and with modifications by Solberg and Hjertager [25]. The geometries are illustrated in figure 5.2

All modules are simulated with two gas types, methane and propane, and three degrees of gas filling; 1/4, 1/2 and 1/1 module filled with gas. For the Piper Alpha C module, the 1/4 filling is taken to be the lower, eastern quadrant. This is an approximation to the actual explosion. For the CMR modules, the lower quart filled with gas was picked randomly. For all modules, the 1/2 filling grade represents the lower half of the module filled with gas.

The flow simulation grids are partly uniform, partly exponential. Within the modules, the control volumes of the size of $1\,m^3$, gradually increasing outside. The calculation domains are extended in all three dimensions outside the modules with approximately the corresponding module length to each side. That is, if the module is 45m long, the calculation domain in the same direction is set up to be approximately $3 \cdot 45 = 135\,m$. The same rule of thumb is kept in the two other directions.

The models contain 8 pressure monitoring points, evenly distributed along the walls. The data from the monitoring point with the highest explosion pressure is selected to be further processed.

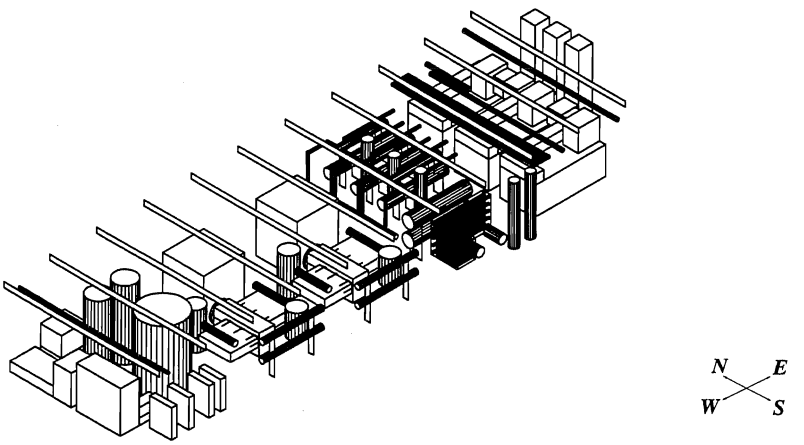

Figure 5.1: Visualisation of the computer model implementation of the Piper Alpha C module. Original model by Førrisdahl [39].

Thus, we have a set of $3 \times 2 \times 3 = 18$ cases. For each of these cases, 400 simulations are performed. The ignition point location is varied randomly for each simulation. Some ignitions points end up within process equipment and therefore produce no explosion. Such cases are discarded, and the effective number of different ignition points generally end up in the interval of 300–350 for each case.

5.2 Observed values

With all the data generated from the simulations, which parameters to process further must be decided.

Explosion simulators offer a wide range of logging information during the progress of the combustion. As an example, EXSIM offers the possibility to register [51]

- turbulent kinetic energy k
- dissipation of turbulent kinetic energy ϵ
- fuel fraction
- enthalpy
- pressure

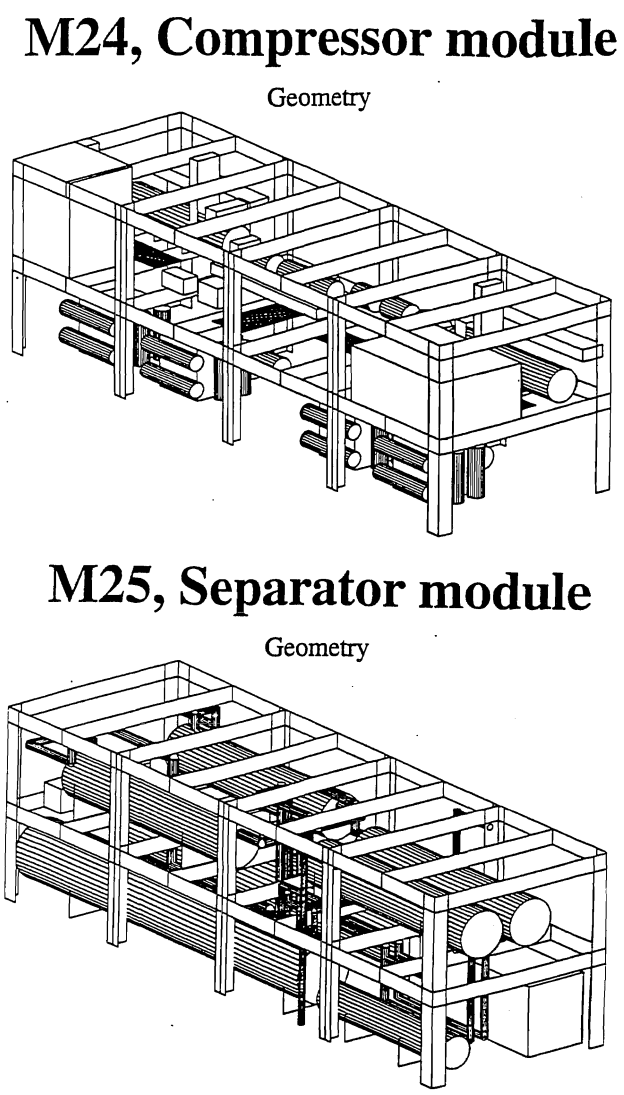

Figure 5.2: Visualisation of the computer model implementation of the CMR M24 and M25 modules as presented by Sæter et al. [24].

- density
- temperature
- effective viscosity
- turbulent timescale ϵ/k
- combustion rate
- oxygen fraction
- combustion production fraction
- turbulent velocity
- turbulent Reynolds number
- mixture fraction
- turbulent length scale

An illustration of a typical explosion pressure as a function of time is shown in figure 5.3. The simulation is a reconstruction of the Piper Alpha C module explosion with a randomly placed ignition point. The result is from a methane explosion with 8 pressure monitoring points.

For offshore structures, the main dependent variable is the explosion pressure. The respones of large structural components subjected to explosion pressure-time profiles with an acceptable rise time will be in the dynamic to quasi-static regime [32]. Furthermore, in the cases where the impulse is of interest, usually only the positive part of the load is considered to be important in determining structural response [32].

The impulse is of interest for "short" durations of the positive phase of the explosion. Let t_1 be the duration of the positive phase and T the structure's natural period. Clough and Penzien [52] then mention $t_1/T < 0.25$ as a "short" duration, while the Steel Construction Institute [32] suggests $t_1/T < 0.40$ as the "shortness" limit.

During the simulations, the pressure as a function of time is calculated. The timesteps in the simulation are irregular, so the postprocessing includes interpolation. The interpolation is done with splines into timesteps of 1 millisecond. Manual inspection proves this interpolation to be an acceptable representation of the original data.

The maximum explosion pressure, $p_{\max} = \max\{p(t)\}$ is extracted from the interpolated function. The positive phase of the explosion pressure is said to start when the explosion pressure reaches 5% of the maximum value. The impulse of the positive explosion phase, $I = \int_{t|_{p=p_{\max}\cdot 0.05}}^{t|_{p=0;\ t>t|_{p=p_{\max}}}} p(t)\,dt$, where $p = 0$ is the first occurrence of zero explosion pressure after maximum. The integration is done with Simpsons formula [53]. The limits of the integral also represent the extents of the duration of the positive phase.

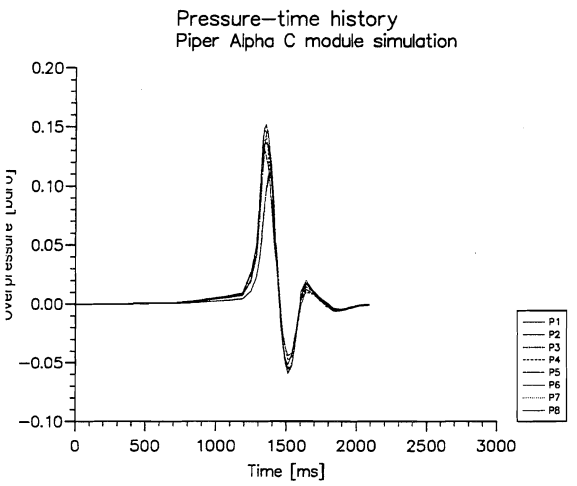

Figure 5.3: Typical pressure-time history for an offshore module with 8 pressure monitoring points.

5.3 The effect of gas cloud size

The Piper Alpha C module and the CMR modules have all been simulated with different amount of gas. Given 400 simulations of each case, the effect of explosion pressure and impulse as a function of module filling grade are illustrated in figures 5.4 and 5.5.

Pappas [36] did some calculations with different gas filling grades and ignition point location far from the module vent openings. The results showed that a filling grade of 30–50% may produce explosion pressures of the same magnitude as a module completely filled with gas.

For the chosen modules and gas filling grades, these observations are not confirmed. A doubling of the explosive gas volume will for the present modules in general produce more than a doubling in explosion pressure and impulse.

A likely explanation for this divergence is the choice of cases. According to Bjerketvedt et al. [12], Pappas [36] chose compartements that were closed at one side and selected ignition point locations far away from the vent opening. This is a delibarately "worst case" choice to show that even a minor-sized gas cloud explosion may produce high overpressures. The present cases do not attempt to reproduce a such situation. They are selected to represent the most realistic situations. For the present cases, the vent openings are at both ends, and the ignition point may be both close to and far away from the vents. This

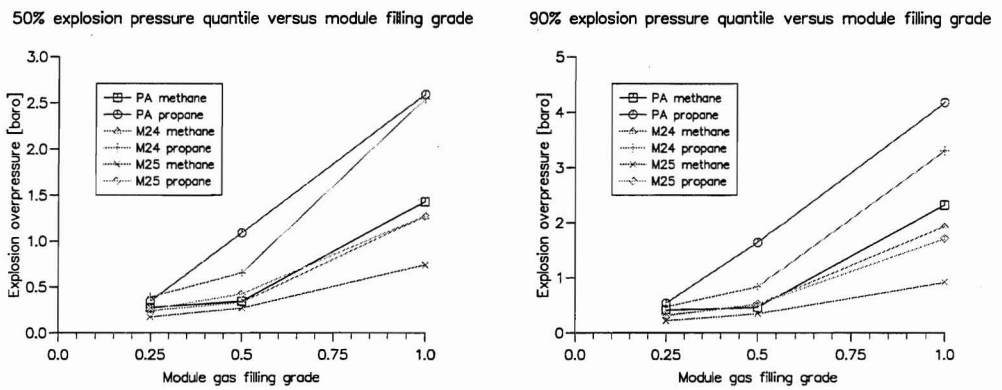

Figure 5.4: Explosion pressure as function of offshore module filling grade, based on 400 simulations.

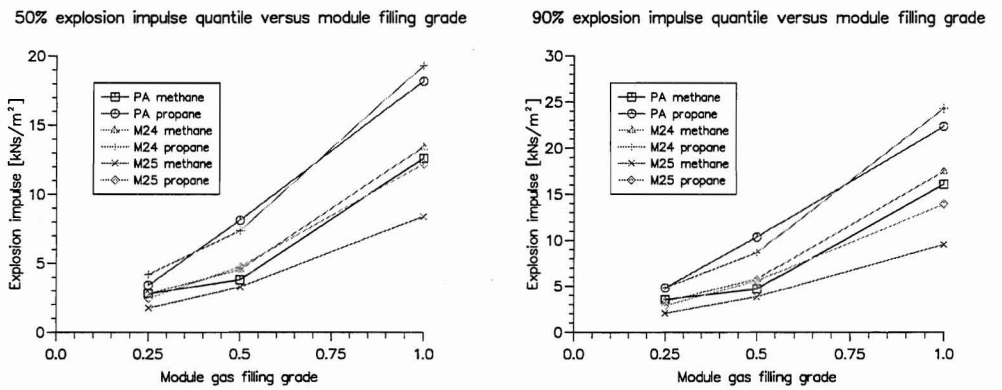

Figure 5.5: Explosion impulse as function of offshore module filling grade, based on 400 simulations.

may well explain the differences in calculated pressures for minor gas filling degrees.

We expect explosion simulators to show comparable results to Pappas' analysis under the same input conditions.

5.4 Impulse versus explosion pressure

While the response of most offshore structures exposed to gas explosion loads rarely are in the impulsive regime [54], a correlation between explosion impulse and explosion pressure may still be interesting to investigate. A plot of the values from all three offshore modules filled completely with gas are shown in figure 5.6. Each sub-figure is made up from the results of 1 200 simulations.

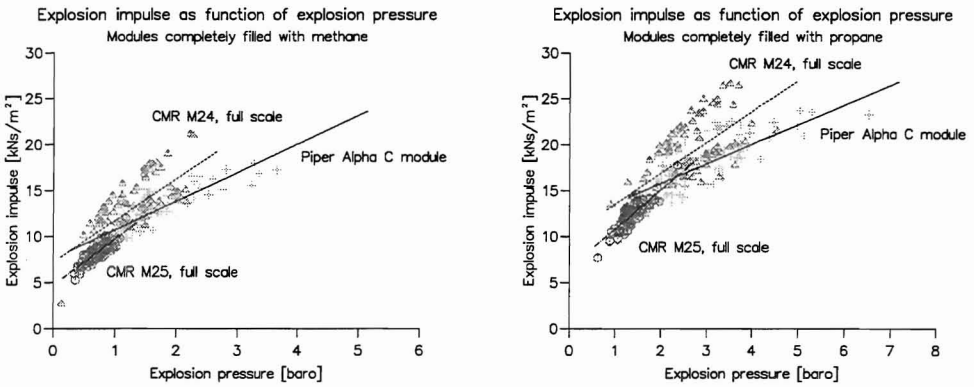

Figure 5.6: Explosion impulse as function of explosion pressure. Left figure: Methane as gas. Right figure: Propane as gas. Straight lines drawn by linear regression. Plotting of scatter values are somewhat reduced to achieve readability.

The results from within each module form nicely grouped plots, which give an overall impression to fit an approximately linear correlation. All three modules show very similar behaviour for both methane and propane, with the CMR modules having slightly steeper linear approximations.

The observations may lead to the somewhat vague conclusion that there exists an approximate, linear relation between explosion pressure and impulse. The actual, individual pressure-time histories are left unpresented, but if we make the assumption that gas explosions in general have a triangular "shape", the observed results *should* lead to the above conclusion. The observation of a linear fit therefore seems explainable.

The linear regression takes the form $y = ax + b$, where x is the explosion pressure and y is the explosion impulse. a and b are constants with appropriate denominations. For the values plotted in figure 5.6, i.e. modules filled completely with gas, we find the constants a and b to be as presented in table 5.1.

The numbers for the a and b constants have obvious limitations. An extrapolation of the lines outside the observed intervals is likely to produce dubious results. A logarithmic fit may produce more reliable values for low pressures, but is not investigated here.

Table 5.1: Constants a and b in the linear regression of the values plotted in figure 5.6.

	Methane		Propane	
	a	b	a	b
Piper Alpha C	3.1	7.6	2.1	11.5
CMR M24	4.5	7.2	3.4	10.2
CMR M25	5.0	4.7	4.3	6.6
Mean	4.2	6.5	3.2	9.4

5.5 Pressure and impulse versus duration

The effect of the duration of the positive phase of the explosion on maximum overpressure and explosion impulse would be interesting to know.

We denote the time from "effective" pressure start, i.e. the time when $p = p_{\max} \cdot 0.05$ to the time when the pressure again reaches zero value, as the duration t_1.

Figure 5.7 shows how the relation between duration and pressure, respectively impulse can be visualised.

Figure 5.8 shows the pressure as a function of duration, $p = p(t_1)$, for increasing methane gas volumes in the Piper Alpha C Module.

The modules show a very similar behaviour; a decreasing magnitude of the parameter in question (pressure or impulse) when increasing the duration of the positive explosion phase. This seems reasonable for the maximum pressure. Given the gas volume, a long duration will a) let the unburnt gas escape away from the module and b) tend to equalise the latent energy over a longer period of time. Both effects will reduce the maximum overpressure.

With respect to the impulse, the conclusion is less well defined. The plots show a more varied relation. However, the overall tendency is larger impulse for shorter duration. This can be explained by flammable gas escaping the module.

For the pressure, the relation seems to be an inverse one. For the impulse the tendency is less clear.

As a special case we notice the CMR M24 module completely filled with propane. The result is shown in figure 5.9. This module has a horizontal grating deck, diving the module into two "storeys". The deck is provided with some holes for pipes and ladders.

The splitting of the observations into two separate "clouds", both of the same shape, can only be explained by the location of the ignition source being either on the upside or downside of the grating deck. The overall impression is nevertheless an inverse relation. However, the physical reason for this "splitted" behaviour is left unanswered.

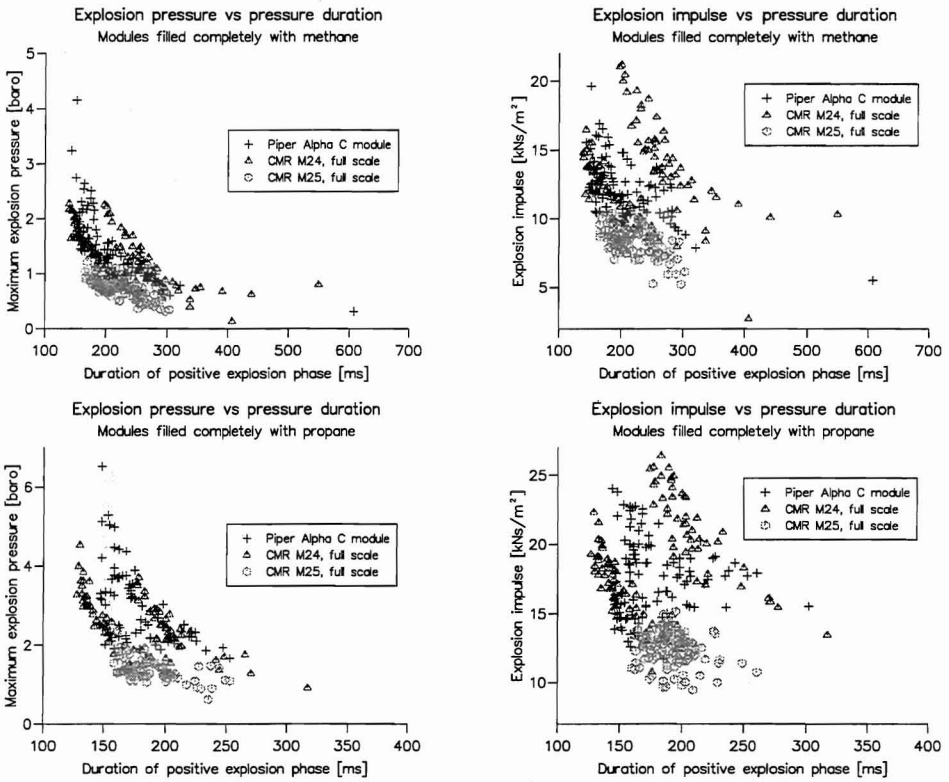

Figure 5.7: Pressure and impulse as function of explosion duration for all modules. Modules filled completely with gas. Upper row: Methane as gas. Lower row: Propane as gas. Left column: Explosion pressure. Right column: Explosion impulse. Plotting of scatter values are somewhat reduced to achieve readability.

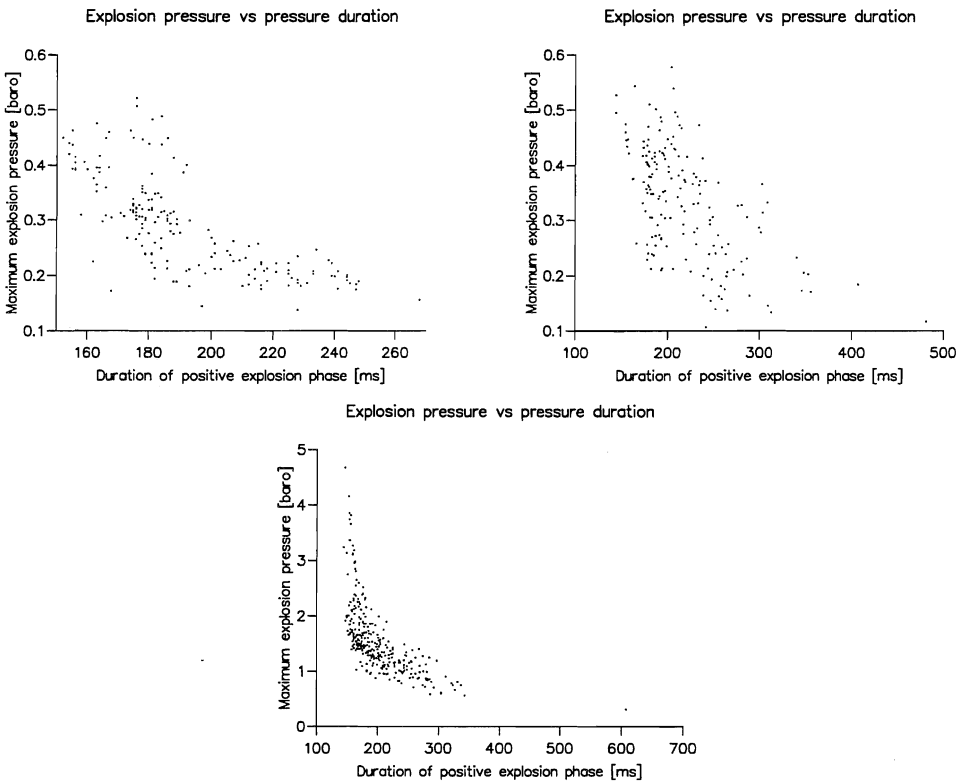

Figure 5.8: Pressure as function of explosion duration. Piper Alpha C Module with methane as gas. Upper, left: low, quart module filled. Upper, right: lower half module filled. Bottom: whole module filled.

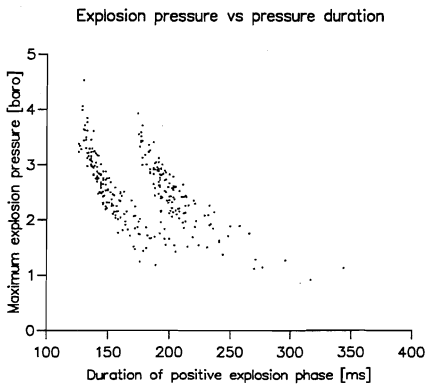

Figure 5.9: Pressure as function of explosion duration. CMR M24 module completely filled with propane.

5.6 Probability of "short" duration

As cited in section 5.2, literature differs with respect to when the impulse is of importance. Clough and Penzien [52] write:

> For short-duration loads, for example, $t_1/T < 1/4$, the maximum displacement amplitude v_{max} depends principally upon the magnitude of the applied impulse $I = \int_0^{t_1} p(t)\,dt$ and is not strongly influenced by the form of the loading impulse.

The t_1 denotes the duration of the positive phase of the explosion pressure, while T is the natural period of the structure.

The volume "Blast Response Series" in the the Steel Construction Institute's Blast and Fire Engineering Project [54] summarises the findings with respect to important factors to be considered when idealising a blast load. The volume denotes the nature of the blast load as *impulsive* when $t_1/T < 0.4$. In this category, preserving of the exact peak value is not critical. Furthermore, preserving the exact load duration is not critical either, but an accurate representation of the impulse is important.

The volume also gives a table for the natural periods of some structural components, as referred in table 5.2.

In the simulated cases, the duration of the positive phase of the explosion can be singled out. The results are given in table 5.3.

The positive phase is taken to start when the pressure reaches 5% of the maximum pressure. This allows some laminar combustion before the explosion escalates. The choice of value was based on visual inspection of numerous explosions.

Table 5.2: Some components with their natural periods for the first mode of vibration [54].

Structural component	Natural period
Stiffened floorplate	15 – 25 ms
Unstiffened floorplate	25 – 35 ms
Vertical stiffeners/columns (pinned)	50 s
Vertical stiffeners/columns (clamped)	$\approx$ 30 ms
Plate panel	50 – 100 ms
Whole wall	$\approx$ 50 ms

Table 5.3: Duration of the positive phase of the explosion pulse in simulated cases [ms]

		Methane			Propane		
	Filling	quantile			quantile		
Module	grade	10%	50%	90%	10%	50%	90%
PA	1/4	164	186	234	162	193	227
	1/2	174	204	286	137	157	237
	1/1	157	188	262	149	167	215
M24	1/4	161	192	244	155	179	229
	1/2	181	229	340	169	202	252
	1/1	153	224	307	136	176	215
M25	1/4	152	200	289	147	184	241
	1/2	183	231	282	175	207	250
	1/1	184	215	270	166	187	219

The positive phase is taken to end when the explosion pressure drops to zero. Negative and positive pressure oscillations after this point are neglected.

From the previous subsections, it is obvious that most of the simulated cases does not fall into the category of "short" duration for typical offshore structures. The exception are plate panels. If we base our discussion on the 50% quantile of the duration, we see that plate panels in some cases will have a t_1/T ratio approximately in the interval 50/350–100/150, i.e. $\frac{t_1}{T} \in [0.14, 0.67]$. Some of these values are larger than the limits given by both Clough and Penzien and the Steel Construction Institute.

This result may argue for taking the impulse load into account when designing "large" offshore structures, with a natural period larger than 50–100 ms, such as plate panels.

The duration of the positive explosion phase seems independent of gas filling grade.

Table 5.4: Loading rate in simulated cases
[bar/s]

Module	Filling grade	Methane quantile 50%	Methane quantile 90%	Propane quantile 50%	Propane quantile 90%
PA	1/4	3.20	6.74	4.54	8.76
	1/2	3.32	5.89	13.22	25.25
	1/1	17.16	39.78	44.30	90.11
M24	1/4	2.36	3.64	3.86	6.60
	1/2	2.67	5.02	5.25	8.51
	1/1	9.22	21.64	28.69	51.58
M25	1/4	1.42	1.60	2.36	2.66
	1/2	2.04	2.35	3.47	4.08
	1/1	5.25	5.61	11.15	11.71

5.7 Loading rate

The rate of loading can in some cases be of importance to the structure. This applies if the duration of the positive impulse is "long". Clough and Penzien [52] write:

> For long-duration loadings, for example $t_1/T > 1$, the dynamic magnification factor depends principally on the rate of the load to its maximum value. A steep loading of sufficient duration produces a magnification factor of 2; a very gradual increase causes a magnification factor of 1.

The volume "Blast Response Series" in the the Steel Construction Institute's Blast and Fire Engineering Project [54] summarises important factors to be considered when idealising a blast load. The blast load is denoted as *dynamic* in the interval $0.4 < t_1/T < 2.0$ and *quasi-static* for $t_1/T > 2.0$. For these cases, preserving the rise time is very important. Neglecting this fact can significantly affect the response.

For the simulations, the loading rate $\Delta p/\Delta t$ is presented in table 5.4 and the rise time $t_{ris} = t|_{p=p_{\max}} - t|_{p=p_{\max}\cdot 0.05}$ is presented in table 5.5.

The start of the explosion pulse follows the convention defined in section 5.6.

Conclusions that can be made from the observations of loading rate are:

1. The loading rate increases with gas volume. We have earlier argued for the whole offshore module being filled with gas as the design case. If this recommendation is acknowledged, the loading rate will be in the higher range.

2. The loading rate increases with geometry complexity. This observation is done with knowledge of the internal layout of the modules. The Piper Alpha C module com-

Table 5.5: Rise time in simulated cases [ms]

Module	Filling grade	Methane quantile 10%	Methane quantile 50%	Methane quantile 90%	Propane quantile 10%	Propane quantile 50%	Propane quantile 90%
PA	1/4	56	88	123	53	76	110
	1/2	61	105	157	62	79	120
	1/1	56	82	144	44	60	100
M24	1/4	74	103	149	77	100	130
	1/2	85	121	170	91	120	178
	1/1	90	133	192	62	88	126
M25	1/4	79	121	199	73	109	156
	1/2	81	130	178	81	122	167
	1/1	101	135	184	93	116	147

puter model contains far more piping than the CMR modules. This can also be argued from a physical point of view. The more obstructions encountered by the gas flow, the more turbulence is produced and faster combustion is achieved. The simulations confirm this physical argument.

3. The loading rate increases with gas reactivity. Propane has a higher reactivity than methane, and the table reflects this fact.

Conclusions that can be made from the observations of rise time are:

1. The rise time seems almost independent of gas volume. The maximum overpressure arrives at approximately the same time for all gas volumes.

2. The rise time can seem to decrease with geometry complexity. The Piper Alpha and CMR M24 modules have the most numerous set of obstructions—small, but turbulence-generating—while the CMR M25 module have more longish obstructions, following the direction of the combustion, and thus producing less turbulence. On the other hand, the CMR M25 module is divided horizontally into two subvolumes by means of an internal deck with some openings. This may delay the ignition of the gas volume on the other side of the deck with respect to the ignition source. Both these explanations may be valid for the rise time values, and with that the loading rate.

5.8 Pressure-time shape function

Looking for ways to present the simulated data and search for different correlations, several interesting discoveries emerge from the background material.

An interesting feature is whether the *shape* of the pressure-time function will have an influence on the resulting maximum overpressure.

Let us disregard the pressure-time history before the pressure starts to gain some magnitude. If we define $t = 0$ when $p = p_{\max} \cdot 0.05$, i.e. about the time when the pressure starts to rise significantly, t_{ris}, the rising time, will be the value when the maximum pressure arrives. The duration of the positive phase, i.e. the time from $t = 0$ to the time when the pressure again reaches zero pressure, is denoted t_1. The ratio t_{ris}/t_1 will then describe the shape of the pressure-time function.

If we approximate the pressure-time function to be triangular-shaped, $t_{\text{ris}}/t_1 \gtrapprox 0$ will denote a steep loading curve, $t_{\text{ris}}/t_1 \approx 0.5$ will describe an isosceles triangle while $t_{\text{ris}}/t_1 \lessapprox 1$ is a slow loading rate followed by an almost immediate decrease to zero explosion pressure.

An example of maximum explosion pressure as a function of the ratio t_{ris}/t_1 is shown in figure 5.10. The example shows the results from 400 simulations of the Piper Alpha C Module, lower half module filled with methane. The ignition point location is varied.

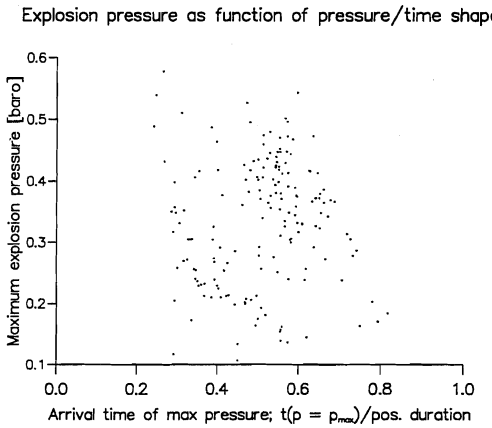

Figure 5.10: Maximum explosion pressure as function of pressure-time shape. Simulated results from the Piper Alpha C Module, lower half module filled with methane.

Other simulations show the same pattern. The conclusion must be that there seems to be no evident relation between the shape of the loading function and maximum explosion

Table 5.6: Quantiles in the distributions of pressure-time shape by means of the ratio t_{ris}/t_1. All modules completely filled with gas. Quantiles from sets of 400 simulations.

	Methane			Propane		
	quantile			quantile		
Module	10%	50%	90%	10%	50%	90%
Piper Alpha C	0.34	0.45	0.60	0.27	0.36	0.48
CMR M24	0.50	0.60	0.69	0.43	0.51	0.62
CMR M25	0.52	0.63	0.73	0.53	0.62	0.70

pressure. Both small and large explosion values can be accompanied by either abrupt or slow explosion loading rates.

However, a visual inspection of figure 5.10 shows that the often assumed triangular shape of a gas explosion is supported for this case. A majority of the observations is placed in the interval $[0.35, 0.60]$, with a value of 0.5 as the triangular fit. For these explosions, an assumption of isisceles triangular shape will not be very wrong.

If we discard the information of the magnitude of the explosion and just observe the ratio t_{ris}/t_1, we can produce diagrams of the distribution of this ratio. These are shown in figure 5.11.

The distributions can also be tabulated to gain information of the quantiles within each distribution. This in done in table 5.6.

Observations that can be done are:

1. The top of an assumed triangular pressure-time pulse will arrive earlier for propane than for methane.

2. The top of an assumed triangular pressure-time pulse will arrive relatively earlier for congested modules.

3. An isosceles triangle seems to be an overall good estimate for methane, but this observation is less definite for propane.

A visual inspection of several pressure-time diagrams (not shown here) comfirms the overall impression of a triangular shape as a usable approximation. We have a loosely based opinion that a skewed sinusoidal shape would fit most of the simulated results.

5.9 The effect of louvres

The EXSIM simulation code allows input of louvres, i.e. panel surfaces with porosity. Some cases have been simulated both with and without louvres at the module longitudinal ends

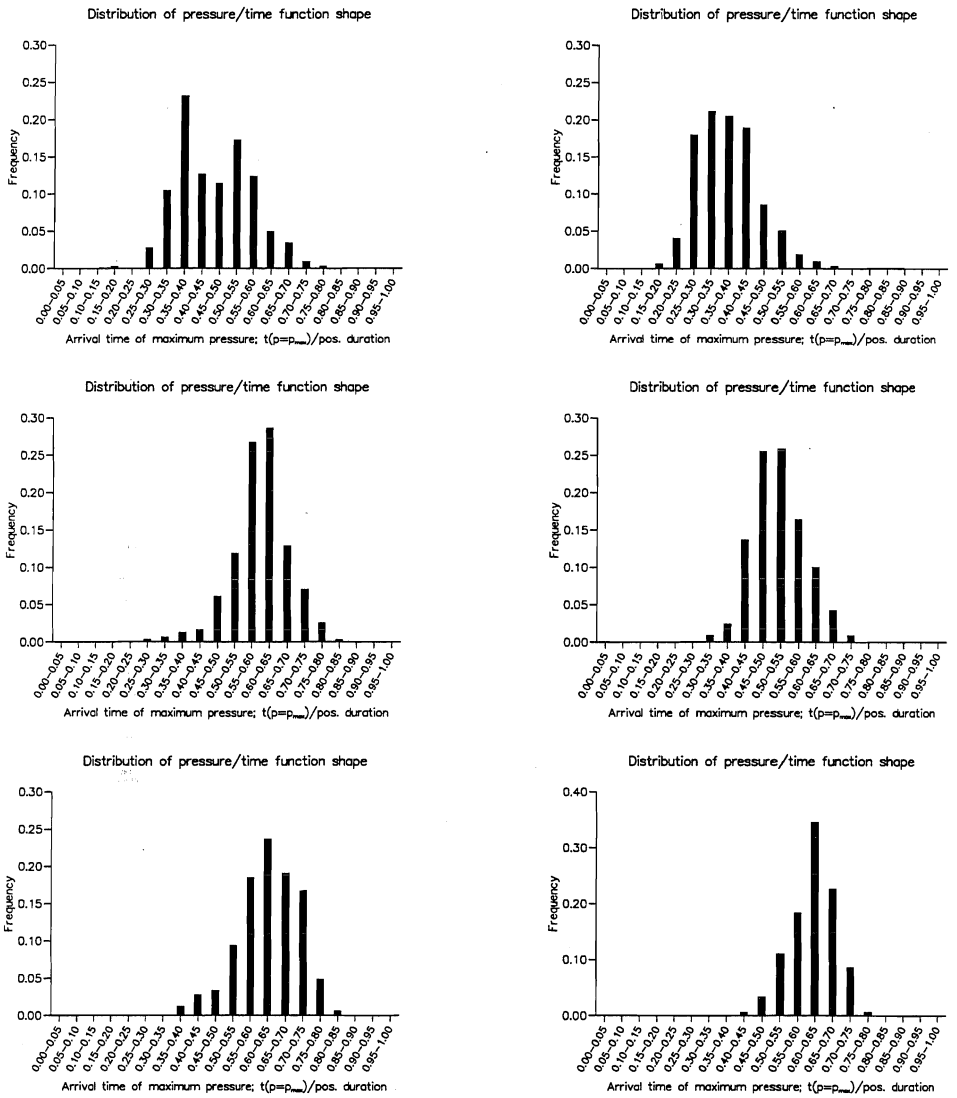

Figure 5.11: The distribution of pressure-time "shape" visualised by the ratio t_{ris}/t_1. Upper row: Piper Alpha C module. Middle row: CMR M24 module. Lower row: CMR M25 module. Left column: Methane as gas. Right column: Propane as gas. All modules filled completely. Each subfigure is based on 400 simulations.

Table 5.7: Explosion pressures for the CMR M25 module, full scale. Quantiles from sets of 400 simulations [baro].

Relative	Methane		Propane	
gas volume	w/o louvres	with louvres	w/o louvres	with louvres
50% quantile				
1/4	0.17	0.55	0.26	0.70
1/2	0.27	1.00	0.42	1.36
1/1	0.74	2.69	1.27	3.56
90% quantile				
1/4	0.23	0.66	0.32	0.85
1/2	0.34	1.14	0.52	1.55
1/1	0.92	3.05	1.71	4.21

Table 5.8: Explosion impulses for the CMR M25 module, full scale. Quantiles from sets of 400 simulations [kNs/m^2].

Relative	Methane		Propane	
gas volume	w/o louvres	with louvres	w/o louvres	with louvres
50% quantile				
1/4	1.75	21.27	2.44	24.89
1/2	3.27	36.07	4.74	41.92
1/1	8.40	71.33	12.19	79.75
90% quantile				
1/4	2.03	24.54	2.86	29.35
1/2	3.84	39.83	5.58	47.51
1/1	9.56	78.09	13.91	86.26

to investigate the effect of such panels.

More specific, explosion simulations have been performed on the CMR M25 module (full scale) in it's original layout (without louvres) and with louvres at each end with a porosity of 0.5.

Values for maximum pressure, explosion impulse, duration of positive phase and loading rate are presented in tables 5.7, 5.8, 5.9 and 5.10 respectively.

An introduction of louvres at the ends of an offshore module have clearly effects on a possible explosion. Both maximum explosion pressure, impulse and explosion duration increases in their respective magnitudes.

For this case, louvres with a porosity of 0.5, the increase in explosion pressure is a factor of 3–4 for methane and $\approx$ 3 for propane. More dramatic is the increase in impulse. We

Table 5.9: Explosion positive phase duration for the CMR M25 module, full scale. Quantiles from sets of 400 simulations [ms].

Relative	Methane		Propane	
gas volume	w/o louvres	with louvres	w/o louvres	with louvres
50% quantile				
1/4	200	807	184	705
1/2	231	639	207	531
1/1	215	470	187	390
90% quantile				
1/4	289	900	241	801
1/2	282	721	250	590
1/1	270	523	219	437

Table 5.10: Loading rate for explosion loads for the CMR M25 module, full scale. Quantiles from sets of 400 simulations [bar/s].

Relative	Methane		Propane	
gas volume	w/o louvres	with louvres	w/o louvres	with louvres
50% quantile				
1/4	1.42	2.07	2.36	3.09
1/2	2.04	3.68	3.47	5.74
1/1	5.25	12.95	11.15	31.83
90% quantile				
1/4	1.60	3.02	2.66	4.46
1/2	2.35	4.96	4.08	7.52
1/1	5.61	16.88	11.71	35.26

register a factor of 8–12 for methane and 6–10 for propane. There is no distinct difference in these factors for the means (50% quantiles) and the extremes (90% quantiles).

Noteworthy are also the increases in positive explosion phase durations. Originally quite "short", some explosions now tend to reach durations near 1 second. This will clearly place the dimensioning regime for structures in the module as "quasi-static", see section 5.7.

Under such conditions one must address the loading rate. We see from table 5.10 that the loading rate increases for the situation with louvres. The dynamic magnification factor as mentioned by Clough and Penzien [52] may, as a result, increase, and thus make the dimensioning circumstances worse.

Chapter 6

The effect of ignition point location

This chapter contains the results from over 7 000 simulations. For each simulation, the ignition point is located at a random place within the explosive cloud. This is done in order to look for probabilistic properties in the distribution of explosion pressure.

6.1 Presentation of data

The influence of the location of the ignition point is illustrated in figures 6.1 and 6.2. Each of the sub-figures are constructed from a sampling of 150 specimens from a set of 400 simulations.

As can be seen from the figures, the maximum explosion overpressure varies with a factor of approximately 4 (all modules, propane) to 20 (CMR M24, methane) within the modules due to ignition point location. The impulse varies with a factor of approximately 2 (all modules, propane) to 10 (CMR M24, methane). Thus the impulse varies less than explosion pressure.

Figures of observed distributions of cases with 1/4 and 1/2 filling grade are not provided, but show similar behaviour.

6.2 Probabilistic properties

As for other loads, e.g. snow and wind, finding some universal *distribution function* for the pressures presented in figures 6.1 and 6.2it would be convenient. With access to probabilistic parameters for explosions, we could estimate, as an example, the 90% quantile in any explosion process, i.e. the value that 90% of all explosion pressures (or impulses) would be less than.

With access to the probabilities of an explosion occurring and its magnitude, we could provide numbers for *the return period of a characteristic explosion*, the characteristic explosion being our choice of quantile.

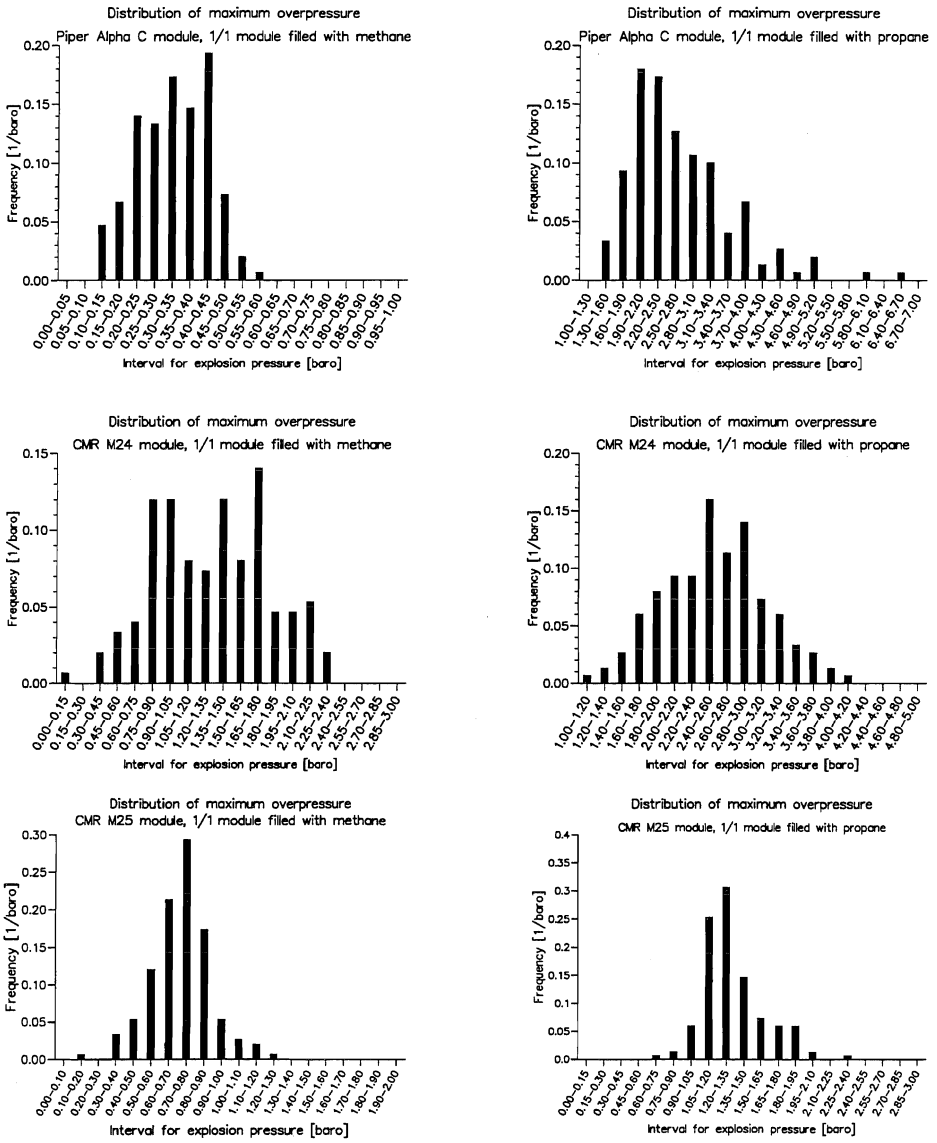

Figure 6.1: The effect on explosion pressure when varying ignition point location. Upper row: Piper Alpha C module. Middle row: CMR M24 module. Lower row: CMR M25 module. Left column: Methane as gas. Right column: Propane as gas. All modules filled completely.

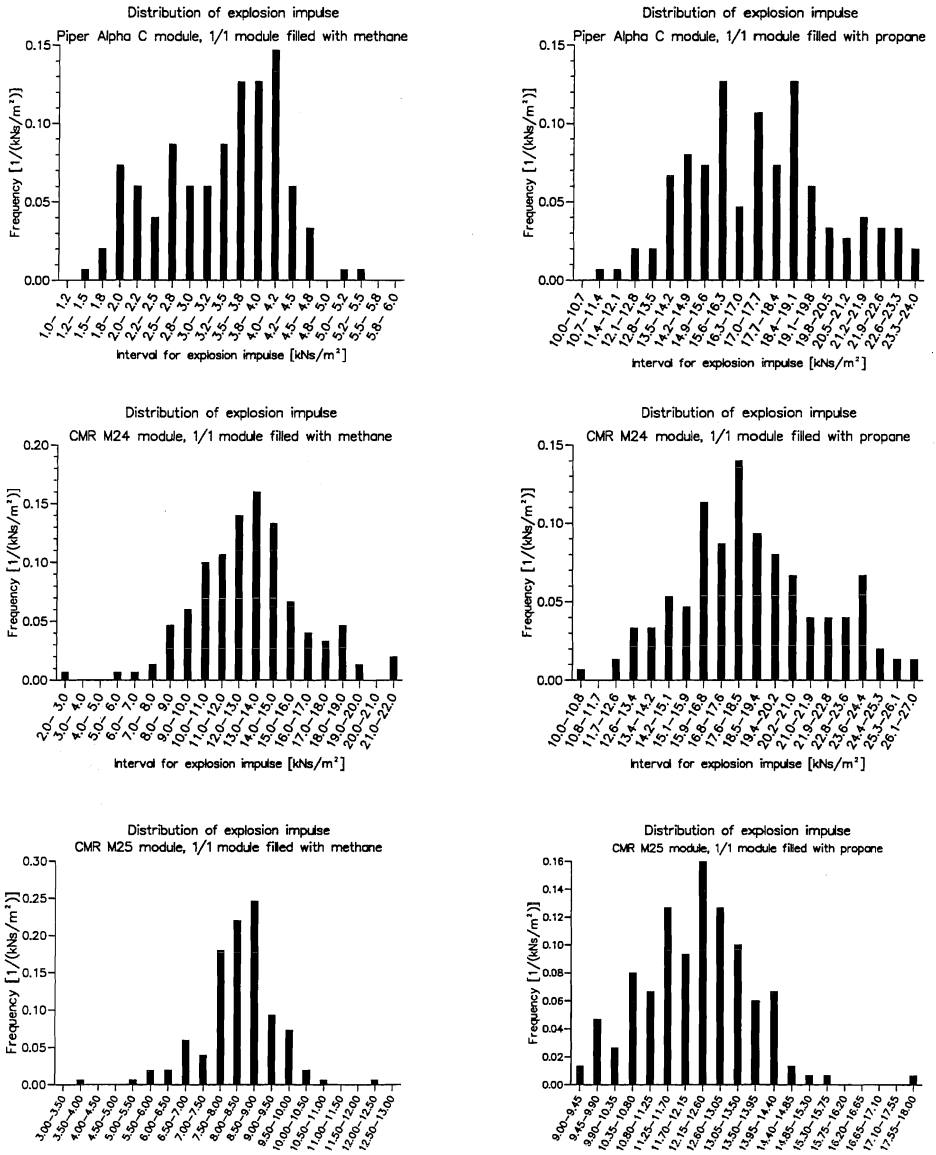

Figure 6.2: The effect on explosion impulse when varying ignition point location. Upper row: Piper Alpha C module. Middle row: CMR M24 module. Lower row: CMR M25 module. Left column: Methane as gas. Right column: Propane as gas. All modules filled completely.

In order to provide probabilistic data for this approach, we must find one or several distribution functions for the presented data. This can be done by tests. Procedures to test versus several distributions can be found in statistical textbooks, e.g. Ang and Tang [27, 30].

The choice of test are based on previous experience. Earlier probabilistic behaviour discovered in load statistics is described in section 3.2.2. Here, explosion data is tested versus normal, lognormal, Gumbel type I and Gumbel type II distributions.

6.3 Testing of data versus normal and lognormal distributions

6.3.1 General

The test of explosion loads versus normal distribution are mostly done as a reference, since variable loads rarely will show up with a such distribution, see section 3.2.2. The possibility of explosion loads taking the form of a lognormal distribution, however, must be considered.

The theory of normal and lognormal distributions are covered in several statistical handbooks, e.g. Ang and Tang [27] and Dougherty [55].

6.3.2 Discussion

Data sets like those shown in figures 6.1 and 6.2 are tested. All in all we have 3 modules with 3 filling grades of 2 gas types. The test are performed for both explosion pressure and impulse. That makes a total of 36 test cases. The test figures are shown in appendix A.

Explosion pressure

Explosion pressure versus normal distribution. The diagrams with probability test plots for explosion pressure versus normal distribution are given in figures A.1, A.5 and A.9. Surprisingly, it must be said, some of these show great concurrence, particularly the CMR M24 module plots. The CMR M25 module plots also show very closeness to the normal distribution, but the Piper Alpha C module must be said to differ. For the Piper Alpha C module, the results from the module filled completely with gas are especially non-confirming in the extreme values. The normal distribution can not be said to apply to maximum explosion pressure in general.

Explosion pressure versus lognormal distribution The diagrams with probability test plots for explosion pressure versus lognormal distribution are given in figures A.2, A.6 and A.10. Just the results from the Piper Alpha C module completely filled with

methane and some of the results from the CMR M25 module can be said to coincide with the lognormal distribution. Clearly the maximum explosion pressure does not fall into the category of lognormal distributions.

Explosion impulse

Explosion impulse versus normal distribution The diagrams with probability test plots for explosion impulse versus normal distribution are given in figures A.13, A.17 and A.21. Many of these plots show great correspondence with the normal distribution. The plots that differ most in the diagrams are CMR M25, lower $\frac{1}{2}$ module filled with methane (fig. A.21), and Piper Alpha C module, low $\frac{1}{4}$ module filled with propane (fig. A.13). The data in the other diagrams must be said to fit relatively well into the normal distribution in some way.

All degrees of gas filling taken into account, the observed values for impulse are in the range $1-25$ kNs/m^2. A direct comparison of the results are therefore of little value, but the observed coefficient of variation, V, may help in the estimation of future impulse values. The calculated results are shown in table 6.1 without any further discussion.

Table 6.1: Observed mean and standard deviation together with calculated coefficient of variation, $V = s/\bar{x}$ for explosion impulse.

		Methane			Propane		
		$\bar{x}$	s	V	$\bar{x}$	s	V
Piper	1/4	2.62	0.61	0.23	3.32	0.79	0.24
Alpha	1/2	3.39	0.83	0.24	7.51	2.16	0.29
C module	1/1	12.29	2.12	0.17	17.76	2.62	0.15
CMR	1/4	2.57	0.47	0.18	3.89	0.65	0.17
M24	1/2	4.34	1.12	0.26	6.97	1.14	0.16
module	1/1	12.77	3.05	0.24	18.42	3.41	0.19
CMR	1/4	1.73	0.23	0.13	2.41	0.35	0.14
M25	1/2	3.29	0.54	0.16	4.76	0.61	0.13
module	1/1	8.46	1.06	0.12	12.12	1.25	0.10

Explosion impulse versus lognormal distribution The diagrams with probability test plots for explosion impulse versus normal distribution are given in figures A.14, A.18 and A.22. Having concluded that this parameter may fit into a normal distribution, it is no surprise that the explosion impulse does not seem to fit into a lognormal distribution.

6.4 Testing of data versus extremal statistics distributions

6.4.1 General

The theory of extremal statistics applies to all kind of loads where the extreme, i.e. "largest" or "smallest", values are the variables of interest. Such distributions and their associated parameters have special characteristics unique to the extreme values [30].

The probability distributions of extremes are derived from the distribution of the initial values. The value of interest, e.g. snow load on roofs, are recorded over some reference period, typically one year. This will represent a continuous stochastic variable. The recording is sampled by n observations, denoted $x_i, i = 1, \ldots, n$. The value of these observations are called $X_i, i = 1, \ldots, n$. The value of interest for the extreme statistics is the maximum of these X_i, i.e.

$$Y_n = \max\{X_1, X_2, \ldots, X_n\} \tag{6.1}$$

Several sets of X_i will form a set of observations $y_i, i = 1, \ldots, n$ with values Y_n, and Y_n itself can be regarded as a stochastic variable. The distribution functions $F_{Y_n}(y)$ and $f_{Y_n}(y)$ are functions of the distribution function of X and the number of observations n, i.e. how many extremal values that are available.

The distribution of Y_n is generally difficult to obtain in analytic form [30]. However, as n, the number of extremal values available, approaches infinity, $F_{Y_n}(y)$ and $f_{Y_n}(y)$ may converge to an asymptotic form [47]. This is known as the *asymptotic theory of statistical extremes.*

Gumbel [29] classified the possible asymptotes into three forms:

1. Type I: The double exponential form
2. Type II: The exponential form
3. Type III: The exponential form with upper bound ω

The Type I form is associated with an initial variate distribution with an exponentially decaying tail, while the Type II form appears when the initial variate has a distribution with a polynomial decaying tail. If the extreme value of the initial variate is limited, i.e. has an upper bound, the distribution may asymptotically approach the Type III form.

Ang and Tang [30] describe the convergence criteria for the three types of Gumbel distributions. The criteria are based on the *hazard function* $h(t) = f(t)/(1 - F(t))$. The hazard function describes the conditional probability of failure in the time interval $(t, t + dt)$, given no failure in the time interval $(0, t)$. For the largest value, the hazard function

of X may be defined as [30]

$$h_n(x) = \frac{f_X(x)}{1 - F_X(x)} \tag{6.2}$$

6.4.2 Application of statistics of extremes to explosions

Specifically for the case of explosion loads, the Type III distribution as described in section 6.4.1 is not applicable. There is no obvious physical limit for the maximum explosion pressure or explosion impulse. Furthermore, convergence criteria based on the hazard function as described in equation 6.2 are difficult to apply on the explosion cases as viewed in this context. In this thesis, the explosion parameters are analysed given that an explosion occurs, while the hazard function necessarily will involve the probability of an explosion occurring. The latter is beyond the scope of this thesis. The procedure to achieve the probability of an explosion occurring is described in risk assessment literature, e.g. by Kortner et al [56].

For this reason, a hypothesis of convergence of explosion pressure and impulse distributions to an asymptotic Gumbel form is difficult to approve or discard. However, it is possible to test the explosion pressure and impulse distributions versus the different Gumbel distributions by means of extremal probability papers.

6.4.3 Extremal probability papers

The Gumbel Type I distribution

The Gumbel Type I distribution is given by it's cumulative distribution function [30]

$$F_{X_n}(x) = e^{-e^{-\alpha_n(x-u_n)}} \tag{6.3}$$

and the probability density function

$$f_{X_n}(x) = \alpha_n e^{-\alpha_n(x-u_n)} e^{-e^{-\alpha_n(x-u_n)}} \tag{6.4}$$

where

u_n is the *characteristic largest value* of the initial variate X

α_n is an inverse measure of dispersion of X_n

The characteristic largest value u_n is defined by

$$n(1 - F_X(u_n)) = 1.0$$

or

$$F_X(u_n) = 1 - \frac{1}{n} \tag{6.5}$$

Let X_n be a rewriting of Y_n in equation 6.1, i.e. the extreme values of n samples. We introduce a *standarised extremal variate*

$$S = \alpha_n(X_n - u_n) \tag{6.6}$$

Introducing equation 6.6 into equation 6.3 yields

$$F_S(s) = e^{-e^{-s}} \tag{6.7}$$

The N largest values from a population of the (assumably) Type I distribution are plotted on an extremal probability paper such that the mth value in increasing order is plotted at the probability $m/(N+1)$. The plotting order is discussed by Gumbel [27, 28]. Thus, if we want to use the standard variate S as abscissa value, we get

$$\begin{aligned} \frac{m}{N+1} = F_S(s) = e^{-e^{-s}} &= e^{-e^{-\alpha_n(x-u_n)}} \\ \ln\left(\frac{m}{N+1}\right) &= -e^{-\alpha_n(x-u_n)} \\ \ln\left(-\ln\left(\frac{m}{N+1}\right)\right) &= -\alpha_n(x-u_n) \\ x &= u_n - \frac{\ln\left(-\ln\left(\frac{m}{N+1}\right)\right)}{\alpha_n} \end{aligned} \tag{6.8}$$

or

$$S = -\ln\left(-\ln\left(\frac{m}{N+1}\right)\right) \tag{6.9}$$

Observation pairs are plotted as (S, X_n) on the *Gumbel Type I probability paper.*

If these observations form a line in the paper, the distribution can be assumed to be of Gumbel Type I extreme distribution.

The straight line can be constructed either by eye, by the *method of moments* (MoM) or by the *order statistics estimators* proposed by Lieblein [31]. The latter two are used in this thesis.

The straight line calculated by MoM is based on the equations for the population moments:

$$\mu_{X_n} = u_n + \gamma/\alpha_n \tag{6.10}$$

$$\sigma_{X_n} = \frac{\pi}{\sqrt{6}\,\alpha_n} \tag{6.11}$$

If we replace the population moments with the sample moments, $\mu_{X_n} \rightarrow \bar{x}_n$ and $\sigma_{X_n} \rightarrow s_{X_n}$, we get:

$$\hat{u}_n = \bar{x}_n - \frac{\sqrt{6}}{\pi}\gamma s_{X_n} \tag{6.12}$$

$$\hat{\alpha}_n = \frac{\pi}{\sqrt{6}\, s_{X_n}} \tag{6.13}$$

and the plotting is done by the formula

$$x = S/\hat{\alpha}_n + \hat{u}_n \tag{6.14}$$

The straight line calculated after Lieblein [31] is done by the estimators

$$\hat{u}_n = \sum_{i=1}^{n} a_i x_i \tag{6.15}$$

$$\frac{1}{\hat{\alpha}_n} = \sum_{i=1}^{n} b_i x_i \tag{6.16}$$

where a_i and b_i are weight factors given in appendix B. The procedure prescribed by Lieblein involves grouping the explosion data into groups of six entries and sorting the entries within each group in increasing magnitude. With several groups, the estimators are given by

$$\hat{u}_n = \frac{1}{k}\sum_{i=1}^{n_s} a_i \left(\sum_{j=1}^{k} x_{ij} \right) \tag{6.17}$$

$$\frac{1}{\hat{\alpha}_n} = \frac{1}{k}\sum_{i=1}^{n_s} b_i \left(\sum_{j=1}^{k} x_{ij} \right) \tag{6.18}$$

where $n_s = 6$, k the number of groups and the plotting is done according to equation 6.14.

The Gumbel Type II distribution

The Gumbel Type II distribution is given by it's cumulative distribution function [30]

$$F_{Y_n}(y) = e^{-(v_n/y)^k} \tag{6.19}$$

and the probability density function

$$f_{Y_n}(y) = \frac{k}{v_n}\left(\frac{v_n}{y}\right)^{k+1} e^{-(v_n/y)^k} \tag{6.20}$$

where
v_n is the characteristic largest value of the initial variate X
k is the shape parameter; $1/k$ is a measure of dispersion

The characteristic largest value v_n is defined by

$$F_X(v_n) = 1 - \frac{1}{n} \tag{6.21}$$

If Y_n has the Type II asymptotic distribution with positive parameters v_n and k, then $\ln Y_n$ has the Type I asymptotic distribution with parameters $u_n = \ln v_n$ and $\alpha_n = k$. Thus,

$$S = \alpha_n(X_n - u_n) = k(\ln Y_n - \ln v_n) = k \ln(Y_n/v_n) \tag{6.22}$$

The Type II distribution paper is equivalent to the Type I distribution paper, except that the Type II has a logarithmic (as opposed to linear) scale for the stochastic variable. The plotting position of the observations are given in equation 6.9.

We use the MoM and order statistics method as described for Type I to produce the value pairs $(0, X_{S=0})$ and $(1, X_{S=1})$, and derive an exponential function that goes through these points. The exponential function will form a straight line in the semilogarithmic diagram.

6.4.4 Discussion

Data sets like those shown in figures 6.1 and 6.2 are tested. All in all we have 3 modules with 3 filling grades of 2 gas types. The test are performed for both explosion pressure and impulse. That makes a total of 36 test cases. The test figures are shown in appendix A.

Explosion pressure

Explosion pressure versus Gumbel type I distribution. The diagrams with probability test plots for explosion pressure versus the Gumbel type I distribution are given in figures A.3, A.7 and A.12. The only diagrams that show some agreement between measured data and theoretical distribution behaviour are the Piper Alpha C module with gas in whole module, both methane and propane, and the CMR M24 module with lower half filled with methane. The other plots seem to differ to a large degree. The conclusion is that the Gumbel type I distribution in general fit poorly for explosion pressure.

Explosion pressure versus Gumbel type II distribution The diagrams with probability test plots for explosion pressure versus Gumbel type II distribution are given in figures A.4, A.8 and A.12. The Gumbel type II distribution does not fit the measured data at all. All simulations show large deviations for low and high data.

Explosion impulse

Explosion impulse versus Gumbel type I distribution The diagrams with probability test plots for explosion impulse versus Gumbel type I distribution are given in figures A.15, A.19 and A.23. A few of the sub-figures may be argued to fit to the Gumbel type I distribution, i.e. Piper Alpha, 1/1 module filled with methane and CMR M24 module, 1/1 and 1/2 module filled with methane, but in general there is more divergence than concurrence. The Gumbel type I distribution can not be said to represent the data material.

Explosion impulse versus Gumbel type II distribution The diagrams with probability test plots for explosion impulse versus Gumbel type II distribution are given in figures A.16, A.20 and A.24. As for explosion pressure, the tests reveal a rather appalling misfit. The Gumbel type II distribution can not be said to represent the simulated results.

6.5 Non-parametric statistics

6.5.1 General theory

When regarding statistical data with unknown distribution, such as the results from explosion simulators, non-parametric or order statistics may be used. Gibbons [57] has deduced the equations used in this thesis. This section contains a short summary.

We let $X_1, X_2, \ldots, X_n$ denote a random sample from a population, such as the maximum overpressures from explosion simulations when varying the ignition point location. The sample is sorted in increasing magnitude, in such a way that $X_{(1)} < X_{(2)} < \ldots < X_{(r)} < \ldots < X_{(s)} < \ldots < X_{(n)}$.

To estimate a confidence interval for a population quantile, κ_p, this can be done by calculating the probability that the quantile will lie between two observations in the sample,

$$P(X_{(r)} < \kappa_p < X_{(s)}) = 1 - \alpha \tag{6.23}$$

where $X_{(r)}$ and $X_{(s)}$ denotes two observations, $r < s$. $1-\alpha$ is the confidence level associated with the inequalities.

The probability is given in it's original notation by

$$P(X_{(r)} < \kappa_p < X_{(s)}) = \sum_{i=r}^{s-1} \binom{n}{i} p^i (1-p)^{n-i} \tag{6.24}$$

where p is the sought quantile level (e.g. 90% $\Rightarrow p = 0.90$), not to be misinterpreted as explosion pressure.

Henceforward we will denote Gibbons' κ_p (quantile in a population) as p_κ (pressure population quantile) in order to avoid misunderstandings regarding the use of the letter p. Also, I_κ will denote κ_p when discussing the impulse population quantile. Later we will derive a set of load factors γ with their corresponding distribution functions, and γ_κ is a quantile based on their sorted sets.

Gibbons suggests to choose r and s such that $s-r$ is a minimum for a fixed α. However, there is also the possibility to choose r and s such that the difference $X_s - X_r$ forms a minimum. Sometimes there will be several equal interval spans $s-r$ that satisfy the same confidence criterion, with no particular clues of which span is the one to favour.

The present calculations is based on the situation "first come", i.e. the first probability found by the computer that satisfies the given confidence criterion is used, not concerning which of the minimum criterion is achieved. This may produce some minor "jumps" in the tables presented, but they are expected to be of less importance.

Given the data in e.g. figure 6.1, the estimation of an explosion overpressure quantile p_κ can be done by using equation (6.24). The quantile will lie within a confidence interval, $p_\kappa \in [p_{\kappa,-l}, p_{\kappa,+l}]$, where l denotes the confidence level. It follows that one can be certain with (at least) the chosen confidence level that the actual quantile p_κ has a lower value than its upper confidence limit, $p_{\kappa,+l}$.

Here, the upper limit for the population quantile within a confidence level is taken to be the population quantile itself. Thus we will denote $p_{\kappa,+l}$ as p_κ. This is formally incorrect, but serves the purpose of this study. $I_{\kappa,+l}$ will likewise be denote as I_κ.

The confidence interval will be case-specific. With enough simulations, non-parametric statistics can always be used to achieve a certain quantile in the explosion pressure with a preferred confidence interval for a given case (i.e. geometry, gas type and cloud size). This is the desired procedure.

The samples presented here can be used to estimate their specific quantiles in the population. Furthermore, they can be used to derive several statistically interesting properties in further risk analysis.

6.5.2 Application of non-parametric statistics to explosion data

As explained, the derivation of such confidence intervals will depend on a certain amount of simulations for each given case. This can be costly and time-consuming, and motivates the search for a simpler and more general — but still statistically correct — method.

A situation may occur where the cost or time only allows a few, say 2, simulations of an explosion with arbitrary ignition points within a module. How can we use data from earlier simulations to obtain a sound statistical platform for the use of these two new simulations?

The situation is illustrated in figure 6.3. The problem is solved by extracting data from sets such as those given in figure 6.1. If we draw randomly 2 data points from a set of 150 observations (as is the case for the results presented in figure 6.1), and take the mean value of these 2, we will gain a set of $\binom{150}{2} = 11\,175$ mean values, denoted $\bar{x}_i, i = 1, \ldots, 11\,175$. The distance from this random mean $\bar{x}_i$ to the sought $p_{\kappa,+l}$ (e.g. the 90% quantile) is denoted d. This d will then be a stochastic variable with an unknown distribution.

The distance d, however, is of little practical value for the general case. It will vary in magnitude for each simulated module, and it's denomination, kPa, fits poorly if we want to provide a factorial approach, as the partial factor method described in section 3.3.3. The solution to generalisation of the problem can be to do some kind of normalisation of the distance. If we divide the distance d with the random mean $\bar{x}_i$, we will get a denomination-free factor that can be used in the reverse case. If we let

$$\gamma_{I,i} = (\bar{x}_i + d)/\bar{x}_i = p_{\kappa,+l}/\bar{x}_i \approx p_\kappa/\bar{x}_i \tag{6.25}$$

we can by picking two arbitrary simulations find a $\bar{x}$ and calculate the desired pressure quantile by multiplying with the γ factor, i.e. $p_\kappa = \bar{x}_i\gamma_I$. The assumption that must be done for this procedure is that the γ factor has a similar distribution for each case.

The problem turns out to be how to estimate γ_I. For two other simulations, we will get a new $\bar{x}_i$ and thus a new γ_I. For a set of 11 175 observations it is trivial to reproduce the distribution of γ_I. We simply let the computer calculate all possibilities. An example of a such calculation is illustrated in figure 6.4.

The distribution of γ is obviously dependent of the choice of acceptable pressure level. As can be seen from figure 6.3, the higher level of safety, by choosing a high pressure quantile, the higher the factor $\gamma_I = p_\kappa/\bar{x}_i$.

The distribution of γ_I in figure 6.4 is much smoother than the distributions of $p_{\max}$ in figure 6.1, and a test of γ_I versus various known distribution functions may well lead to a result. If we, however, continue our non-parametric treatment of the observed data, we can, after some computations, present a $\gamma_{I_{\kappa,+l}}$, i.e. an upper limit for a quantile for γ_I with a specific confidence level l in a set of $\gamma_{I,i}$. Although slightly incorrect, we will also here call this upper confidence limit of the population quantile for γ_{I_κ}. With a set of observations of order 10 000, the confidence interval will be relatively narrow.

The quantile κ_p (Gibbons' notation, see sec. 6.5) and confidence level l will generally be different for $p_{\max,i}$ or I_i, and their corresponding $\gamma_{I,i}$. As an example, we can decide that the 90% quantile of the explosion pressure presents an acceptable safety level. This quantile can be estimated with a confidence level of 95%. This value is a number on the pressure axis. Given this value, we can calculate a set of γ, and in turn decide that this factor can be represented by it's 90% quantile with 98% confidence.

The combinations of quantiles, confidence levels, gas types, gas filling and choice of module turn out to be numerous. For this reason, the presented data are limited to observe the 75, 90, 95 and 98% quantiles in the pressure and impulse distributions with

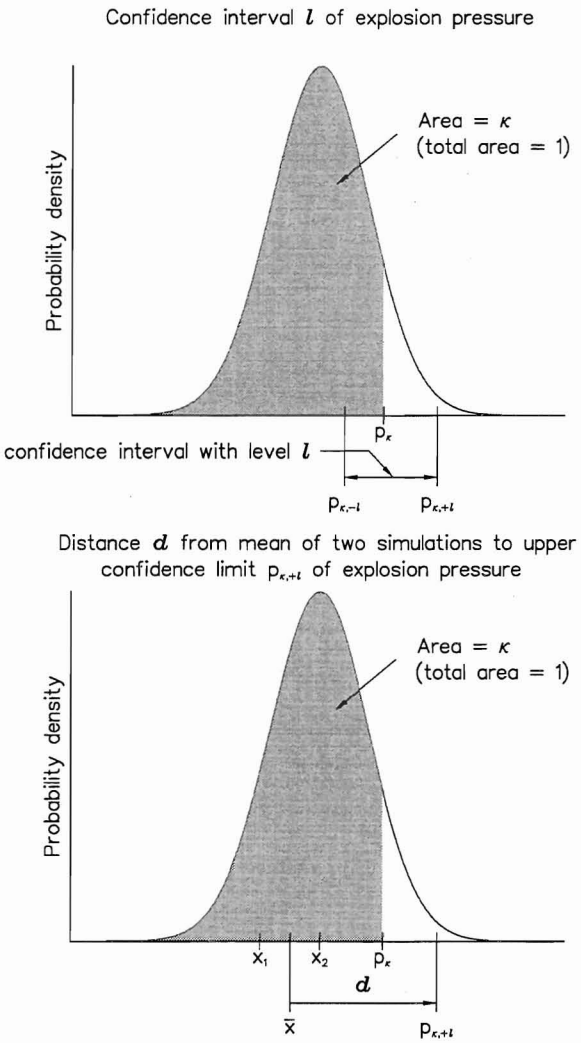

Figure 6.3: Calculating confidence level and ignition point location uncertainty factor $\gamma = (\bar{x} + d)/\bar{x} = p_{\kappa,+l}/\bar{x} \approx p_\kappa/\bar{x}$.

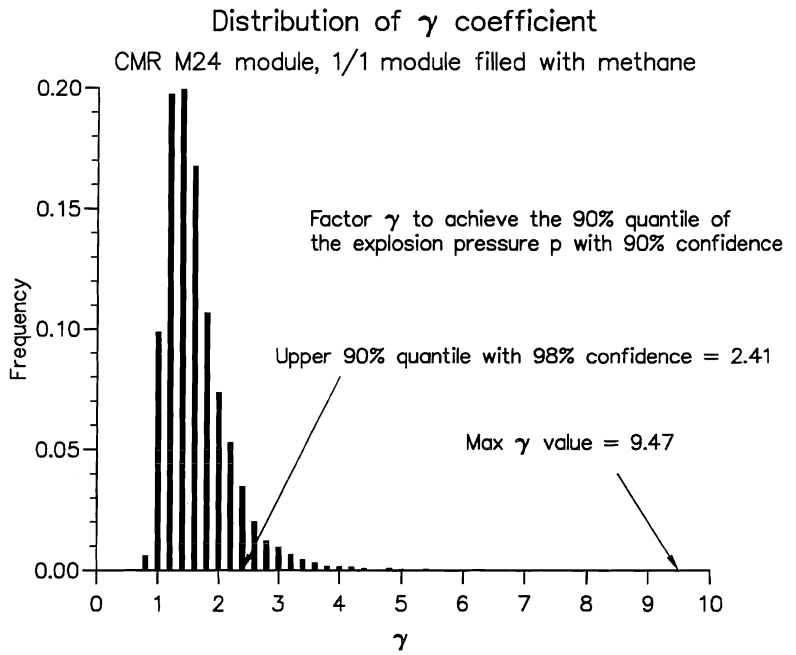

Figure 6.4: Distribution of $\gamma_I = p_\kappa/\bar{x}$, where p_κ is the explosion pressure quantile sought.

90% confidence and the 90% quantile of the factor γ with 98% confidence. The relevance of this choice for direct use in consequence analysis is unknown. Other combinations can be tabulated, but are not shown here.

More simulations than 2 can be done to get a value of $\bar{x}_i$. The number 2 was chosen to illustrate the procedure. A higher number of simulations will produce lower factors γ with less dispersion. The effect is documented in the following chapters.

6.5.3 Calculations of ignition point location uncertainty factors

Calculations to gain values for the ignition point location uncertainty factor are done for both pressure and impulse for all offshore modules and each filling grade. The calculations are done with basis in 2, 3 and 4 simulations.

The presented tables are organised by gas volume cloud. Within these categories, each module is presented with gas type, number of simulations and selected distribution quantiles as variables. Thus, we have a set of *ignition point location uncertainty factors* in

tables 6.2–6.10. The pressure and impulse quantile levels are calculated with 90% confidence. The γ factors are presented as the 90% quantile with 98% confidence to achieve the (in the tables) given pressure quantile with 90% confidence.

Table 6.2: Ignition point location uncertainty factor γ for Piper Alpha C module, 1/4 module filled with gas.

	Gas type					
	Methane			Propane		
	no. of simulations			no. of simulations		
Load type	2	3	4	2	3	4
75% quantile						
Pressure	1.71	1.66	1.60	1.91	1.83	1.76
Impulse	1.39	1.36	1.33	1.49	1.45	1.42
90% quantile						
Pressure	2.14	2.07	1.99	2.16	2.07	2.00
Impulse	1.84	1.79	1.76	1.90	1.86	1.81
95% quantile						
Pressure	2.36	2.28	2.20	2.37	2.28	2.19
Impulse	1.94	1.89	1.85	1.95	1.90	1.86
98% quantile						
Pressure	2.55	2.46	2.37	2.48	2.38	2.29
Impulse	2.01	1.96	1.92	2.13	2.08	2.03

Table 6.3: Ignition point location uncertainty factor γ for CMR M24 module, 1/4 module filled with gas.

	Gas type					
	Methane			Propane		
	no. of simulations			no. of simulations		
Load type	2	3	4	2	3	4
	75% quantile					
Pressure	1.47	1.43	1.39	1.41	1.39	1.36
Impulse	1.33	1.32	1.29	1.29	1.28	1.26
	90% quantile					
Pressure	1.62	1.58	1.53	1.53	1.51	1.48
Impulse	1.50	1.48	1.45	1.36	1.35	1.33
	95% quantile					
Pressure	1.76	1.71	1.67	1.65	1.63	1.60
Impulse	1.72	1.71	1.67	1.43	1.41	1.39
	98% quantile					
Pressure	1.86	1.80	1.76	1.72	1.71	1.67
Impulse	1.93	1.91	1.87	1.71	1.70	1.67

Table 6.4: Ignition point location uncertainty factor γ for CMR M25 module, 1/4 module filled with gas.

	Gas type					
	Methane			Propane		
	no. of simulations			no. of simulations		
Load type	2	3	4	2	3	4
	75% quantile					
Pressure	1.55	1.54	1.50	1.51	1.48	1.44
Impulse	1.27	1.25	1.23	1.30	1.30	1.28
	90% quantile					
Pressure	1.78	1.74	1.69	1.71	1.67	1.63
Impulse	1.36	1.34	1.32	1.40	1.40	1.38
	95% quantile					
Pressure	1.83	1.79	1.73	1.83	1.79	1.74
Impulse	1.45	1.43	1.41	1.47	1.47	1.44
	98% quantile					
Pressure	1.85	1.80	1.75	1.93	1.89	1.84
Impulse	1.66	1.63	1.61	1.58	1.58	1.54

Table 6.5: Ignition point location uncertainty factor γ for Piper Alpha C module, 1/2 module filled with gas.

	Gas type					
	Methane			Propane		
	no. of simulations			no. of simulations		
Load type	2	3	4	2	3	4
	75% quantile					
Pressure	1.78	1.70	1.63	2.50	2.21	2.08
Impulse	1.58	1.53	1.48	1.74	1.68	1.61
	90% quantile					
Pressure	1.99	1.89	1.82	2.92	2.58	2.42
Impulse	1.72	1.66	1.61	1.96	1.90	1.82
	95% quantile					
Pressure	2.11	2.01	1.93	3.70	3.28	3.08
Impulse	1.78	1.72	1.66	2.09	2.03	1.94
	98% quantile					
Pressure	2.28	2.17	2.10	4.03	3.56	3.35
Impulse	1.85	1.79	1.73	2.18	2.12	2.03

Table 6.6: Ignition point location uncertainty factor γ for CMR M24 module, 1/2 module filled with gas.

	Gas type					
	Methane			Propane		
	no. of simulations			no. of simulations		
Load type	2	3	4	2	3	4
	75% quantile					
Pressure	1.97	1.86	1.78	1.57	1.52	1.47
Impulse	1.49	1.44	1.40	1.31	1.29	1.27
	90% quantile					
Pressure	2.57	2.43	2.23	1.81	1.75	1.70
Impulse	1.77	1.71	1.66	1.43	1.41	1.38
	95% quantile					
Pressure	2.75	2.60	2.48	1.95	1.88	1.82
Impulse	1.82	1.75	1.70	1.45	1.42	1.39
	98% quantile					
Pressure	3.38	3.19	3.04	2.35	2.26	2.19
Impulse	2.12	2.04	1.99	1.50	1.47	1.44

Table 6.7: Ignition point location uncertainty factor γ for CMR M25 module, 1/2 module filled with gas.

	Gas type					
	Methane			Propane		
	no. of simulations			no. of simulations		
Load type	2	3	4	2	3	4
	75% quantile					
Pressure	1.54	1.52	1.47	1.36	1.36	1.34
Impulse	1.32	1.33	1.30	1.21	1.22	1.20
	90% quantile					
Pressure	1.71	1.69	1.64	1.52	1.53	1.50
Impulse	1.46	1.47	1.44	1.36	1.37	1.35
	95% quantile					
Pressure	1.84	1.82	1.76	1.70	1.70	1.67
Impulse	1.52	1.53	1.50	1.49	1.49	1.47
	98% quantile					
Pressure	1.99	1.97	1.90	1.88	1.89	1.86
Impulse	1.63	1.64	1.60	1.53	1.53	1.51

Table 6.8: Ignition point location uncertainty factor γ for Piper Alpha C module, 1/1 module filled with gas.

	Gas type					
	Methane			Propane		
	no. of simulations			no. of simulations		
Load type	2	3	4	2	3	4
	75% quantile					
Pressure	1.84	1.76	1.68	1.68	1.61	1.56
Impulse	1.64	1.59	1.54	1.32	1.30	1.27
	90% quantile					
Pressure	2.06	1.97	1.87	2.16	2.07	2.01
Impulse	1.78	1.72	1.66	1.50	1.48	1.45
	95% quantile					
Pressure	2.19	2.08	1.99	2.51	2.47	2.34
Impulse	1.89	1.83	1.77	1.56	1.54	1.51
	98% quantile					
Pressure	2.52	2.40	2.29	3.25	3.12	3.03
Impulse	2.16	2.09	2.02	1.60	1.57	1.54

Table 6.9: Ignition point location uncertainty factor γ for CMR M24 module, 1/1 module filled with gas.

	Gas type					
	Methane			Propane		
	no. of simulations			no. of simulations		
Load type	2	3	4	2	3	4
	75% quantile					
Pressure	2.00	1.90	1.81	1.49	1.45	1.41
Impulse	1.46	1.46	1.41	1.40	1.38	1.35
	90% quantile					
Pressure	2.41	2.29	2.18	1.75	1.70	1.66
Impulse	1.75	1.75	1.70	1.54	1.51	1.48
	95% quantile					
Pressure	2.51	2.38	2.26	1.80	1.75	1.70
Impulse	1.85	1.86	1.80	1.62	1.60	1.57
	98% quantile					
Pressure	2.57	2.44	2.32	2.00	1.95	1.90
Impulse	2.04	2.05	1.98	1.68	1.66	1.63

Table 6.10: Ignition point location uncertainty factor γ for CMR M25 module, 1/1 module filled with gas.

	Gas type					
	Methane			Propane		
	no. of simulations			no. of simulations		
Load type	2	3	4	2	3	4
	75% quantile					
Pressure	1.49	1.45	1.41	1.36	1.35	1.33
Impulse	1.25	1.26	1.24	1.22	1.22	1.21
	90% quantile					
Pressure	1.73	1.69	1.64	1.63	1.62	1.59
Impulse	1.33	1.34	1.32	1.30	1.30	1.28
	95% quantile					
Pressure	1.99	1.94	1.89	1.74	1.73	1.69
Impulse	1.45	1.46	1.43	1.35	1.35	1.33
	98% quantile					
Pressure	2.14	2.09	2.03	1.78	1.76	1.73
Impulse	1.66	1.67	1.64	1.41	1.41	1.39

The effect of all modules combined are presented in table 6.11. Assuming that the design case in many cases will be the whole module filled with gas, the mean of the γ factor for all 3 offshore modules completely filled with gas are shown.

Table 6.11: The mean of ignition point location uncertainty factor γ for all modules, modules completely filled with gas.

	Gas type					
	Methane			Propane		
	no. of simulations			no. of simulations		
Load type	2	3	4	2	3	4
	75% quantile					
Pressure	1.78	1.70	1.63	1.51	1.47	1.43
Impulse	1.45	1.44	1.40	1.31	1.30	1.28
	90% quantile					
Pressure	2.07	1.98	1.90	1.85	1.80	1.75
Impulse	1.62	1.60	1.56	1.45	1.43	1.40
	95% quantile					
Pressure	2.23	2.13	2.05	2.02	1.98	1.91
Impulse	1.73	1.72	1.67	1.51	1.50	1.47
	98% quantile					
Pressure	2.41	2.31	2.21	2.34	2.28	2.22
Impulse	1.95	1.94	1.88	1.56	1.55	1.52

6.5.4 Immediate observations

Given the factors presented in table 6.11 and those for the individual modules, some immediate results can be observed:

1. Deviations in explosion impulse is lower than for explosion pressure.
2. Deviations for propane are in general lower than for methane, i.e. the explosion propagation for methane is more dependent on the ignition point location than that for propane.
3. Relatively, there seems to be no evident effect of gas cloud volume.
4. By increasing the number of simulations from 2 to 4, we will get a reduction in the ignition point uncertainty load factor γ. For explosion pressure, this reduction is of order 8% for methane and 5% for propane. For explosion impulse, the reduction is approximately 4% for methane and 3% for propane.

5. The γ factor is very case-dependent with respect to quantile choice. For Piper Alpha, we get an increase in the γ factor of approximately 100% from the 75% to the 98% quantile in the distribution. For the CMR M25 module, we get an increase of approximately 15% in the same interval.

6.5.5 Discussion of properties of the ignition point location uncertainty load factor

The properties described in section 6.5.4 can be discussed as follows:

1. The observation that the explosion impulse is more "stable" than the maximum explosion pressure seems natural. While the pressure is a peak value, the impulse is an integrated value, and will thus tend to vary less than the pressure function. Thus, a lower ignition point uncertainty factor for impulse than for pressure seems sensible.

2. The observation that methane should be more sensitive to ignition point location than propane may be correct, or at least can be explained. Propane is a more reactive gas than methane, and may tend to produce higher overpressures no matter where the ignition point is located. Methane has a slower combustion rate than propane under undisturbed conditions, but if the ignition is in a very confined area, an early turbulence will occur and result in a quicker combustion rate. While the arrival of an early maximum pressure does not need to imply a high explosion value (see figure 5.10), this may be the case for a methane cloud ignited in a congested area.

3. The explosion pressure as a function of ignition point location being seemingly independent of the gas cloud size is just an observation. There are no evident explanations why it should be, or, for that matter, not be so. If of any worth, it may be taken as an argument for the γ factor being a property of a set of explosions, independent of gas cloud size.

4. The small difference in ignition point uncertainty factor with 2 and 4 simulations shows that even such small numbers provide a good estimate of the overall pressure or impulse level in the module. They do not provide information of the variations of the possible explosions, the deviation, but even 2 simulations give a good estimate of the mean value.

5. The γ factor seems to be case-dependent. However, the overall level of the γ factor seems to be well settled. For explosion pressure, the γ factor for the 90% quantile will for the three modules lie within the interval 1.3–2.9, $\gamma \in [1.3, 2.9]$ with an approximated mean of 1.7–1.8, i.e. a little under 2. For explosion impulse, the 90% quantile will for the three modules lie within the interval 1.2–1.9, $\gamma \in [1.2, 1.9]$, with an approximated mean about 1.5.

The effect of the relative gas cloud size is illustrated in an example in figure 6.5. The picture is typical. While there are some variations within each module, the tendency is that the γ factor *does* have an overall value for a given module.

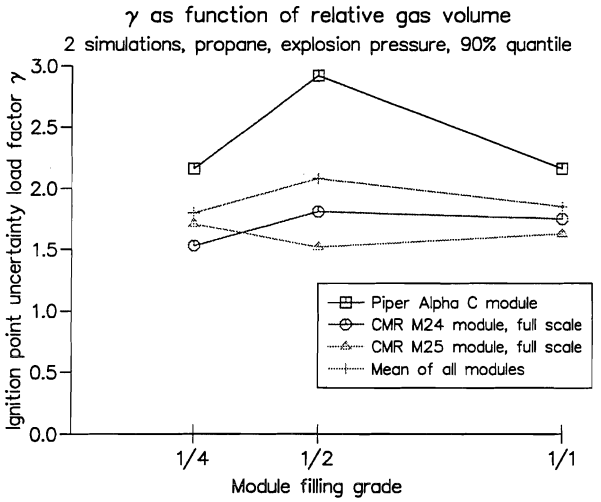

Figure 6.5: The ignition point location uncertainty factor γ as a function of module filling grade.

The influence of number of simulations on the γ factor is shown in figure 6.6. The figure is an example, and shows clearly the relative moderate effect an increase in number of simulations has on the γ factor.

Methane will in general produce larger or similar γ factors than propane. An example is shown in figure 6.7.

The ignition point location uncertainty factor γ will rely on the chosen pressure (and impulse) quantile. This effect is illustrated in figure 6.8.

6.5.6 Non-parametric statistics conclusions

Non-parametric statistics can, with large enough number of simulations, be used to calculate pressure quantiles that satisfy given safety levels in the design process. This must be the desired procedure in any planning phase of industrial processes involving explosive gases, both offshore and onshore.

However, the large number of simulations necessary to achieve such a safety level is inconvenient. This is tried solved by finding the distribution produced when picking 2,

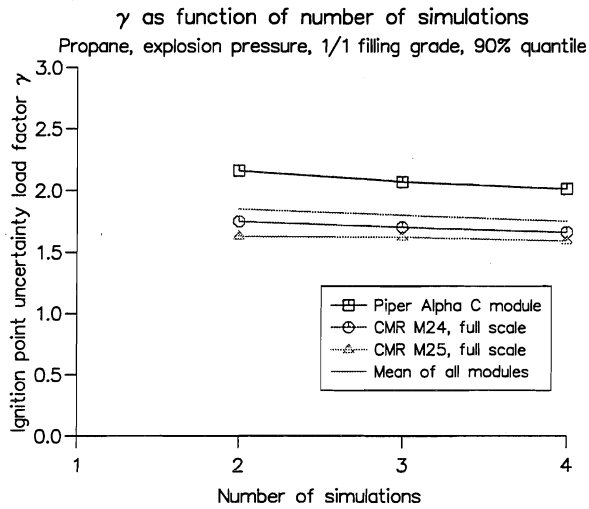

Figure 6.6: The ignition point location uncertainty factor γ as a function of number of simulations.

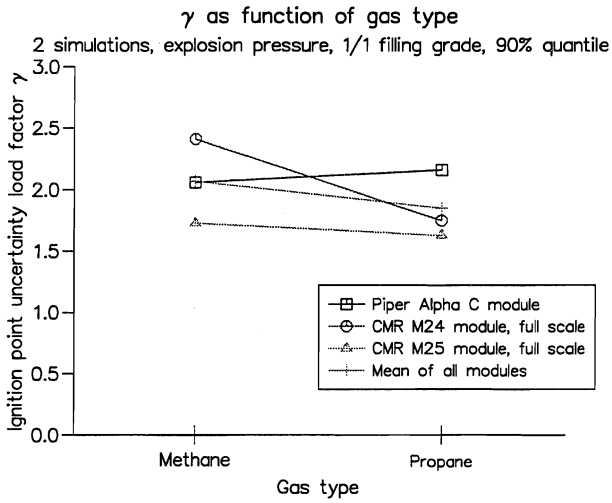

Figure 6.7: The ignition point location uncertainty factor γ as a function of gas type.

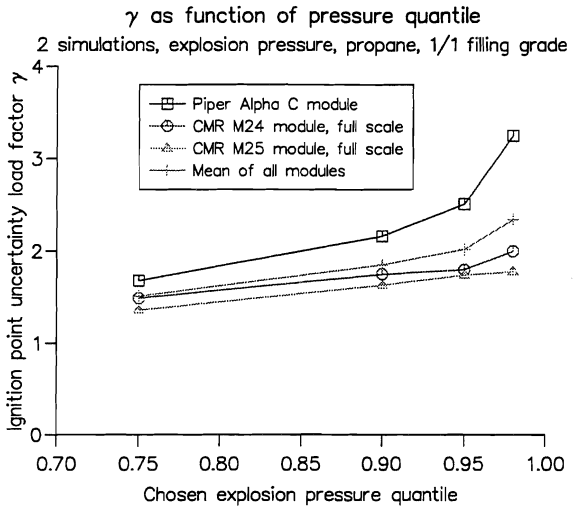

Figure 6.8: The ignition point location uncertainty factor γ as a function of chosen pressure quantile.

3 and 4 arbitrary simulations and let the mean of these enter as the denominator in a fraction where the known quantile represents the numerator. This will produce a *ignition point location uncertainty factor.*

The question of relevance of the ignition point uncertainty factor being a measurement of real dispersion of the effect of ignition point location remains. This will be discussed in chapter 8.

With these limitations, the non-parametric statistics approach is recommended, and—taken the presented data into view—the only general probabilistic method currently applicable to explosion loads.

6.6 Error sources in data treatment

At this point it may be necessary to remind the reader that the only subject discussed here is the ignition point location. Other sources to possible errors in the estimation process, such as explosion simulator behaviour and assumptions of initial turbulence field are kept out of the discussion.

In spite of narrowing down the error sources to the treatment of the ignition point location, there are still several sources that should be investigated.

6.6.1 Placement of ignition point

In the computer simulations, the ignition point is placed randomly within the flammable cloud. This is hardly the actual case. The ignition point location will presumably be connected to some obstruction surface. Possible ignition sources may be hot surfaces or electrical switches.

The procedure of picking randomly placed ignition points was done due to three main reasons.

1. The available data models were not accurate enough. Minor pipes and electrical cabling are not shown in the cited literature. Furthermore, an implementation of these are rarely done in the computer models due to the flow nature of the problem. Single, small pipes, although turbulence-generating to some degree, often have little influence on the total flow and turbulence pattern.

2. Lack of procedure for picking points close to surfaces. Although a such procedure can be established from the internal simulator representation of the obstacles, it would have been time-consuming. Judgment resulted in emphasis put on establishing a statistical method of data treatment.

3. The necessity of investigating close-to-surface ignitions in stead of arbitrary ignitions is unclear.

Given that an explosion occur in the vicinity of a surface, one might expect a boundary condition that produces turbulence when the gas flow passes along. The turbulence results in a higher combustion rate and thus quicker pressure loading rate. However, the influence of the loading rate on maximum explosion pressure seems vague, as illustrated in figure 5.10 on page 49. Furthermore, as explained earlier, *closeness* to a surface may not be a sufficient criterion. Just a closeness criterion may not produce significant early turbulence. The critical parameter is the *confinement* of the ignition source. A procedure describing confinement instead of closeness is hard to formalise.

The error produced by the chosen location procedure will presumably be a one-sided one, i.e. the simulated pressures (chosen in free air) will be higher or lower than similar values obtained from close-to-surface simulations.

The effect of choosing an arbitrary ignition point within the gas cloud, as opposed to the vicinity of a surface, remains unknown. If it exists, the resulting error will presumably be a constant, thus making the achieved factors being either too low or too high. The presented reasoning that the maximum explosion pressure seems relatively independent of the loading rate argues for that the possible error will be small.

6.6.2 Biased explosion simulator

There is a possibility of explosion simulators calculating certain ignition point locations with more or less accuracy than other points. We can e.g. imagine a simulator tackling the flow and combustion equations especially well for ignition in corners of a module.

There is no published data confirming or rejecting a such hypothesis as a general property of any explosion simulator. While a such behaviour may be present in single cases, a general trend have not be traced.

A biased explosion simulator will, if it exists, produce a constant error in the data, and thus influence the data either in safe or unsafe direction.

The lack of demonstrateable biased cases in literature does not prove the non-existence of such behaviour. Biasing in ignition point location is a matter of great importance, and must be viewed with great attention in the future.

6.6.3 Error in statistical values

Given the non-parametric statistics approach, the simulated results represent a *set* of observations, but the selected value $p_{\kappa,+l}$ represents the quantile in the *population*. Thus, the estimation of the explosion quantile should be robust and conservative, as the chosen value is taken to be the upper confidence limit.

In the postprocessing of the explosion data, the calculated mean $\bar{x}$ is done from the *set*, not the *population*, as the value is calculated from a subset of the already simulated data. This may introduce an error in the estimation of $\bar{x}$. The size of the set is 150 specimens, so the conclusion is that an approximation of $\bar{x}$ in the set to μ in the population can be done. The resulting error is arbitrary, and thus may lead to both higher and lower values. The magnitude of this error is unknown.

The ignition point uncertainty factor γ_I is deduced from a set of observations, but the resulting value taken to be the upper limit in the confidence interval of the population value. This estimation is also on the safe side.

6.6.4 Error summary

Thus, the statistical procedure from the raw data to the final γ_I contains two numerical roundings to the safe side and one approximation with arbitrary sign. The effect of this will be a γ giving a reasonable measurement of the dispersion in ignition point location, mostly on the conservative side.

Chapter 7

The Flixborough accident

7.1 Introduction

The Flixborough accident is thoroughly documented [58, 38, 50, 59]. Only a brief summary is given here; On 1st June 1974 there was an uncontrolled leakage of about 30 tons [58] of cyclohexane on the Nypro (UK) Ltd plant at Flixborough, England. A short minute after the leakage started the explosive cloud was ignited. A violent explosion occurred, causing the death of 28 men and severe damage to the buildings on the site.

A plan of the plant is shown in figure 7.1.

7.2 Literature

Several authors have estimated the maximum overpressure in the exploding gas cloud ([58], [50], [59]). The estimates are either based on observation of the damage or calculations of the energy release in the explosion.

7.2.1 Estimation of ignition point and gas cloud volume and location

Sadee et al. [58] have made an estimation of the explosive cyclohexane air mixture to a total volume of about 400 000 m^3, shaped like a banana or boomerang in its footprint, containing 30 tons of cyclohexane at a concentration of 2% per volume. The authors also pointed out that a likely source of ignition was the reformer furnace of the nearby hydrogen plant. Gugan [50] stated 36 tons as a likely cyclohexane mass. Marshall [59] also stated the hydrogen plant as a probable point of ignition. Generally, there seems to be an agreement with respect to the general conditions of the leakage and the location of ignition in most reports of the Flixborough accident.

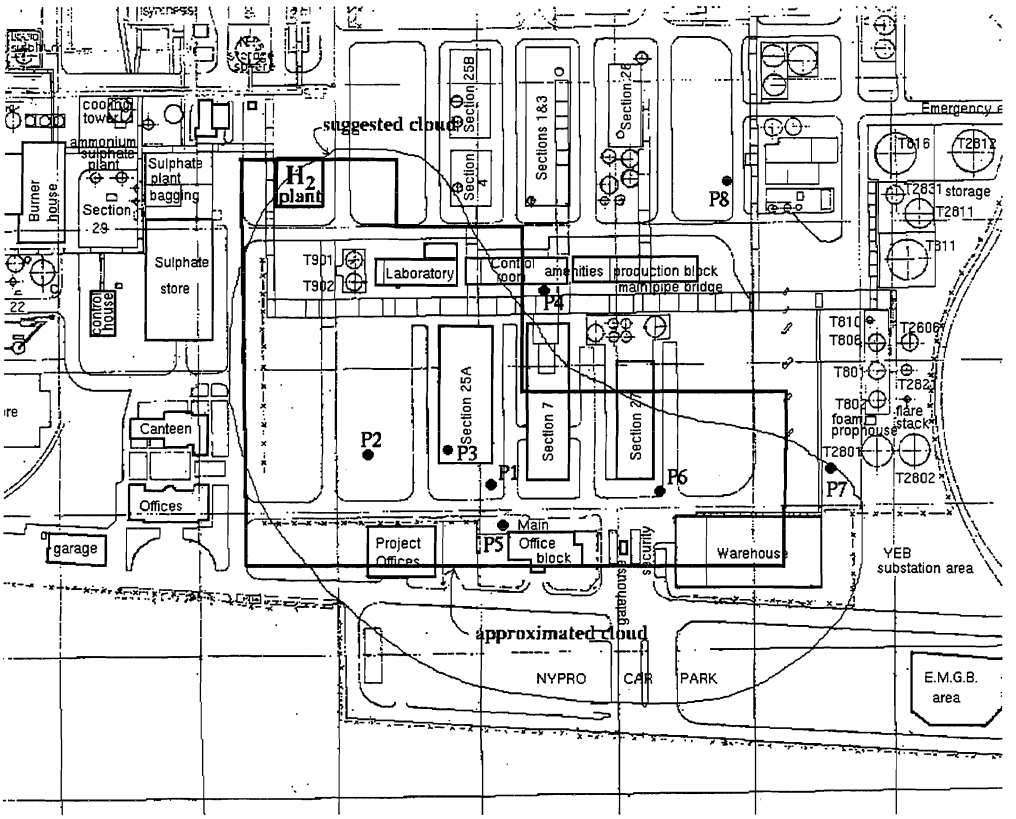

Figure 7.1: Plan of Flixborough plant. Assumed gas cloud reconstructed from Sadee et al. [58]. Pressure monitoring points P1 ... P8 are described in the text.

7.2.2 Estimation of explosion pressure

Sadee et al., 1976

The site survey performed by Sadee et al. [58] describes 11 selected structures that substained damage. The maximum explosion pressure are visually estimated at 9 of these locations and compared to an "equivalent" TNT explosion.

Where the damage was particularly severe, i.e. at the apparent explosion centre and at the caprolactam control building, Sadee et al. made no estimation of the explosion pressure. The caprolactam building was just described as demolished. Further from the explosion centre several structures and their damage was thoroughly documented. The authors estimated overpressures in the range 70–15 kPa (0.70–0.15 bar) at corresponding approximately distances 100–300 m.

Gugan, 1979

Gugan [50] describes the damage done on the reactors R2525 (here called P2) and R2526 (here called P3) and concludes that the net crushing pressure on the skirts of these vessels must have been in excess of 760 kPa (7.6 bar). The skirts were provided with several apertures for ventilation and access, and a rise in the outside pressure would quickly be followed be a rise in the inside pressure, thus reducing the net load on the skirts. Depending on the assumption of the pressure rising rate, Gugan estimates a free atmospheric pressure in the interval 1 039–1 518 kPa (10.4–15.2 bar), the latter mentioned first.

A parked road tanker (here called P7) was estimated to have been exposed to an explosion pressure in the interval 340–1 000 kPa (3.4–10 bar) [50, 60].

A drain cover (here called P6) of cast iron sustained damage from a pressure in excess of 10 00 kPa (10 bar).

Based on the energy release in the exploding cyclohexane-air mixture and the pressure rising rate, Gugan argues that the pressure in the centre of the flammable cloud probably was of the order 2 500 kPa (25 bar) and maybe as high as 4 400 kPa (44 bar).

Roberts and Pritchard, 1982

Scattered over the site was a large number of lamp posts. Roberts and Pritchard [61] carried out an examination of the deformation of 17 of these lamp posts. The deformation of such hollow cylinders can be calculated for force per unit length for a given period of duration. The other way round; given the deformation, one can calculate force per unit length for a given period, i.e. the impulse, these lamp posts were subjected to.

Some lamp posts were knocked completely down by the explosion pulse, thus the impulse must have been greater than their internal resistance. One of the lamp posts sustained a large deflection, but from the deformed shape it was possible to calculate an

assumed impulse. The lamp post is here denoted as "P8".

Roberts and Pritchard estimated the total impulse on this lamp post to be $I = 3.7\,\text{kPa s}$. With an estimated value for the duration of the positive phase of the impulse of $t_d = 200\,\text{ms}$, the "dynamic pressure" was calculated to be $P_d = I/t_d = 3.7/0.2 = 18.5\,\text{kPa}$. The air velocity was found by the equation $P_d = \frac{1}{2}\rho U^2$ with $\rho = 1.3\,\text{kg/m}^3$, thus $U = \sqrt{2P_d/\rho} = \sqrt{2 \cdot 18.5 \cdot 10^3/1.3} = 169\,\text{m/s}$

Marshall, 1987

The remains of the Nypro plant was also inspected by Marshall [59]. His classification is based on visual inspection.

Marshall concluded that the main office building (here called P5) had been subjected to an overpressure in excess of 70 kPa (0.7 bar). He further estimates a reasonable overpressure for the oleum plant control building to be 50 kPa (0.5 bar). For the caprolactam plant control building (here called P4) Marshall suggested a best estimate of overpressure to be circa 100 kPa (1 bar).

Comments to results found in the literature

It is interesting to note that the two authors basing their estimates on visual inspection (Sadee, Marshall) to a large degree conform in the assumed pressure values, i.e. on the low side of 1 bar. Gugan, on the other hand, is basing his estimates on calculations that produce explosion pressures of magnitude 10 bar.

According to Bjerketvedt et al. [12], Gugan's estimates of the pressure in the center of the explosion (25–44 bar) are only likely if there has been a detonation. It is uncertain whether Gugan's calculations are applicable to detonations.

7.3 Computer implementation

7.3.1 Plant layout and gas cloud

The geometry of the Flixborough plant is reconstructed in the computer solely for this thesis on the basis of drawings and photos provided by the Health and Safety Executive [41] supplemented with details from The Inquiry report [38] and Gugan [50]. A visualisation of the computer model is shown in figure 7.2. The final computer model hold 3 500 – 4 000 obstructions. The gas is selected to be cyclohexane, as in the real case.

The computer model implements a $400\,000\,\text{m}^3$ stoichiometric vaporised cloud of cyclohexane and air, with equal height and an approximated banana-shaped footprint as described by Sadee et al. [58]. The approximation to the prescribed cloud is done with three rectangular parallelepipedes combined to one large cloud. The ignition point is taken to be somewhere inside the H_2 plant.

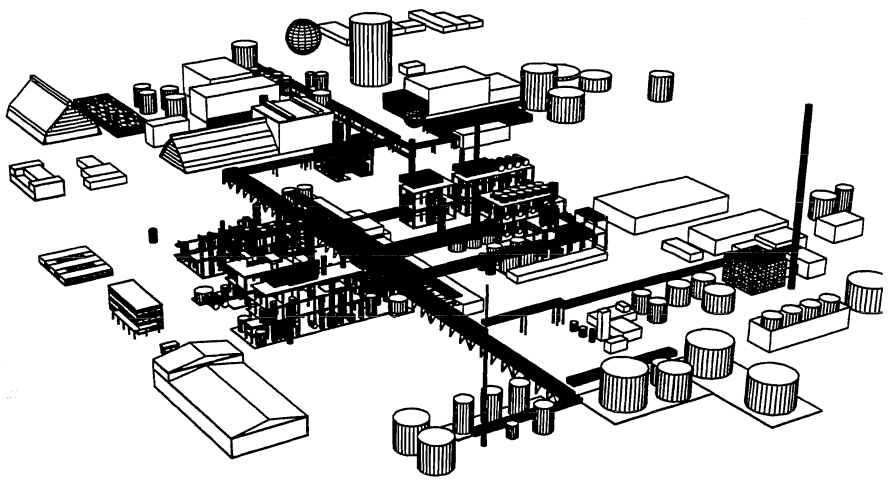

Figure 7.2: Visualisation of the computer model implementation of the Flixborough plant.

The Flixborough simulation cases are built up of approximately 180 000 control volumes. The grid is exponential, with the smallest control volumes cubes with sidelengths of about 1.5 m. The total calculation domain is approximately 300 m·300 m·100 m, the smallest value being the height, and the smallest control volumes located in the most congested areas within the flammable cloud.

These simulations put large demands on the computer, so only 200 simulations are done. However, due to the selected number of pressure monitoring points (16), only 100 simulations are available for each point.

7.3.2 Pressure monitoring points

The pressure monitoring points in the simulation are chosen so that comparison with the visual or calculated pressure levels in literature can be done. The 8 chosen pressure monitoring points are described in table 7.1.

Table 7.1: Description of pressure monitoring points.

Pressure monitoring point	Reference to literature[a]	Description
P1	S1	Appearant explosion centre
P2	G12	Freestanding reactor 5 from sec. 25A
P3	G13	Reactor 6, sec. 25 A
P4	S3/M3	Control building, south side
P5	M2	NW corner of main office building
P6	G16	Cast steel drain cover
P7	G15	Parked road tanker
P8	R15	Lamp post

[a]S = Sadee et. al [58], G = Gugan [50], M = Marshall [59], R = Roberts and Prithcard [61]

7.4 Simulation results

The pressure values in table 7.2 are shown as mean maximum overpressure over 1 ms and explosion impulse for 100 different simulations, all of them with their ignition point located on the ground floor of the H_2 plant.

Table 7.2: Maximum explosion overpressure over 1 ms and explosion impulse. Mean values from 100 different simulations with ignition point located at the ground floor of the H_2 plant.

Pressure monitoring point	Distance from "explosion centre"[a] [m]	Maximum explosion overpressure [kN/m^2 (bar)]	Explosion impulse [kNs/m^2]
P1	0	1360 (13.6)	27.3
P2	55	1290 (12.9)	26.0
P3	30	1650 (16.5)	27.6
P4	90	400 (4.0)	14.1
P5	20	1310 (13.1)	26.1
P6	70	1400 (14.0)	25.4
P7	150	220 (2.2)	7.9
P8	170	100 (1.0)	6.7

[a]As denoted by Sadee et al.

7.5 Comparisons

A collocation of previous estimated values from the literature and simulated is shown in table 7.3.

Table 7.3: Results from literature compared to simulated results.

Pressure monitoring point	Literature estimated explosion overpressure [kN/m^2 (bar)]	Simulated explosion overpressure [kN/m^2 (bar)]
P1	—	1360 (13.6)
P2	1039–1518 (10.4–15.2)^G	1290 (12.9)
P3	1039–1518 (10.4–15.2)^G	1650 (16.5)
P4	100 (1.0)^M/70 (0.7)^S	400 (4.0)
P5	$>$ 70 (0.7)^M	1310 (13.1)
P6	$>$ 1000 ($>$ 10.0)^G	1400 (14.0)
P7	340–1000 (3.4–10.0)^G	220 (2.2)
P8	3.7 kNs/m^2 (impulse)^R	6.7 kNs/m^2 (impulse)

^{G} = Gugan (1979), ^{M} = Marshall (1987), ^{S} = Sadee et al. (1976), ^{R} = Roberts and Pritchard (1982)

7.6 Discussion

The concurrence of results from Gugan's estimations [50] and the simulated results (P2, P3, P6, P7) is striking. The values are very similar. Gugan has investigated the Flixborough case thoroughly and done a great number of calculations to quantify the magnitude of the explosion. It seems that his estimations and further mathematical treatment based on data from the observed damage to a large degree confirm the simulation results.

The explosion pressure estimations of Sadee et al. [58] and Marshall [59] are much lower than the values from the simulations. The reason might be that their values are based on visual inspection, not calculations. The collapse of buildings such as the control room and main office block has resulted in their conclusion of an explosion pressure of magnitude 1 bar, while the simulations show that the actual pressure might be 4.0 bar (P4) and 13.1 bar (P5). This may indicate that an assumption of explosion pressure estimation based on visual inspection alone can lead to large assessment errors.

7.7 Ignition point location at the Flixborough plant

With the given geometry, gas type and cloud size, the ignition point location is varied inside the ground floor of the H_2 plant. Explosion pressure and impulse are registered for 100 simulations with different ignition source locations.

The results show very little variations around the mean values for the 8 pressure monitoring points described in the previous chapter. The mean value, $\bar{x}$, standard deviations, s and coefficient of variance, $V = s/\bar{x}$, of these simulations are shown in table 7.4.

Table 7.4: Mean, standard deviation and coefficient of variation for 100 simulations of explosion pressure and impulse at Flixborough. Pressure in bar, impulse in kNs/m^2.

Pressure monitoring point	Approx. dist. from explosion centre [m]	Explosion overpressure [baro]			Explosion impulse [kNs/m^2]		
		$\bar{x}$	s	V	$\bar{x}$	s	V
P1	0	13.6	0.18	0.0135	27.3	0.30	0.0111
P2	55	12.9	0.25	0.0195	26.0	0.06	0.0024
P3	30	16.5	0.36	0.0218	27.6	0.14	0.0050
P4	90	4.0	0.01	0.0016	14.1	0.33	0.0237
P5	20	13.1	0.33	0.0249	26.1	0.23	0.0088
P6	70	14.0	0.24	0.0172	25.4	0.64	0.0254
P7	150	2.2	0.22	0.1021	7.9	0.81	0.1027
P8	170	1.0	0.19	0.1865	6.7	1.60	0.2374

As can be seen, at these distances from the ignition point, the exact location of the source is not significant. Other parameters, such as turbulence generation due to congested areas, will override the importance of the initial ignition effects.

A natural effect is the increasing coefficient of variance in both explosion pressure and impulse as the distance from the explosion centre (and also from the ignition point) increases. A little more noteworthy is the observation that the coefficient of variation is of the same order for both pressure and impulse. Taking the integrating aspect of the impulse under consideration, we would expect less variance from the impulse than the pressure.

Chapter 8

Partial factors

This chapter summarises the model presented and the respective values found, based on the simulations.

8.1 The presented model

The proposed model tries to establish a statistically sound characteristic explosion load based on the results from 2, 3 or 4 simulations of the case in interest.

The model was proposed in chapter 4, and we summarise:

$$A_k = p\gamma_G\gamma_I\gamma_M \tag{8.1}$$

where

- A_k is the characteristic explosion load
- p is the sample explosion action, usually $\bar{p}$, based on the mean of 2, 3 or 4 simulations
- γ_G is a gas volume uncertainty load factor
- γ_I is an ignition point uncertainty load factor
- γ_M is an explosion simulator model uncertainty load factor

This characteristic accidental action A_k is inteded to be used in the accidental design situaion in the ultimate state limit described in Eurocode 1.1 [8] and the proposal to the equivalent Norwegian standard [44]. The procedure to obtain the sample explosion action, p or $\bar{p}$, is described in section 6.5.2. The uncertainty load factors are described in the following sections.

8.2 Factors for gas cloud size and location

For *offshore modules*, it is argued in section 2.2.2 for a design case being the whole module filled with gas. This will in general represent a conservative assumption, and can be formulated with a gas volume uncertainty load factor with value 1, i.e. $\gamma_G = 1.0$.

There has been no calculations of the volume uncertainty load factor for smaller gas volumes. We can, however, point to figures 5.4 and 5.5. These show that the maximum loads (pressure and impulse) are approximately linear functions of the gas volume. Combined with a probabilistic representation of different explosive gas cloud volumes occurring, it is possible to estimate approximate gas volume uncertainty load factors.

For *onshore process plants* the γ_G factor has not been calculated.

8.3 Factors for ignition point location

The usefulness of the calculations of ignition point uncertainty load factor relies upon the assumption of the existance of a universal (but unknown) distribution for this factor. The existance of a universal distribution has not been proved here, nor have there been any quantitative assessments of the assumption of this existance. The assumption is based on observations done in chapter 6.

For *offshore modules*, chapter 6 has described the values obtained for the ignition point uncertainty load factors. The load factor are presented as mean values for modules completely filled with gas in table 6.11. The values depend on the chosen level of safety. The examples throughout this thesis have been the 90% quantiles in the explosion or impulse distributions. This choice of example values is based on our subjective assessment. Other quantiles may be more representative for actual design situations. While background material may lack for other quantiles, final values are provided earlier.

If we base the value of the load factor on the approximated mean of the 90% quantiles in the three modules investigated, as referred in section 6.5.5, we get approximate ignition point uncertainty load factors $\gamma_I = 2.0$ for explosion pressure and $\gamma_I = 1.5$ for impulse. For a more precise assessment and for other quantiles, see chapter 6.

For *onshore process plants* only the reconstruction of the Flixborough accident in chapter 7 has been evaluated. For this particular case, the exact ignition point location was of little interest, i.e. $\gamma_I = 1.0$ for both pressure and impulse. It is not recommended to use such a small value without further research.

8.4 Factors for computer code uncertainties

There are no evidences for the computer simulation code uncertainties to be different for offshore modules and onshore process plants. While some effects, e.g. the time of the laminar phase of the combustion, may be more dominant for one or the other, explosion

simulators are validated against both large and small geometries. The author have no reports of simulators performing exceptionally well or bad for offshore modules or onshore plants alone.

The uncertainty being a computer code property, it can be calculated from validation data. Reported results are referred to in section 4.5.

For the EXSIM explosion simulator, the simulator model uncertainty load factors can be calculated to the values presented in table 8.1.

Table 8.1: Values of the simulator model uncertainty load factor γ_M to produce a statistical quantile for maximum pressure values from the EXSIM gas explosion simulator.

Quantile in simulated explosion pressure to achieve	Model uncertainty load factor γ_M
75%	1.30
90%	1.52
95%	1.65
98%	1.86
99%	1.90

Thus, if we want to be 90% sure that the explosion simulator results are on the "safe side", we get a factor $\gamma_M \approx 1.5$.

8.5 Remarks

The factorial approach is done on the assumption of individual events, that the three different uncertainties are independent. This assumption is discussed in section 4.6.

Note that if we choose the conservative approach of the design case for an offshore module being completely filled with explosive gas and the 90% quantiles for both ignition point (see sec. 8.3) and simulator (see sec. 8.2) factors, we get

$$A_k = \bar{p} \cdot 1.0 \cdot 2.0 \cdot 1.5 = 3 \cdot \bar{p} \tag{8.2}$$

i.e. a design load being 3 times larger than the mean of the simulations with arbitrary ignition point.

The combined probability of exceeding this characteristic load will be

$$P(L > L_k) = 1 \cdot (1 - 0.90) \cdot (1 - 0.90) = 0.01 \tag{8.3}$$

i.e. given that an explosion actually occurs, our estimate of the characteristic load will be exceeded in 1% of the cases. It will be exceeded in *less* than 1% of the cases if we allow the gas cloud to be ignited before filling the whole module.

The probability of exceeding the characteristic load must be multiplied with the probability of an explosion occurring to get the correct picture of the risk.

Chapter 9

Conclusions

9.1 Summary and conclusions

This thesis has addressed a number of factors associated with uncertainties in the explosion load estimation process. Using numerical explosion simulators in the design phase, several sources to possible errors are introduced. This thesis tries to isolate and quantify several of these possible errors.

The main sources to uncertainties discussed in this thesis are the gas cloud volume, the location of the ignition point and the quality of the computer code used in simulations.

Statistical methods are used to quantify the named uncertainties. In order to get enough statistical data to provide safety factors, approximately 10 000 explosions simulations were done, collecting properties from the simulated explosions.

During the data collection, a number of properties were registered for gas explosions in offshore structures. Graphs and/or tables are presented for:

1. explosion pressure and impulse as function of gas cloud volume.
2. the relation between explosion pressure and explosion impulse.
3. explosion pressure and impulse as function of explosion duration.
4. the probability of a "short" explosion with respect to the natural periods of typical offshore structures.
5. the loading rate for several gas volumes and gas types.
6. the pressure-time shape function, i.e. an investigation of the often assumed triangular shape of a gas explosion.
7. the effect of louvres on explosion pressure and impulse in offshore modules.

The corresponding conclusions were:

1. for large numbers, there is an approximate linear relation between the pressure or impulse and gas volume.
2. it seems possible to produce a linear relation between explosion pressure and impulse in the investigated pressure interval.
3. there seems to be a inverse relation between explosion pressure and explosion duration, but this effect is not so clear for explosion impulse.
4. the literature statements of offshore structures rarely being in the impulsive regime is confirmed; "short" explosion durations are uncommon.
5. loading rates vary a lot, they are observed in the interval 1.5–90 bar/sec.
6. the triangular shape assumption is supported by the observed data.
7. introducing louvres of infinite strength will significantly increase explosion pressure, impulse and duration

Only one onshore plant explosion was investigated; a reconstruction of the Flixborough accident. Explosion pressures up to 16.5 bars was simulated. The simulated results were compared with estimated values in the literature. The simulated results agreed to a large degree with estimations based on actual explosion calculations, but differed a lot from estimations based on observed damage. Estimations based on building damage were typically much lower than simulated and calculated results. This can imply that for severe building damage, an observational estimation of the pressure may be insufficient if the buildings are demolished, as is the case from Flixborough.

The effect of ignition point location was investigated in detail for offshore modules. Simulations confirmed variations with a factor of 20 in explosion pressure with respect to ignition point location. The pressure and impulse distributions while varying the ignition point were tested versus normal, lognormal and Gumbel type I and II distributions. Explosion impulse seems to follow a normal distribution, while explosion pressure hardly can be classified into a parametric distribution.

The distribution of explosion pressure was treated with non-parametric statistics. In this way it was possible to tabulate several interesting quantiles in the pressure distribution with base in just a few simulations. The factor used to multiply the mean of the results from some few simulations to achieve a wanted quantile was called the γ factor, or *the ignition point location uncertainty factor*. Values for the γ factor are tabulated for several cases. The relevancy of these values relies upon the assumption of the existance of a universal distribution for the γ factor.

The value and properties of this γ factor were discussed. It seems relatively independent of gas cloud volume and surprisingly independent of the number of initial simulations. The

γ factor seems lower for impulse than for pressure and just slightly lower for propane than for methane. It is, however, dependent of the chosen safety level.

For the onshore plant — the Flixborough plant — the effect of the ignition point location was negligible. This observation was explained with the large gas cloud, the numerous obstructions and the omnipresent sources to turbulence generation. Is was, however, documented that the effect of the ignition point location increased as the distance from the presumed explosion centre increased.

A model for taking into account the quantified uncertainties was proposed. The model is based on the uncertainties being independent events and results in a design explosion load. The effect of simultaneous load events are left to the prescriber of the accidental limit state.

Partial factors for the design load model was presented in the text. The value of these rely heavily on the user's choice of safety level.

9.2 Recommendation for further work

Although numerous hours of CPU time has been used, both in explosion simulations and non-parametric statistics calculations, the data collection could be more extensive to get a better basis for the statistical evaluations.

Recommendations for further research into factors applicable to the proposed model are:

- Investigate the effect of the initial turbulence field on explosion pressure and impulse. The result from such an investigation may lead to an introduction of another uncertainty factor, γ_T, introductory turbulence uncertainty.
- Investigate the possibility of biased explosion simulators, e.g. the possible case of a particular simulator being extremely good at or bad at simulating ignitions in e.g. corners of modules.
- Produce an algorithm for selecting ignition points close to surfaces or a table of likely ignition points with corresponding igniting frequencies.
- Investigate the effect of ignition point location for several medium-sized, land-based process plants. Although insightful for this particular case due the existence of earlier reports, the Flixborough accident simulation produced little generalisable data.
- The increasing popularity of Floating Production Storage Off-loading installations (FPSOs) justify that a similar route of data collection and statistical assessments and generalisation should be done for these to extend the use of the model.

- The γ factor is treated with non-parametric statistics in this thesis. A test of this factor versus parametric distributions may lead to a better understanding of the properties of γ.
- The statistics in this thesis are based on non-parametric processing of sampled sets. Another approach would be the Bootstrap resampling method as described by Efron [62] and Efron and Tibshirani [63]. It is our impression that the resampling method would enhance the accuracy of the statistical data.

As the model is presented in this thesis, it is a stand-alone design tool for structure dimensioning. In a wider range, it could be coupled to other models for risk analysis.

Of interest is the fit of an explosion event into the hazard function described in section 6.4.1. This may ease the fit of explosion pressure into an extremal distribution and thus may provide parametric properties.

Other applications of the model, such as the extension into e.g. a Monte Carlo-model for explosions or risk analysis in general are also possible.

Nomenclature

Latin letters

a_i	Lieblein weight factors, see appendix B
b_i	Lieblein weight factors, see appendix B
e	natural base, $e = 2.718281\ldots$
e_i	relative error in simulation of an explosion
f_c	material strength of concrete
f_{dc}	material strenght of concrete exposed to fast loading
f_{ds}	material strenght of steel exposed to fast loading
f_s	material strength of steel
f_L	probability density function for L, i.e. load effect
f_R	probability density function for R, i.e. resistance
$f_X(x)$	probability density function for X
$f_{X_n}(x)$	probability density function for X_n
$f_{Y_n}(y)$	probability density function for Y_n
$h(t)$	the hazard function
$h_n(x)$	the hazard function for the largest value of X
$g(\ldots)$	limit stat function
k	the number of groups in Lieblein order statistics; the shape parameter of X_n in Gumbel Type II distribution; factor for calculating quantiles in a distribution
k_L	factor for calculating qunatiles in load distributions
k_R	factor for calculating qunatiles in resistance distributions
l	confidence level
n	number
n_s	number of observations within each group for Lieblein order statistics, chosen to $n_s = 6$ for our purpose
p	explosion pressure; sample explosion pressure or impulse action
$\bar{p}$	the mean of several sample explosion actions
p_k	characteristic explosion pressure
$p_{\max}$	maximum explosion pressure, $\max\{p(t)\}$

p_κ	quantile in an explosion pressure distribution
r	subsript; number in a sequence
s	standarised extremal variate; subscript; number in a sequence
s_{X_n}	standard deviation of a sample of X_n
t	time
t_1	time of positive phase of explosion
t_{ris}	rising time of explosion pressure
u_n	the characteristic largest value of the initial variate X in the Gumbel Type I distribution
$\hat{u}_n$	estimation of u_n
v	displacement of structure
$v_{\max}$	maximal displacement of structure
v_n	the characteristic largest value of the initial variate X in the Gumbel Type II distribution
x	stochastic variable
$\bar{x}_n$	mean value of a sample of X_n
y	stochastic variable
A_d	design value of an accidental action
A_k	characteristic value of an accidental action
$D[\cdot]$	deviation
$E[\cdot]$	expected value
F_L	accumulated probability function for L, i.e. load effect
F_R	accumulated probability function for R, i.e. resistance
F_X	cumulative distribution function
G_k	characteristic value of permanent action
G_{kj}	characteristic value of permanent action j
$F_X(x)$	accumulated probability function for X
L	load effect
L_d	design load value; $L_d = \gamma_F L_k$
L_i	any of several L's
L_k	characteristic load value
M	safety margin
N	a given number
$P(\dots)$	probability
P_F	probability of failure
P_N	probability of non-failure
Q_k	characteristic value of a single variable action
Q_{k1}	characteristic value of the dominant variable action
Q_{ki}	characteristic value of a non-dominant variable action i
P_k	characteristic value of a prestressing action
R	resistance, i.e. structure strength

	(both actual and calculated based on probabilistic properties)
R_d	design value of structure strength; $R_d = R_k/\gamma_M$
R_k	characteristic strength
R_n	nominal strength
$\mathcal{S}$	the set of all non-failure states
S	value of standarised extremal variate
T	natural period of structure
V	coefficient of variation, i.e. $V = \hat{\sigma}/\hat{\mu}$
V_R	coefficient of variation for the ratio R_n/R
$\mathrm{Var}[\cdot]$	variance, i.e. σ^2
$\boldsymbol{X}$	a vector of stochastic values; $\boldsymbol{X} = [X_1 \quad X_2 \quad \dots \quad X_n]$
X	the stochastic value of x
X_n	the nth observation; a synonym for Y_n
Y	the stochastic value of y
Y_n	the maximum value of $\boldsymbol{X}$, i.e. $Y_n = \max\{X_1, X_2, \dots, X_n\}$

Greek letters

α_n	inverse measure of dispersion of X_n in Gumbel Type I distribution; fraction in determination of confidence level
$\hat{\alpha}_n$	estimation of α_n
β	safety index, defined by $E[M]/D[M]$
γ	partial factor; Euler constant, $\gamma = 0.577216\dots$
γ_i	any of several γ's
γ_A	partial factor for accidental action
γ_F	partial factor for load effects or actions
γ_{GA}	partial factor for permanent actions in accidental design situations
γ_{GAj}	partial factor for permanent action j in accidental design situations
γ_G	partial factor for gas cloud size and location uncertainty
γ_I	partial factor for ignition point location uncertainty
γ_M	partial factor for a material property; partial factor computer model uncertainty
γ_P	partial factor for prestressing actions
γ_{PA}	partial factor for prestressing actions in accidental design situations
κ	denotes the quantile in a population, e.g. p_κ,
$\boldsymbol{\mu}$	a vector of mean values; $\boldsymbol{\mu} = [\mu_1 \quad \mu_2 \quad \dots \quad \mu_N]$
μ	mean value
μ_{X_n}	mean value of the population of X_n
π	$3.141592\dots$
σ	standard deviation

σ_k	characteristic material strength
σ_m	mean value of material strength
σ_L	standard deviation in the load distribution
σ_R	standard deviation in the resistance distribution
σ_{X_n}	standard deviation of the population of X_n
ψ	weight function on the volume defined by $\mathcal{S}$
ψ_1	coefficient for frequent value of a variable action
ψ_2	coefficient for quasi-permanent value of a variable action
ω	the upper bound in the Gumbel Type III distribution
Φ	component resistance factor
$\Phi(\cdot)$	the standarised normal distribution function
$\Phi^{-1}(\cdot)$	the inverse standarised normal distribution function

Abbreviations

API	American Petroleum Institute
CMR	Christian Michelsen Research
CPU	Central Processing Unit
DIF	Dynamic Increase Factor
ENV	Europeische Vor-Norm *(European Pre-Standard)*
EMERGE	Extended Modelling and Experimental Reseach into Gas Explosions
EXSIM	EXplosion SIMulator
FLACS	FLame ACcelration Simulator
FORM	First Order Reliability Method
FPSO	Floating Processing Storage Off-loading installation
LRFD	Load and Resistance Factor Design
MoM	Method of Moments
NBS	National Bureau of Standards
NKB	Nordisk Komité for Bygningsbestemmelser *(Nordic Committee for Building Regulations)*
NS	Norsk Standard *(Norwegian Standard)*
QRA	Quantitative Risk Assessment
RP	Recommended Practice
SORM	Second Order Reliability Method

Appendix A

Figures with probability test plots

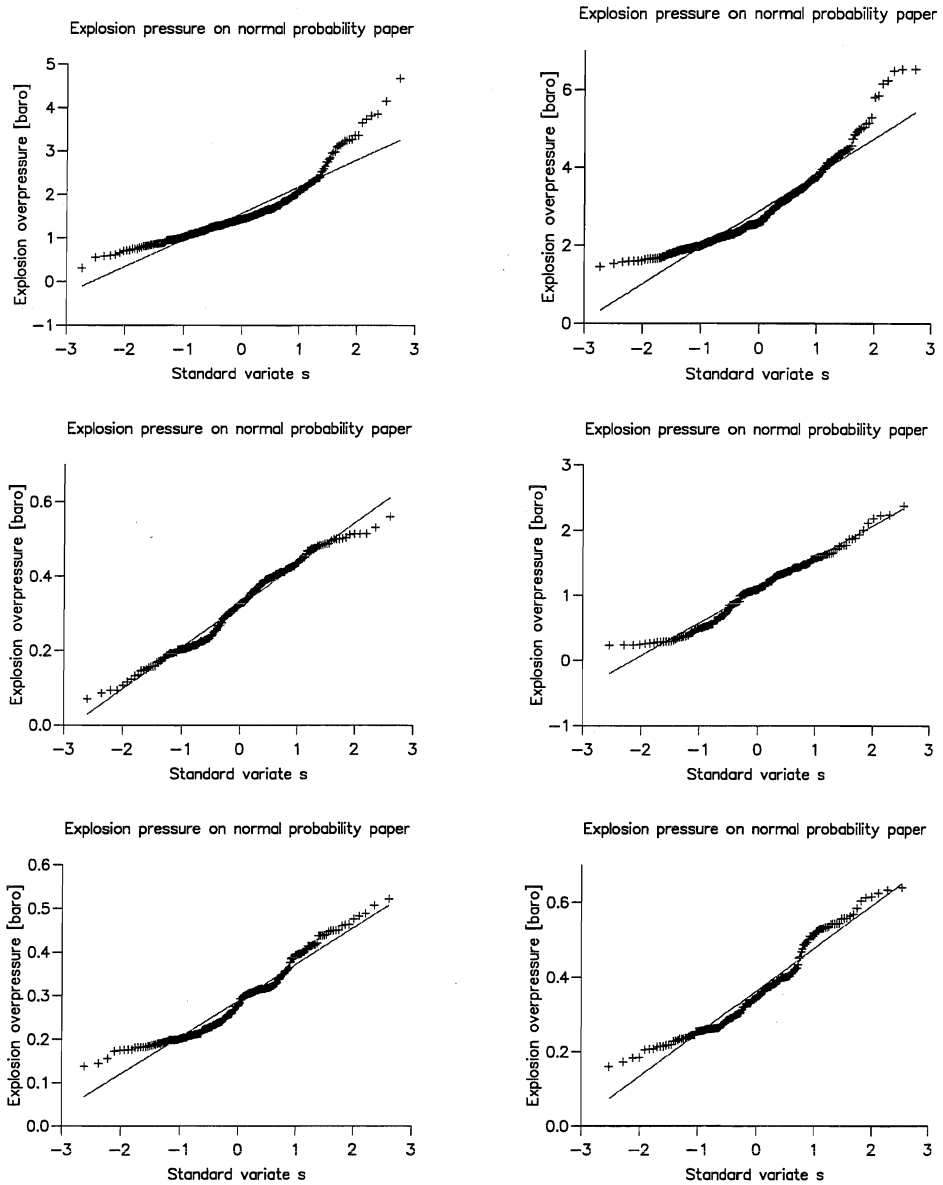

Figure A.1: Piper Alpha C Module. Test of maximum explosion pressure versus normal distribution. Left column methane as gas, right column propane as gas. Upper row: gas in whole module, middle row: gas in lower half of module, lower row: gas in low quart of module. Straight line drawn by linear regression.

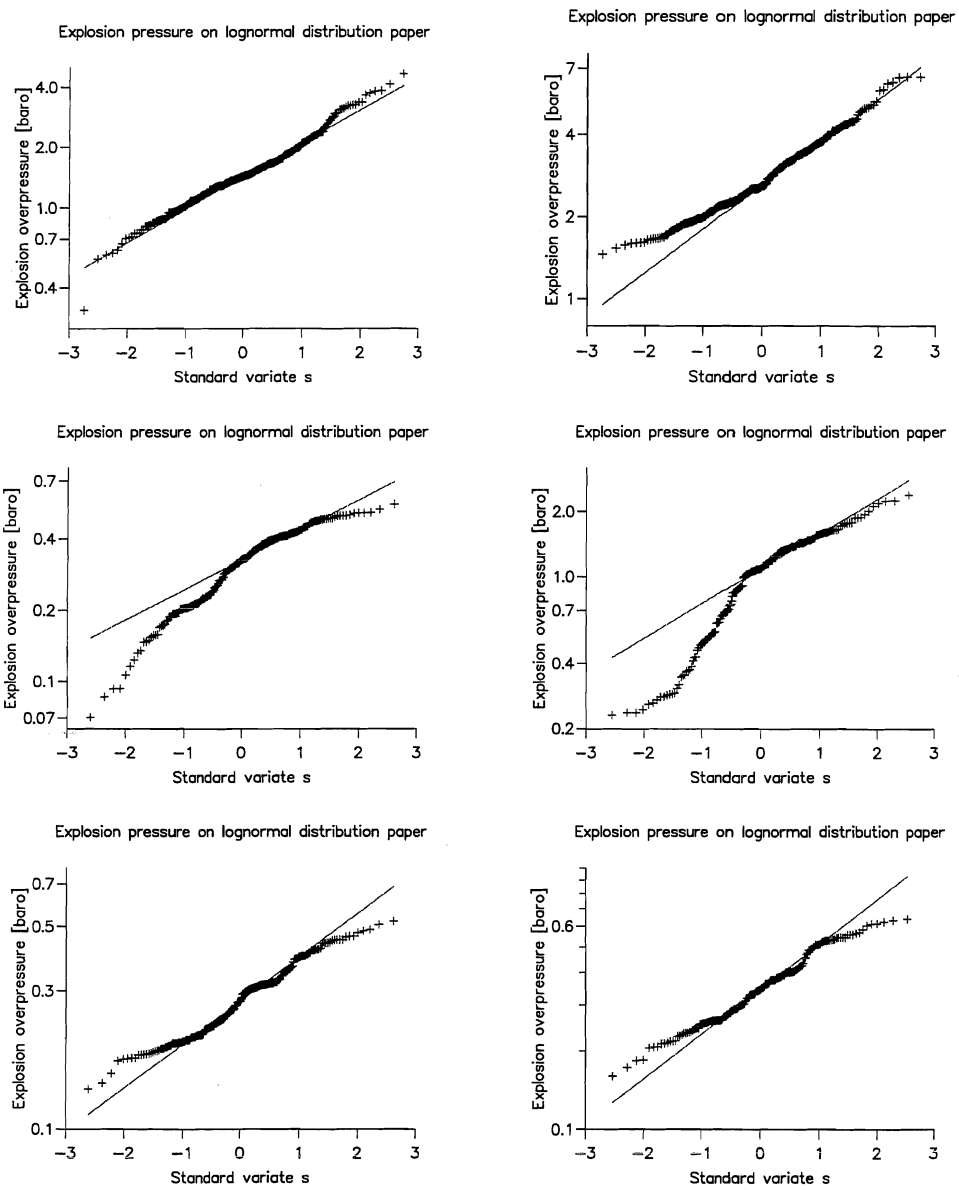

Figure A.2: Piper Alpha C Module. Test of maximum explosion pressure versus lognormal distribution. Left column methane as gas, right column propane as gas. Upper row: gas in whole module, middle row: gas in lower half of module, lower row: gas in low quart of module. Straight line drawn by exponential interpolation between the points $(0, X_{0.50})$ and $(1, X_{0.84})$.

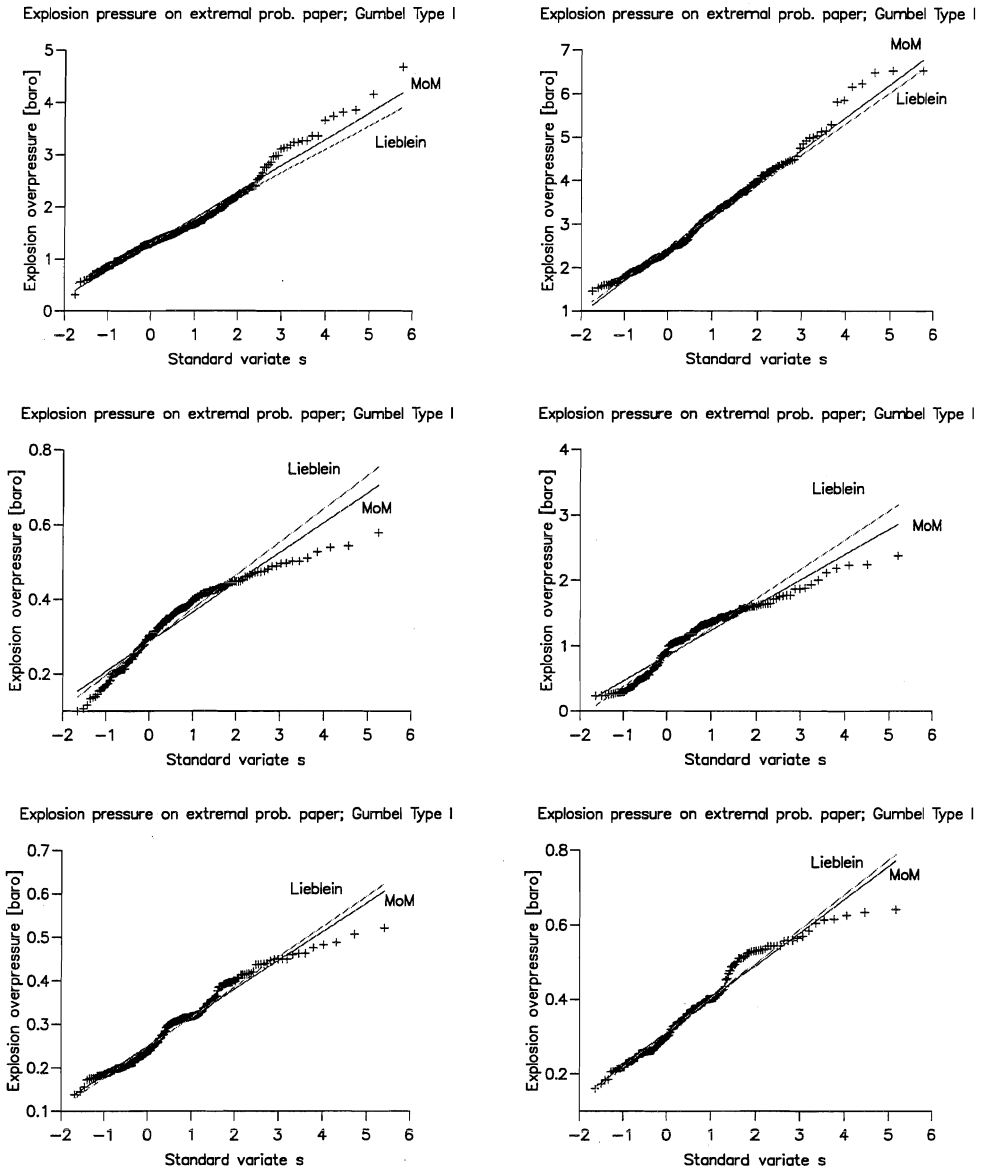

Figure A.3: Piper Alpha C Module. Test of maximum explosion pressure versus Gumbel Type I distribution. Left column methane as gas, right column propane as gas. Upper row: gas in whole module, middle row: gas in lower half of module, lower row: gas in low quart of module. Straight lines are drawn by Method of Moments (MoM) and Lieblein order statistics.

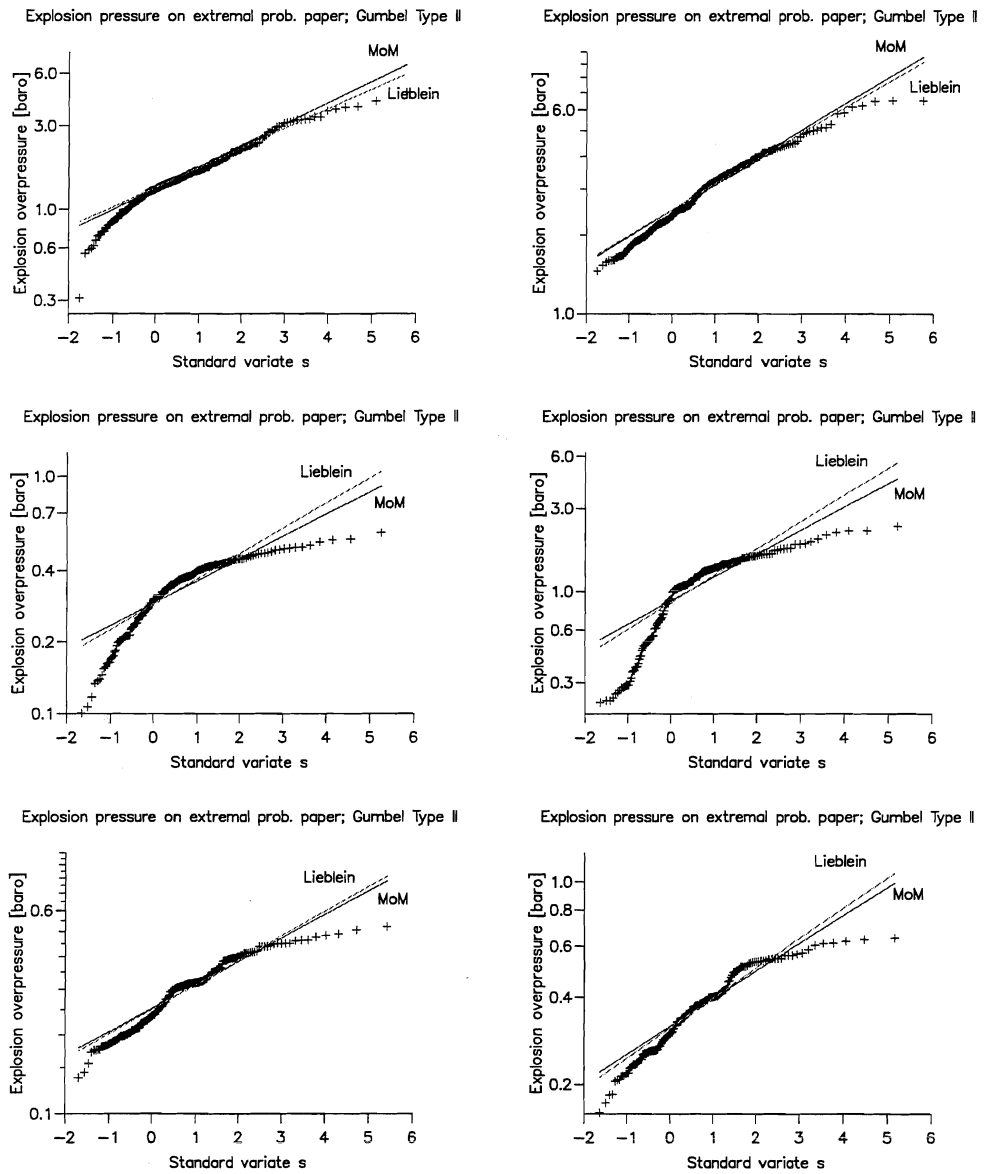

Figure A.4: Piper Alpha C Module. Test of maximum explosion pressure versus Gumbel Type II distribution. Left column methane as gas, right column propane as gas. Upper row: gas in whole module, middle row: gas in lower half of module, lower row: gas in low quart of module. Straight lines are drawn by exponential interpolation between the points $(S_{0.50}, X_{0.50})$ and $(S_{0.84}, X_{0.84})$ calculated by Method of Moments (MoM) and Lieblein order statistics.

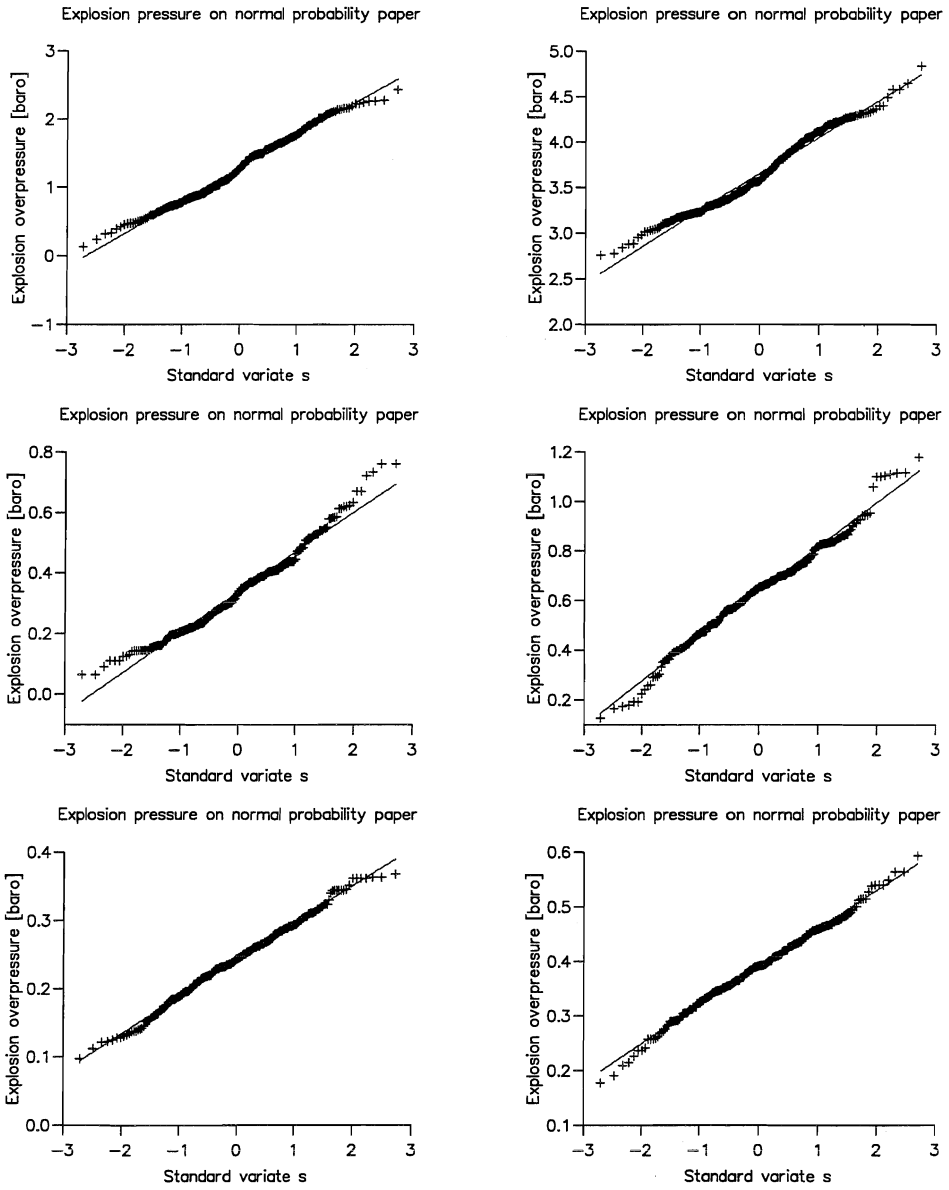

Figure A.5: CMR M24 Module. Test of maximum explosion pressure versus normal distribution. Left column methane as gas, right column propane as gas. Upper row: gas in whole module, middle row: gas in lower half of module, lower row: gas in low quart of module. Straight line drawn by linear regression.

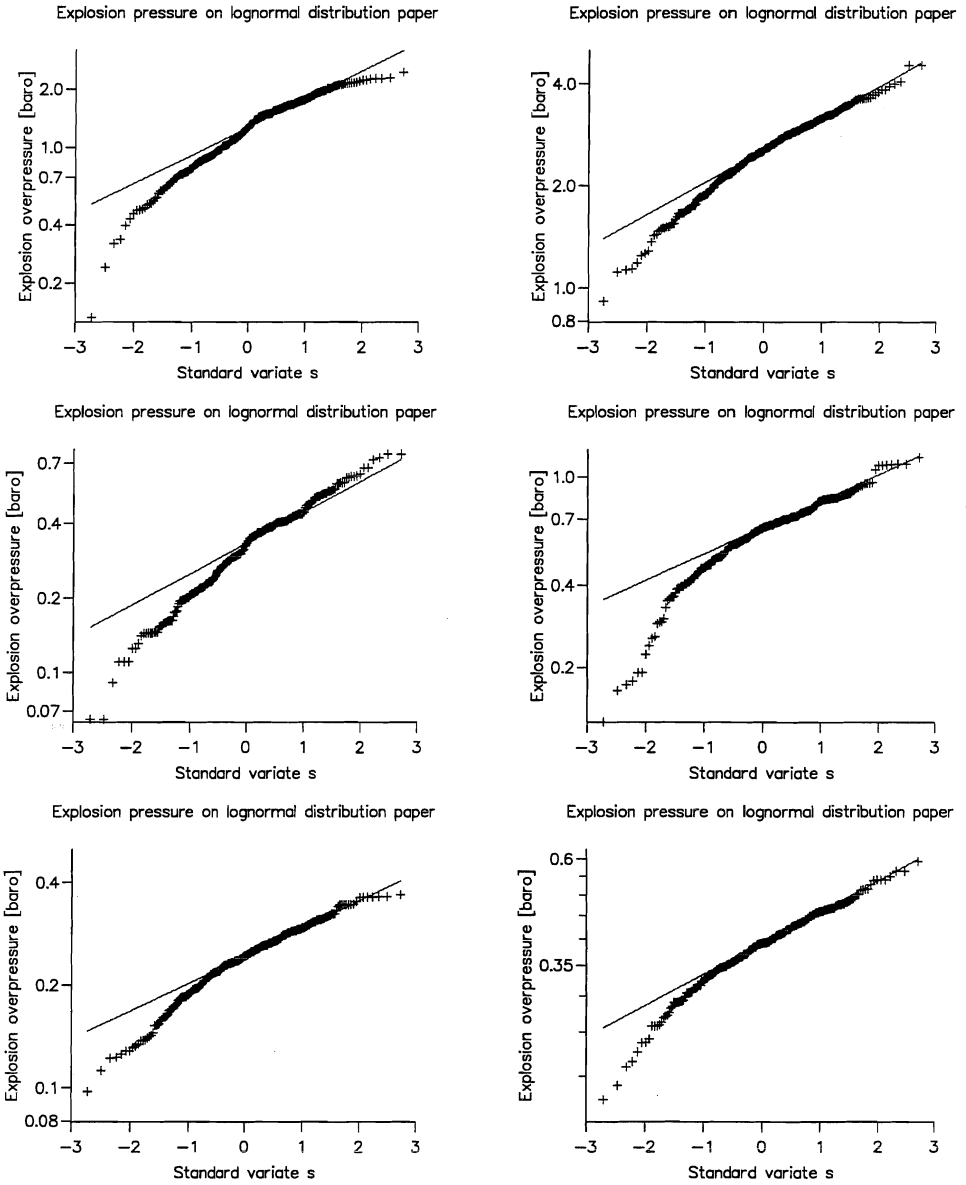

Figure A.6: CMR M24 Module. Test of maximum explosion pressure versus lognormal distribution. Left column methane as gas, right column propane as gas. Upper row: gas in whole module, middle row: gas in lower half of module, lower row: gas in low quart of module. Straight line drawn by exponential interpolation between the points $(0, X_{0.50})$ and $(1, X_{0.84})$.

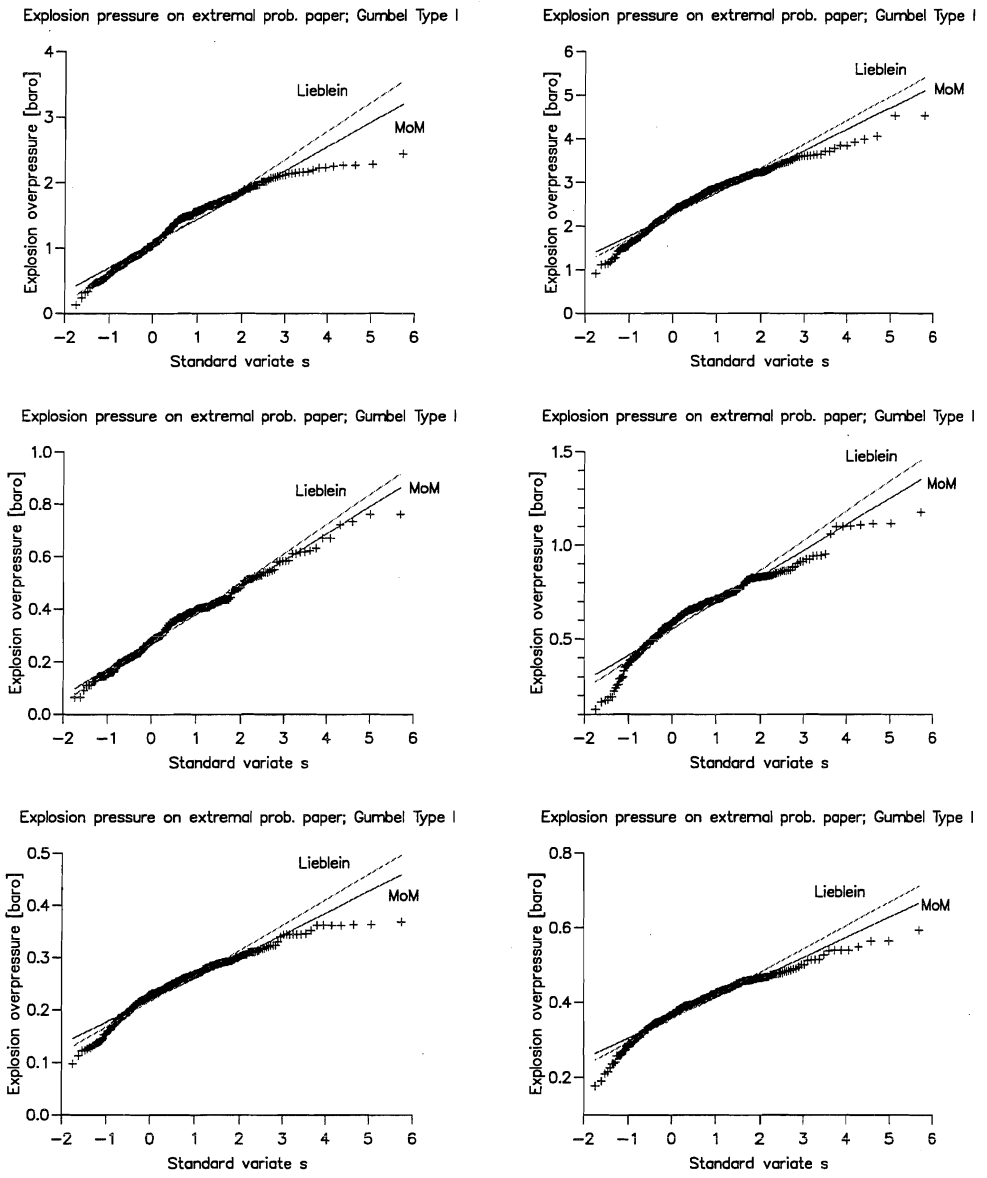

Figure A.7: CMR M24 Module. Test of maximum explosion pressure versus Gumbel Type I distribution. Left column methane as gas, right column propane as gas. Upper row: gas in whole module, middle row: gas in lower half of module, lower row: gas in low quart of module. Straight lines are drawn by Method of Moments (MoM) and Lieblein order statistics.

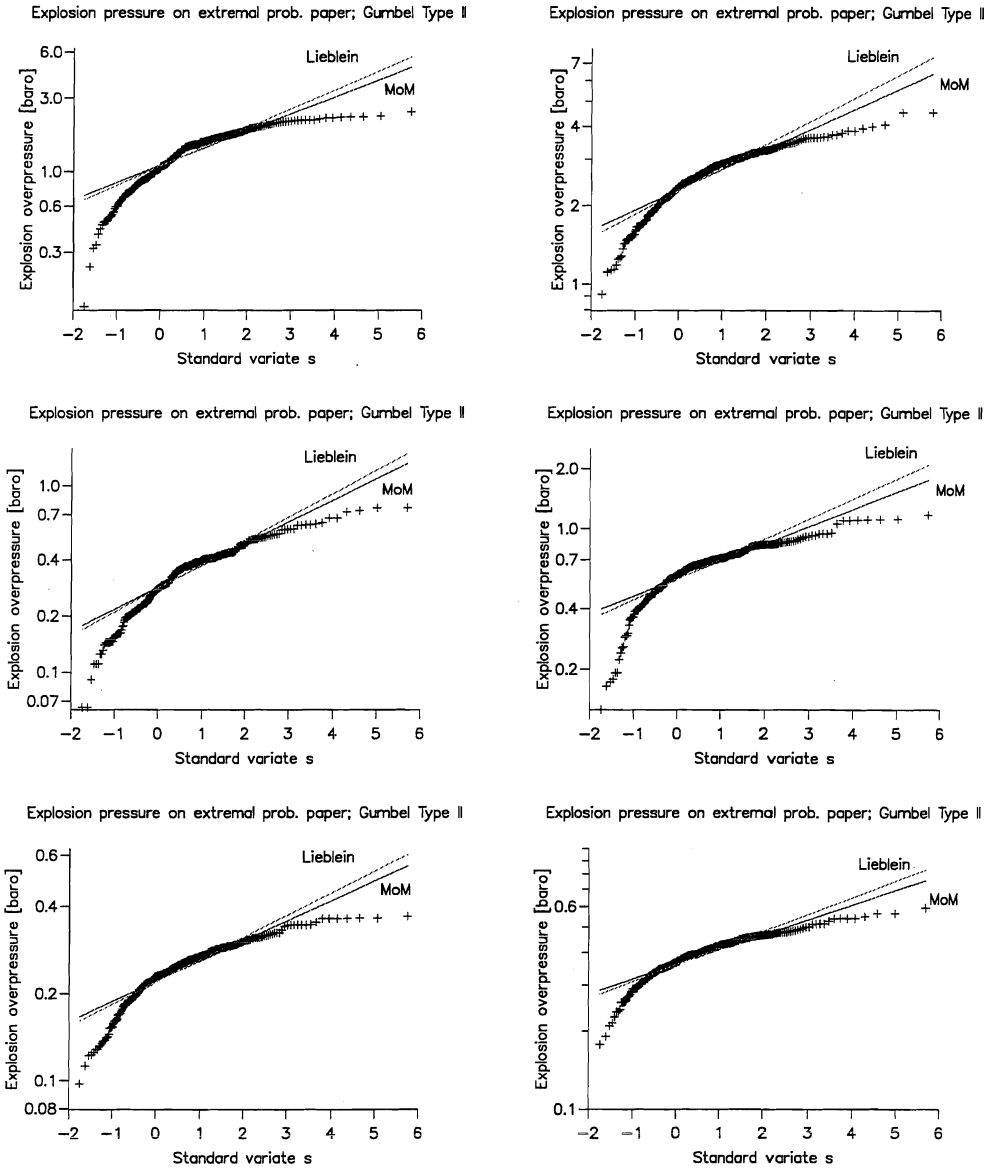

Figure A.8: CMR M24 Module. Test of maximum explosion pressure versus Gumbel Type II distribution. Left column methane as gas, right column propane as gas. Upper row: gas in whole module, middle row: gas in lower half of module, lower row: gas in low quart of module. Straight lines are drawn by exponential interpolation between the points $(S_{0.50}, X_{0.50})$ and $(S_{0.84}, X_{0.84})$ calculated by Method of Moments (MoM) and Lieblein order statistics.

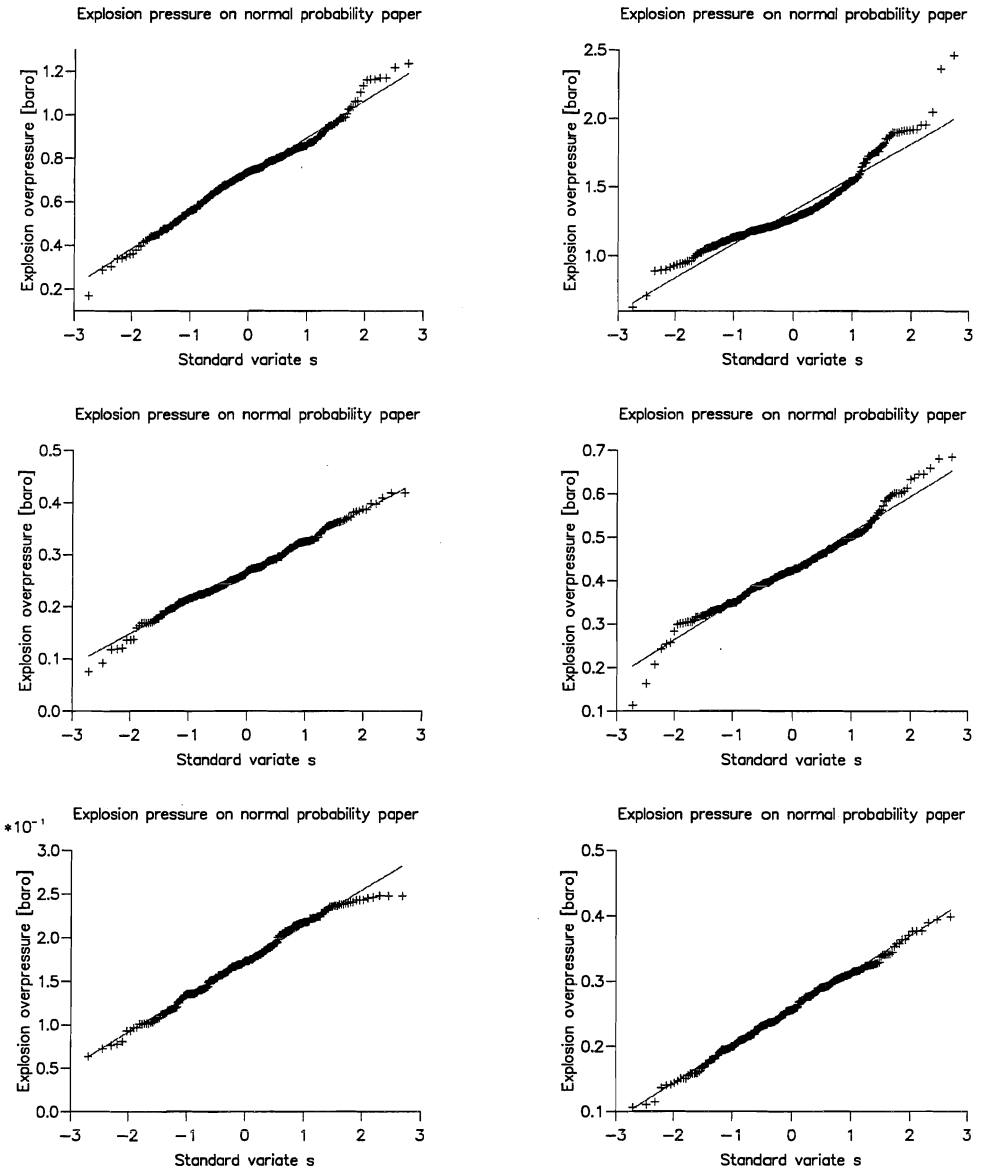

Figure A.9: CMR M25 Module. Test of maximum explosion pressure versus normal distribution. Left column methane as gas, right column propane as gas. Upper row: gas in whole module, middle row: gas in lower half of module, lower row: gas in low quart of module. Straight line drawn by linear regression.

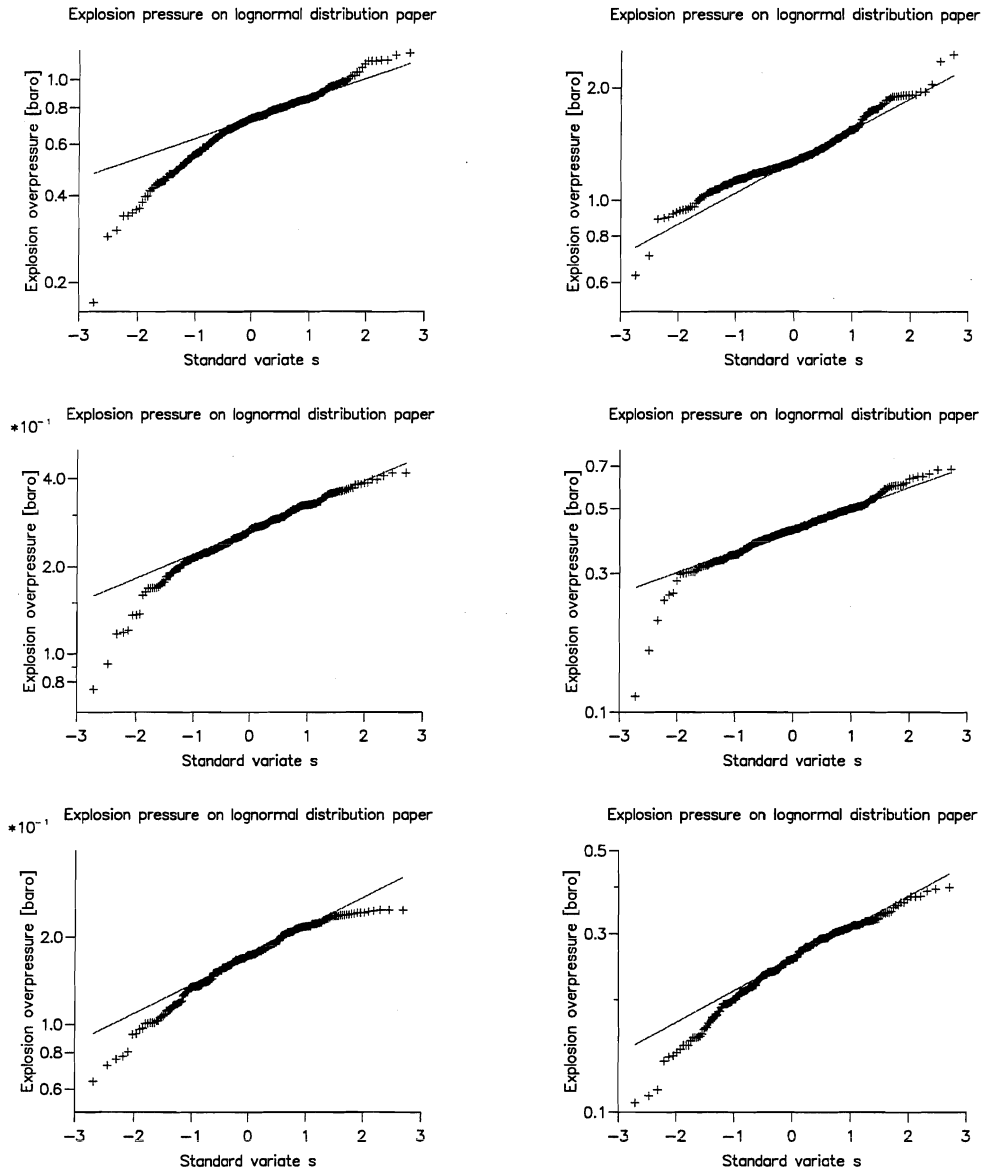

Figure A.10: CMR M25 Module. Test of maximum explosion pressure versus lognormal distribution. Left column methane as gas, right column propane as gas. Upper row: gas in whole module, middle row: gas in lower half of module, lower row: gas in low quart of module. Straight line drawn by exponential interpolation between the points $(0, X_{0.50})$ and $(1, X_{0.84})$.

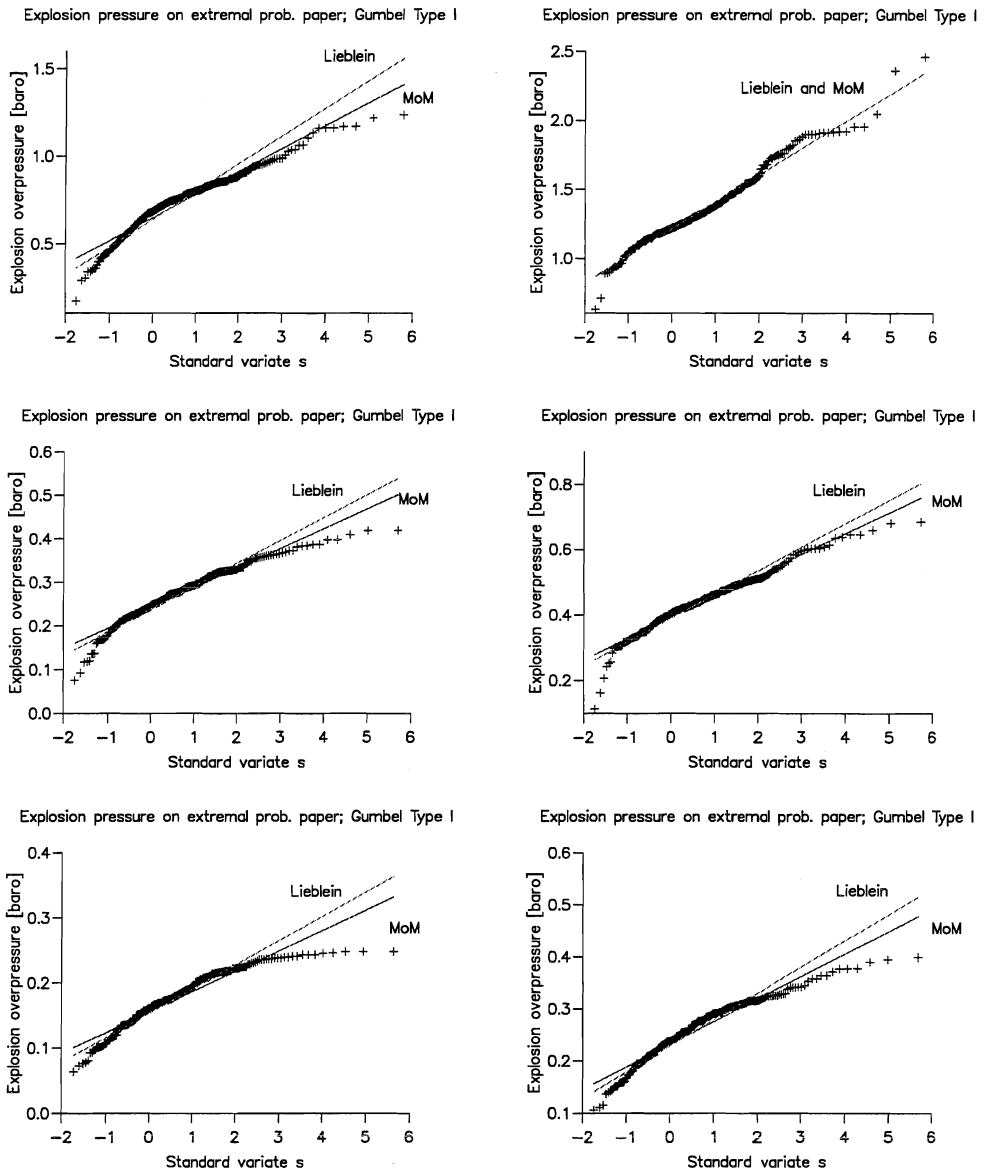

Figure A.11: CMR M25 Module. Test of maximum explosion pressure versus Gumbel Type I distribution. Left column methane as gas, right column propane as gas. Upper row: gas in whole module, middle row: gas in lower half of module, lower row: gas in low quart of module. Straight lines are drawn by Method of Moments (MoM) and Lieblein order statistics.

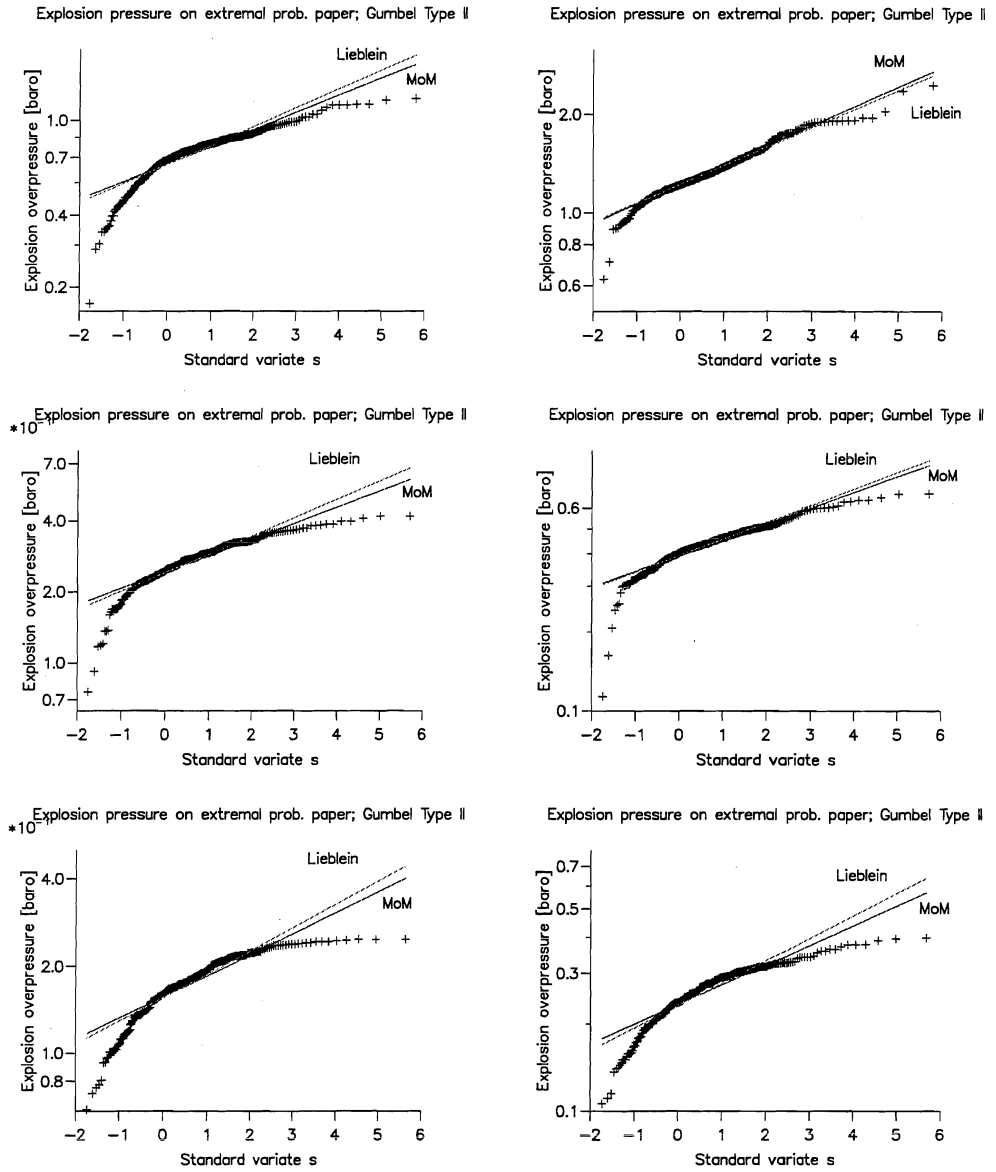

Figure A.12: CMR M25 Module. Test of maximum explosion pressure versus Gumbel Type II distribution. Left column methane as gas, right column propane as gas. Upper row: gas in whole module, middle row: gas in lower half of module, lower row: gas in low quart of module. Straight lines are drawn by exponential interpolation between the points $(S_{0.50}, X_{0.50})$ and $(S_{0.84}, X_{0.84})$ calculated by Method of Moments (MoM) and Lieblein order statistics.

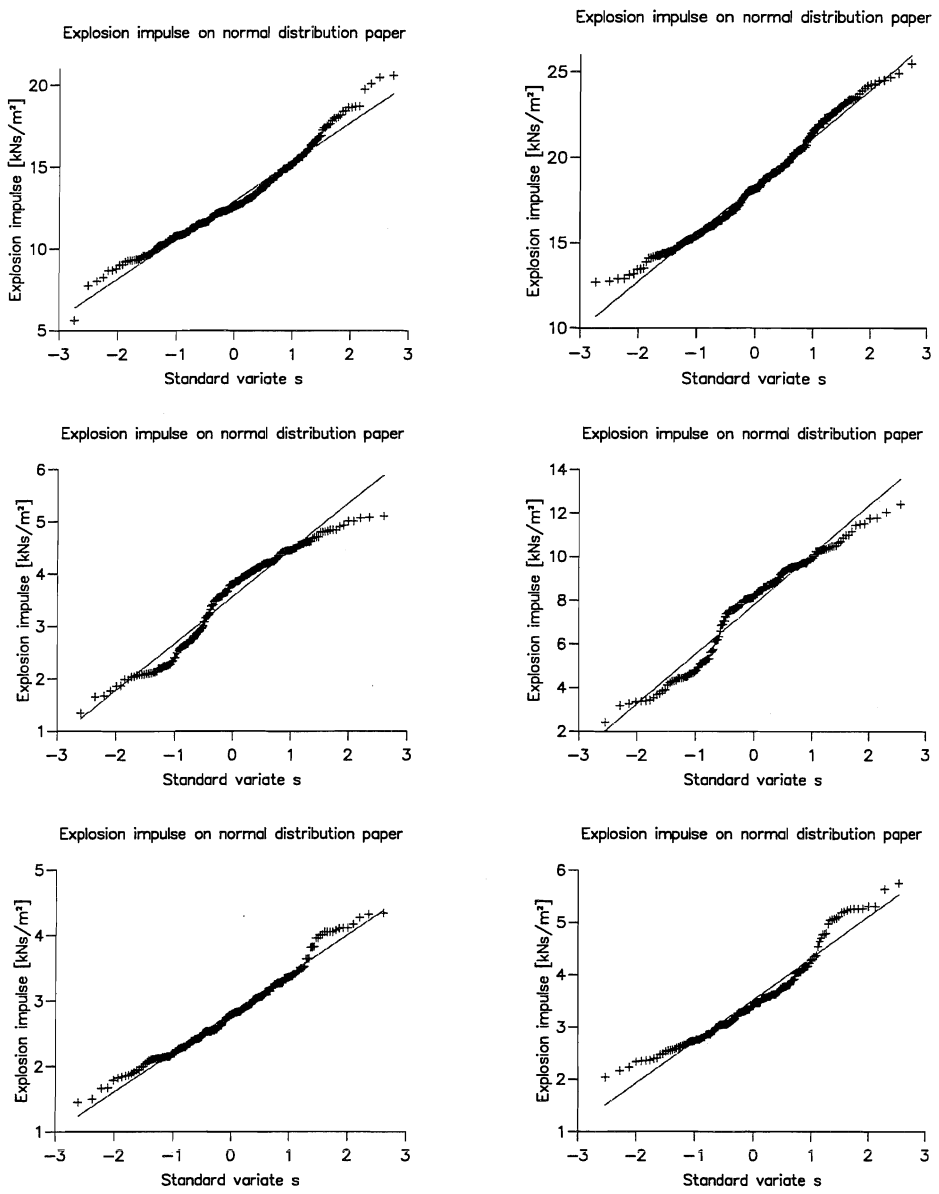

Figure A.13: Piper Alpha C Module. Test of explosion impulse versus normal distribution. Left column methane as gas, right column propane as gas. Upper row: gas in whole module, middle row: gas in lower half of module, lower row: gas in low quart of module. Straight line drawn by linear regression.

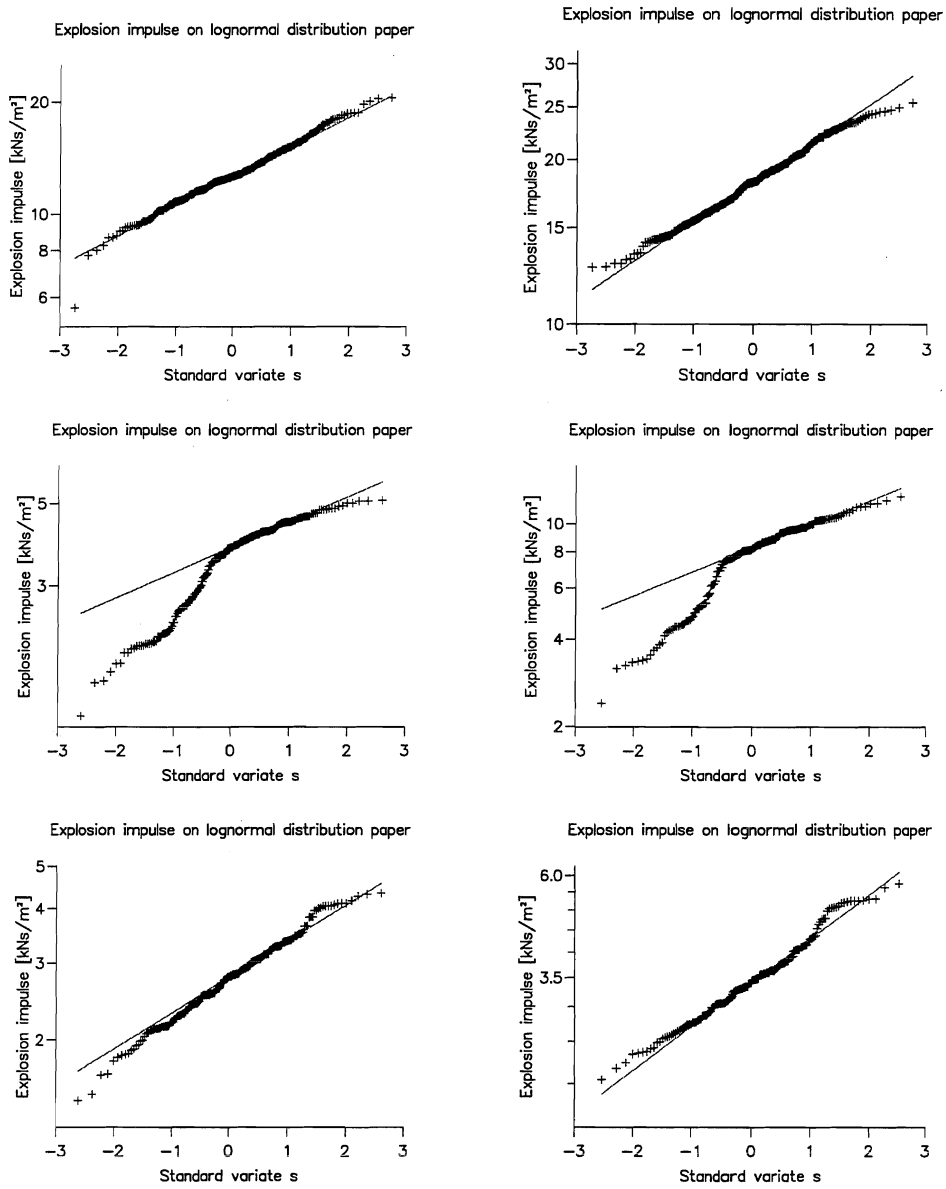

Figure A.14: Piper Alpha C Module. Test of explosion impulse versus lognormal distribution. Left column methane as gas, right column propane as gas. Upper row: gas in whole module, middle row: gas in lower half of module, lower row: gas in low quart of module. Straight line drawn by exponential interpolation between the points $(0, X_{0.50})$ and $(1, X_{0.84})$.

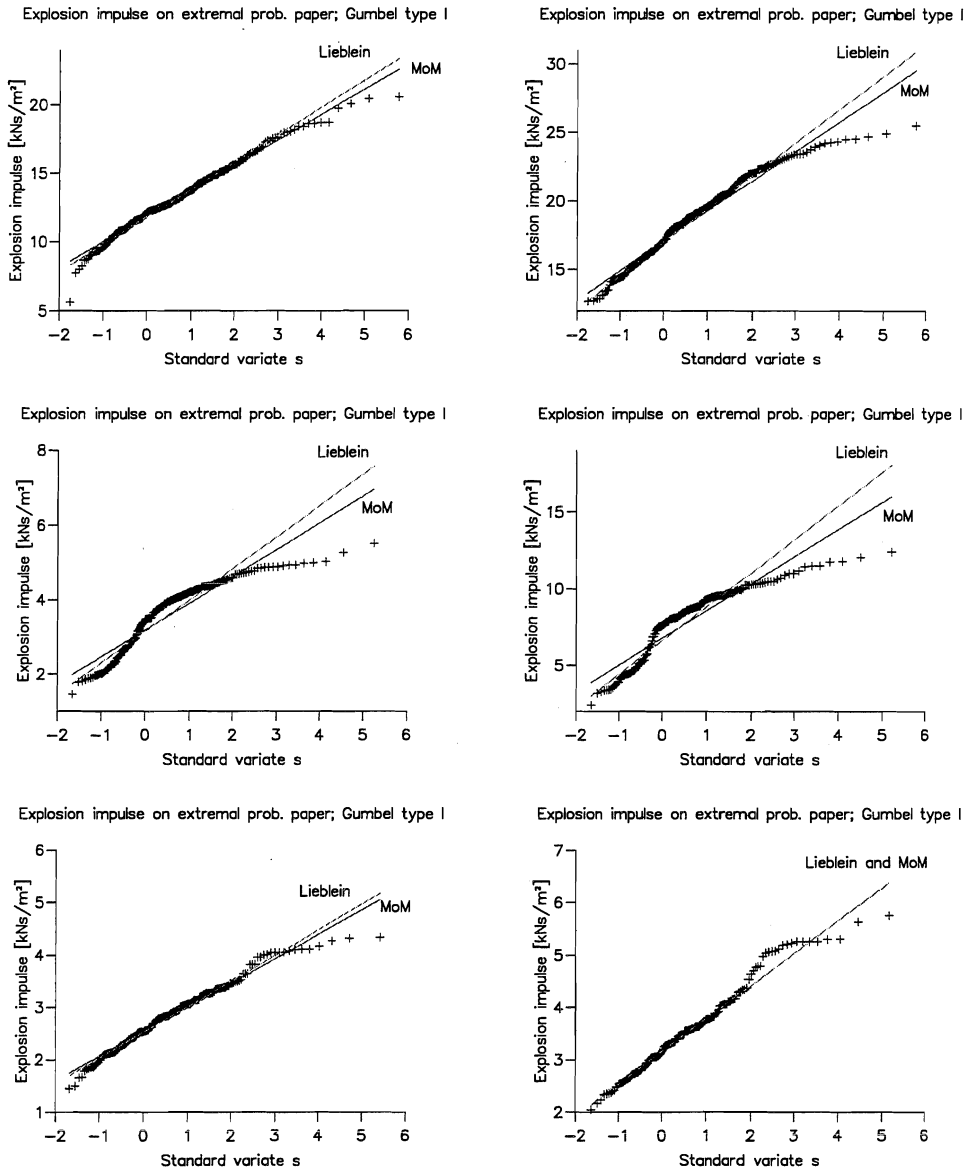

Figure A.15: Piper Alpha C Module. Test of explosion impulse versus Gumbel Type I distribution. Left column methane as gas, right column propane as gas. Upper row: gas in whole module, middle row: gas in lower half of module, lower row: gas in low quart of module. Straight lines are drawn by Method of Moments (MoM) and Lieblein order statistics.

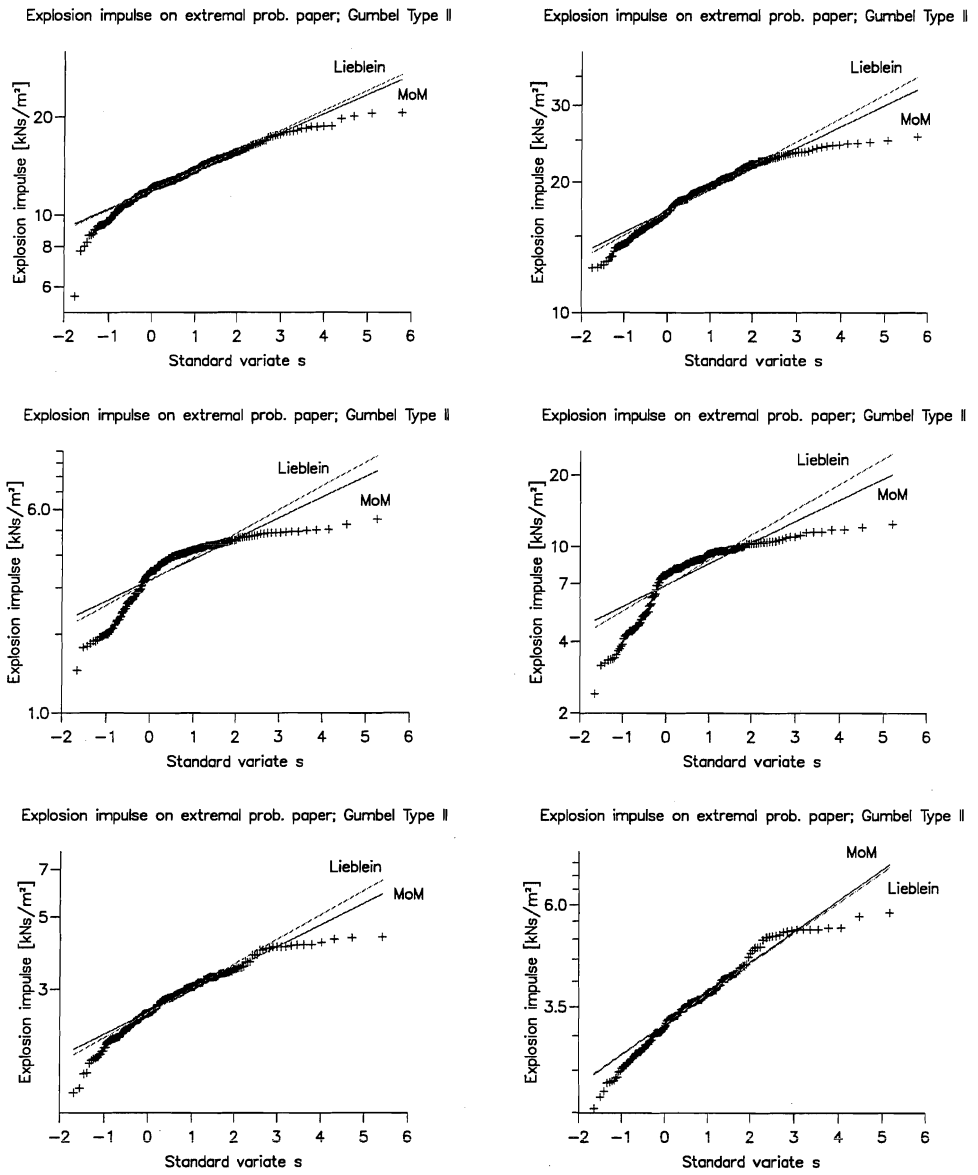

Figure A.16: Piper Alpha C Module. Test of explosion impulse versus Gumbel Type II distribution. Left column methane as gas, right column propane as gas. Upper row: gas in whole module, middle row: gas in lower half of module, lower row: gas in low quart of module. Straight lines are drawn by exponential interpolation between the points $(S_{0.50}, X_{0.50})$ and $(S_{0.84}, X_{0.84})$ calculated by Method of Moments (MoM) and Lieblein order statistics.

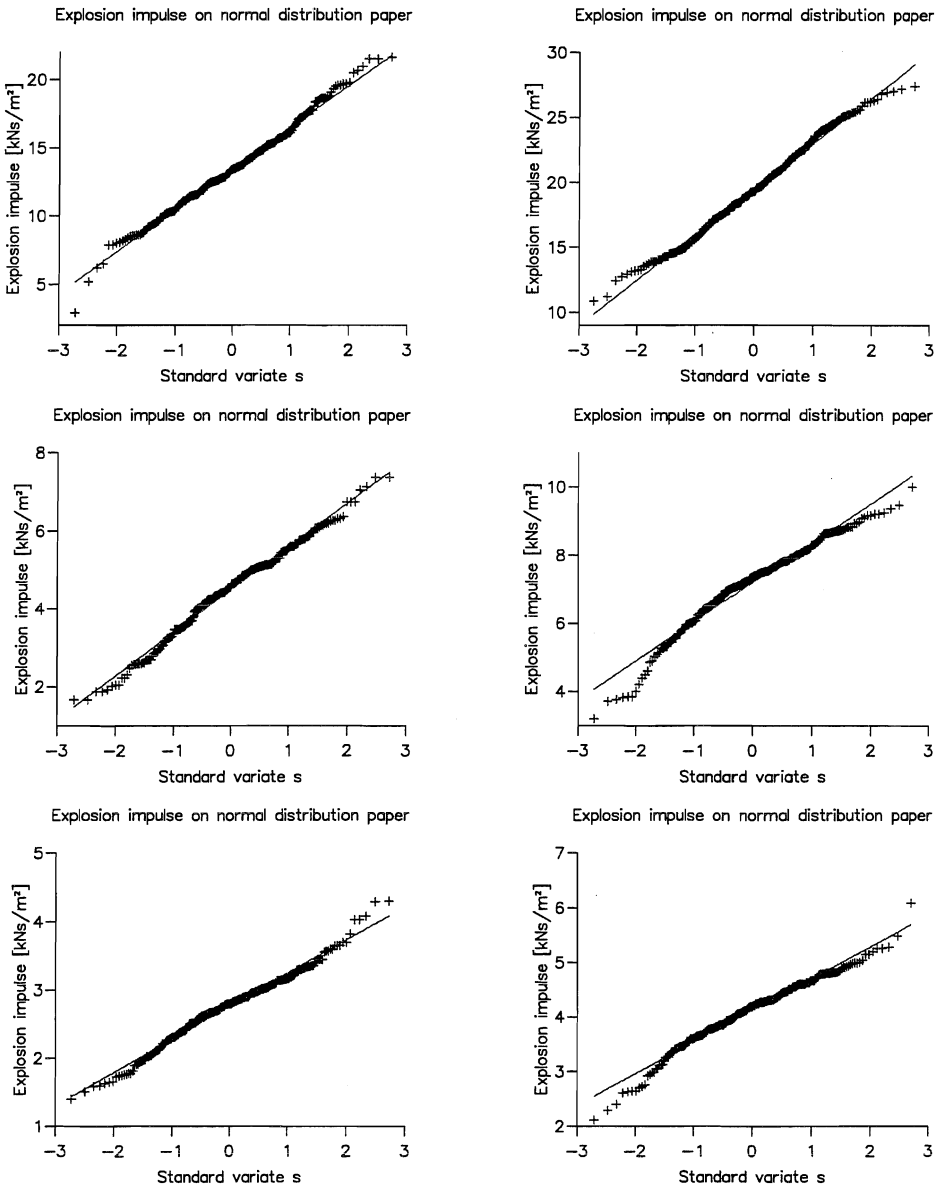

Figure A.17: CMR M24 Module. Test of explosion impulse versus normal distribution. Left column methane as gas, right column propane as gas. Upper row: gas in whole module, middle row: gas in lower half of module, lower row: gas in low quart of module. Straight line drawn by linear regression.

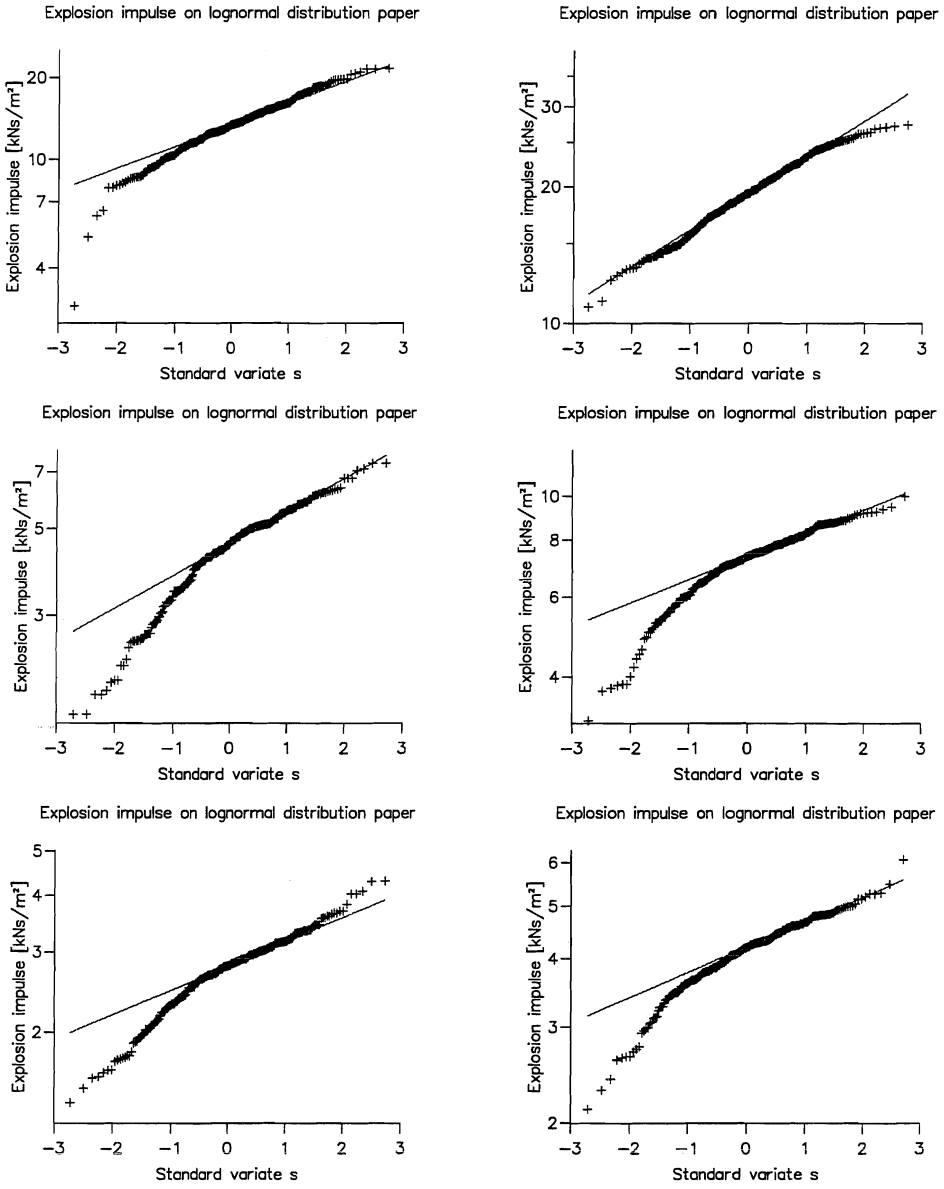

Figure A.18: CMR M24 Module. Test of explosion impulse versus lognormal distribution. Left column methane as gas, right column propane as gas. Upper row: gas in whole module, middle row: gas in lower half of module, lower row: gas in low quart of module. Straight line drawn by exponential interpolation between the points $(0, X_{0.50})$ and $(1, X_{0.84})$.

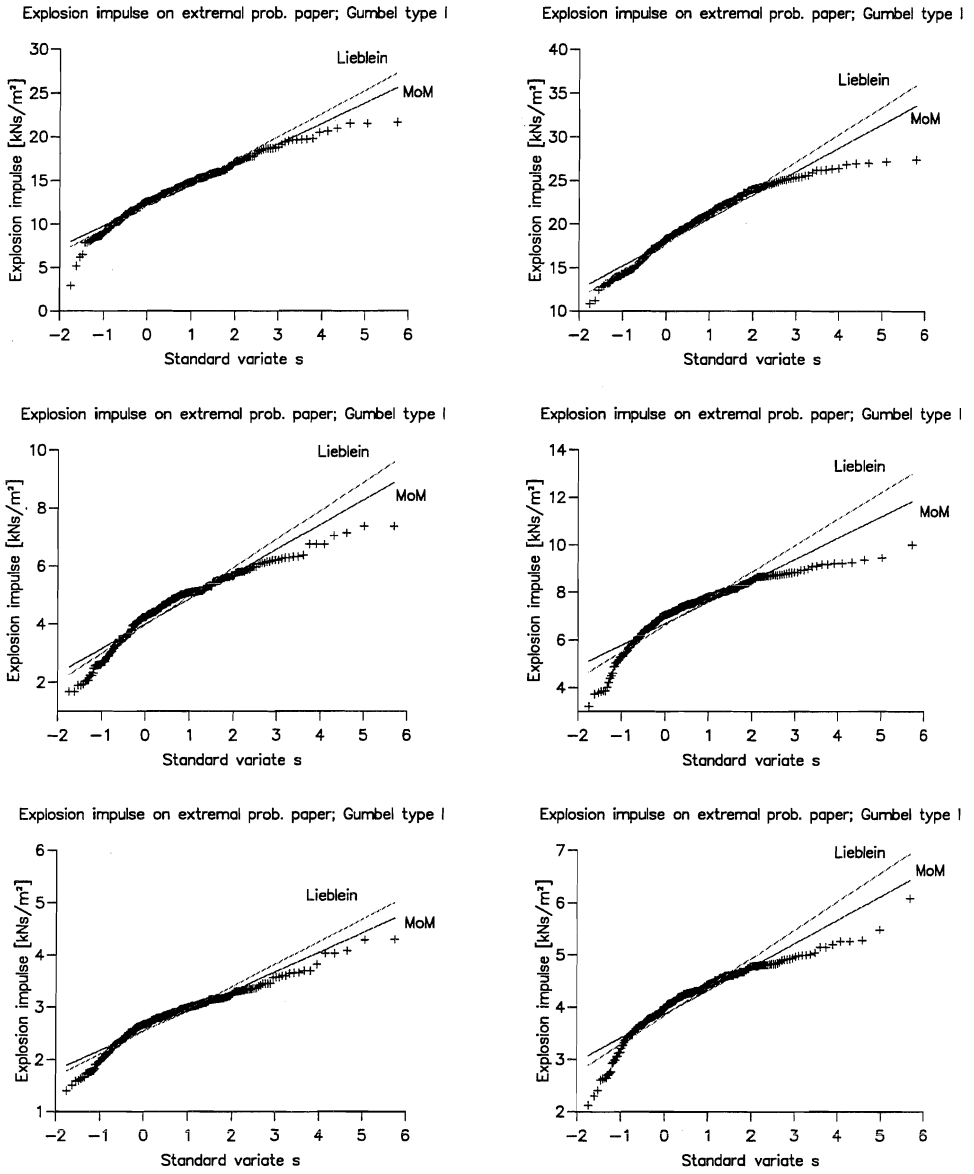

Figure A.19: CMR M24 Module. Test of explosion impulse versus Gumbel Type I distribution. Left column methane as gas, right column propane as gas. Upper row: gas in whole module, middle row: gas in lower half of module, lower row: gas in low quart of module. Straight lines are drawn by Method of Moments (MoM) and Lieblein order statistics.

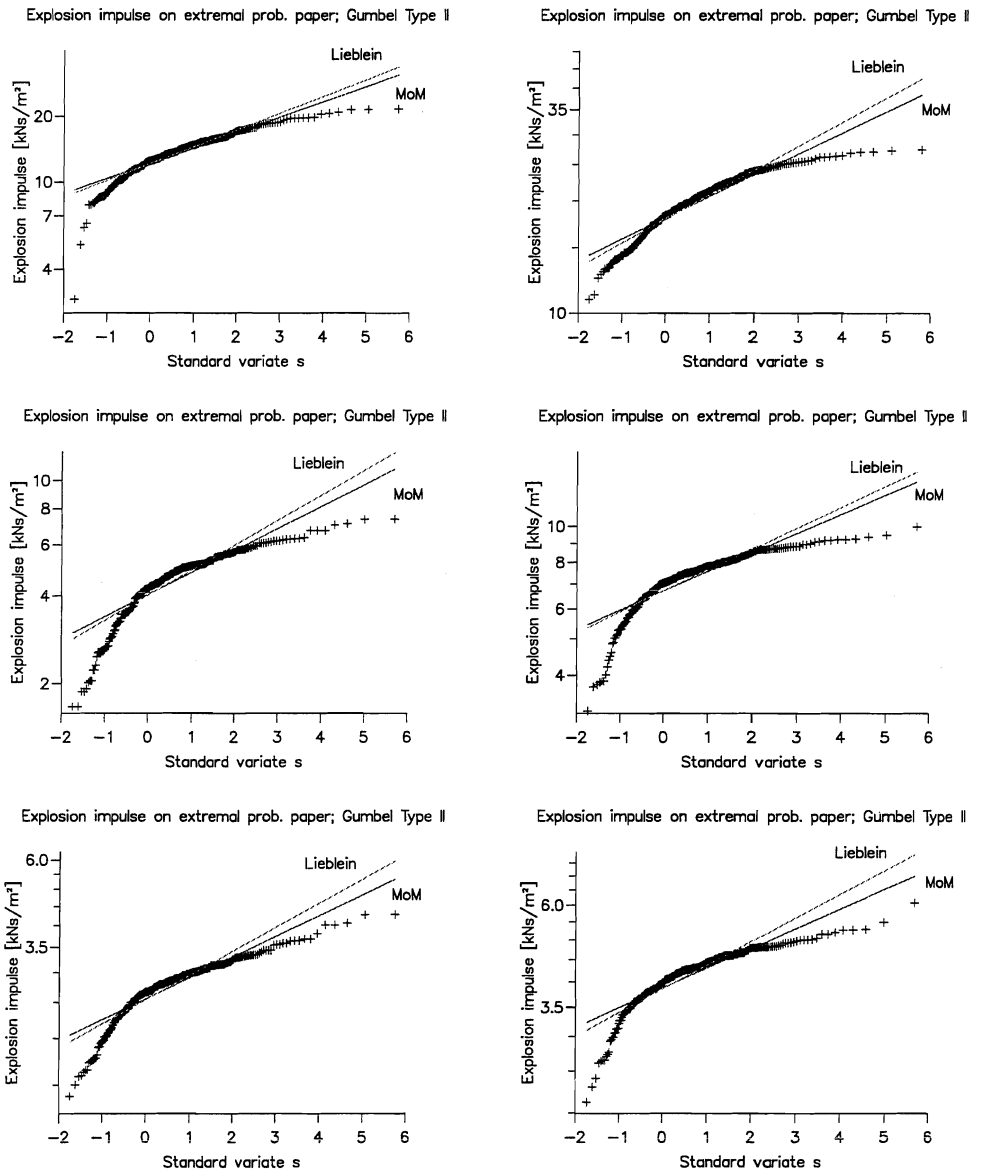

Figure A.20: CMR M24 Module. Test of explosion impulse versus Gumbel Type II distribution. Left column methane as gas, right column propane as gas. Upper row: gas in whole module, middle row: gas in lower half of module, lower row: gas in low quart of module. Straight lines are drawn by exponential interpolation between the points $(S_{0.50}, X_{0.50})$ and $(S_{0.84}, X_{0.84})$ calculated by Method of Moments (MoM) and Lieblein order statistics.

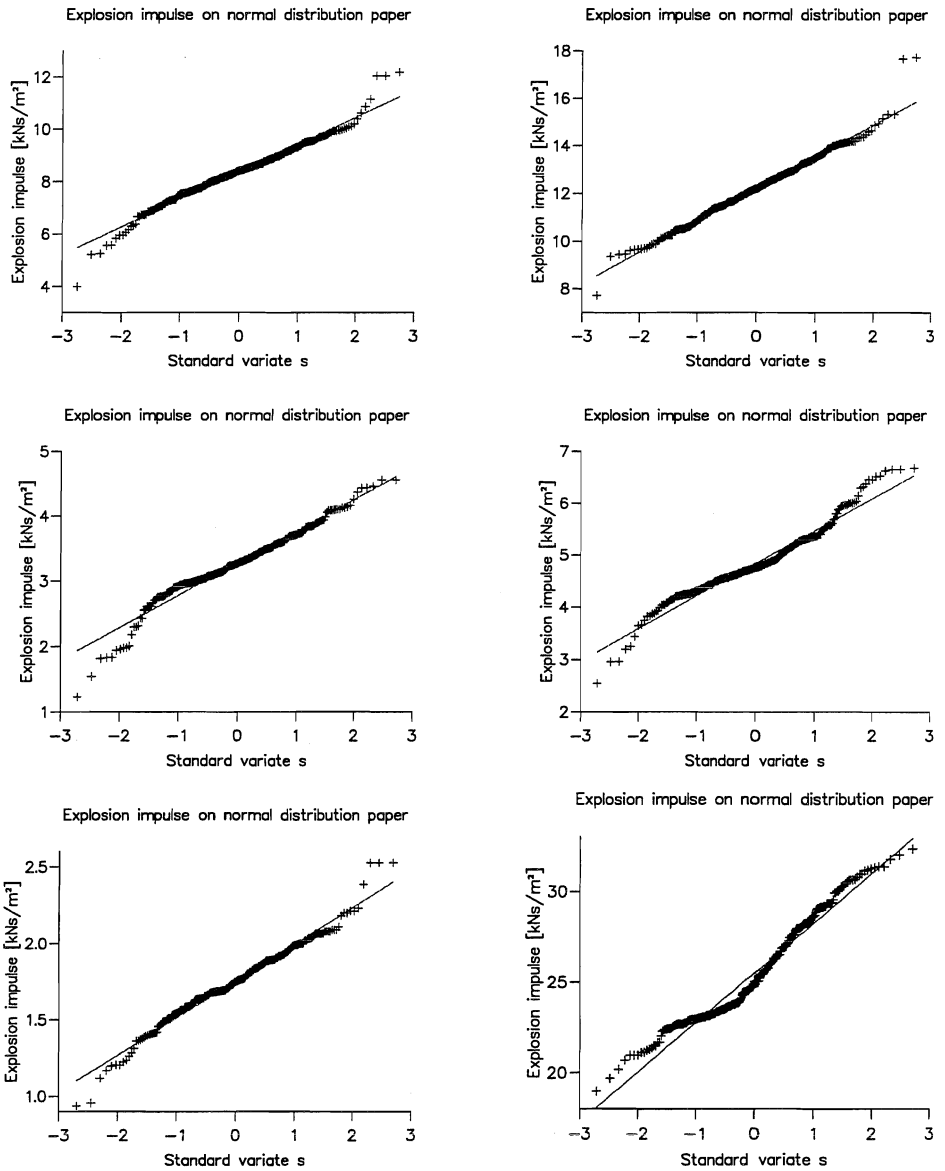

Figure A.21: CMR M25 Module. Test of explosion impulse versus normal distribution. Left column methane as gas, right column propane as gas. Upper row: gas in whole module, middle row: gas in lower half of module, lower row: gas in low quart of module. Straight line drawn by linear regression.

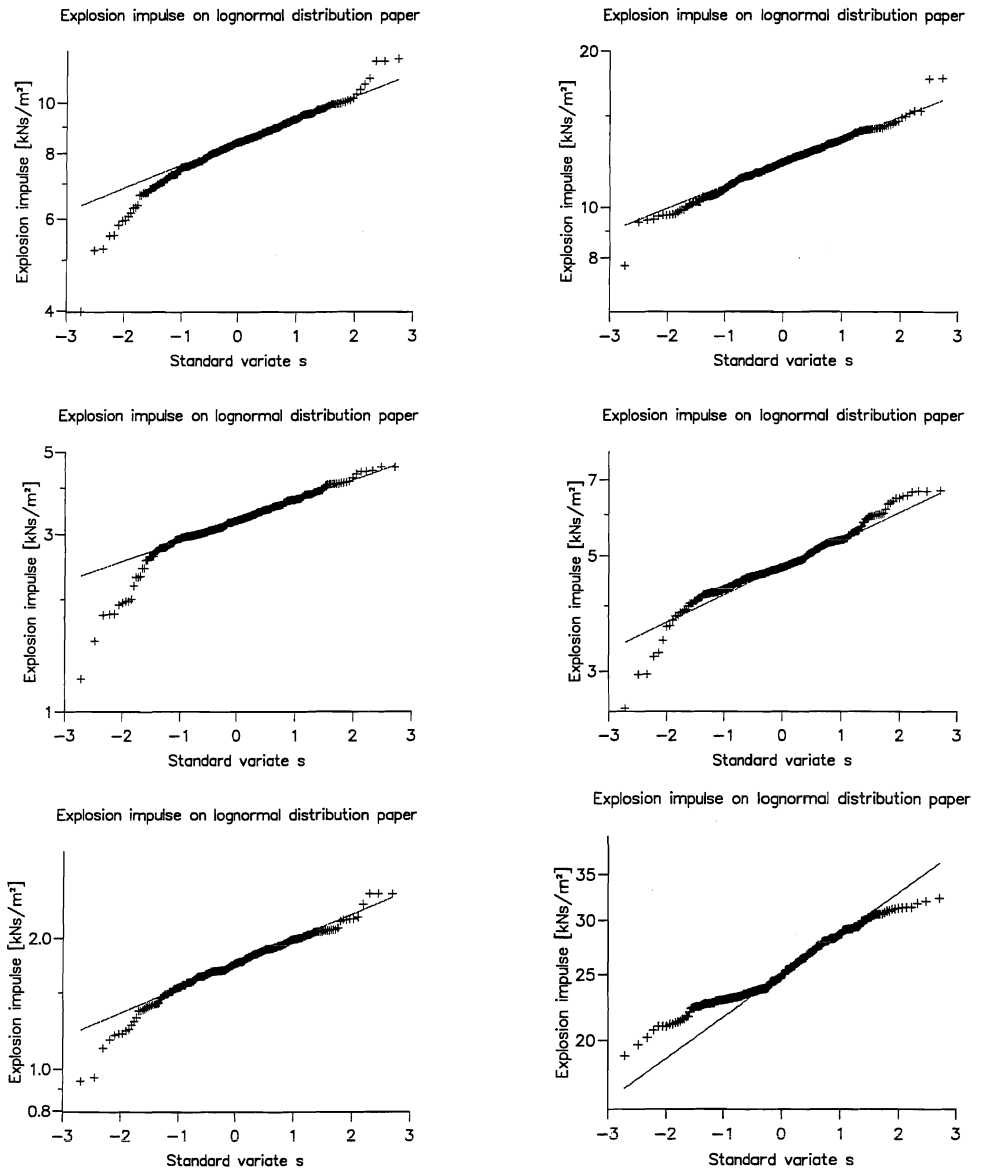

Figure A.22: CMR M25 Module. Test of explosion impulse versus lognormal distribution. Left column methane as gas, right column propane as gas. Upper row: gas in whole module, middle row: gas in lower half of module, lower row: gas in low quart of module. Straight line drawn by exponential interpolation between the points $(0, X_{0.50})$ and $(1, X_{0.84})$.

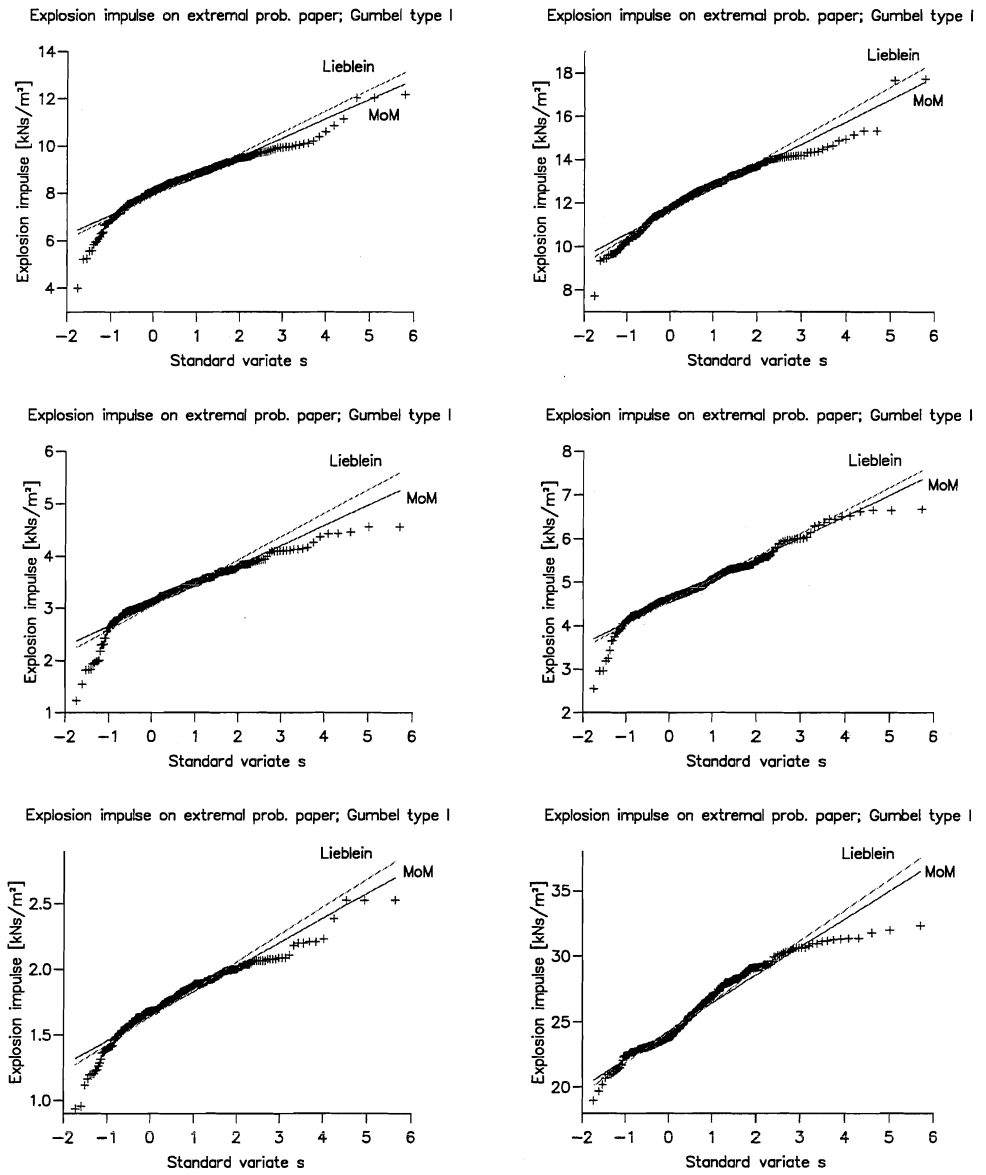

Figure A.23: CMR M25 Module. Test of explosion impulse versus Gumbel Type I distribution. Left column methane as gas, right column propane as gas. Upper row: gas in whole module, middle row: gas in lower half of module, lower row: gas in low quart of module. Straight lines are drawn by Method of Moments (MoM) and Lieblein order statistics.

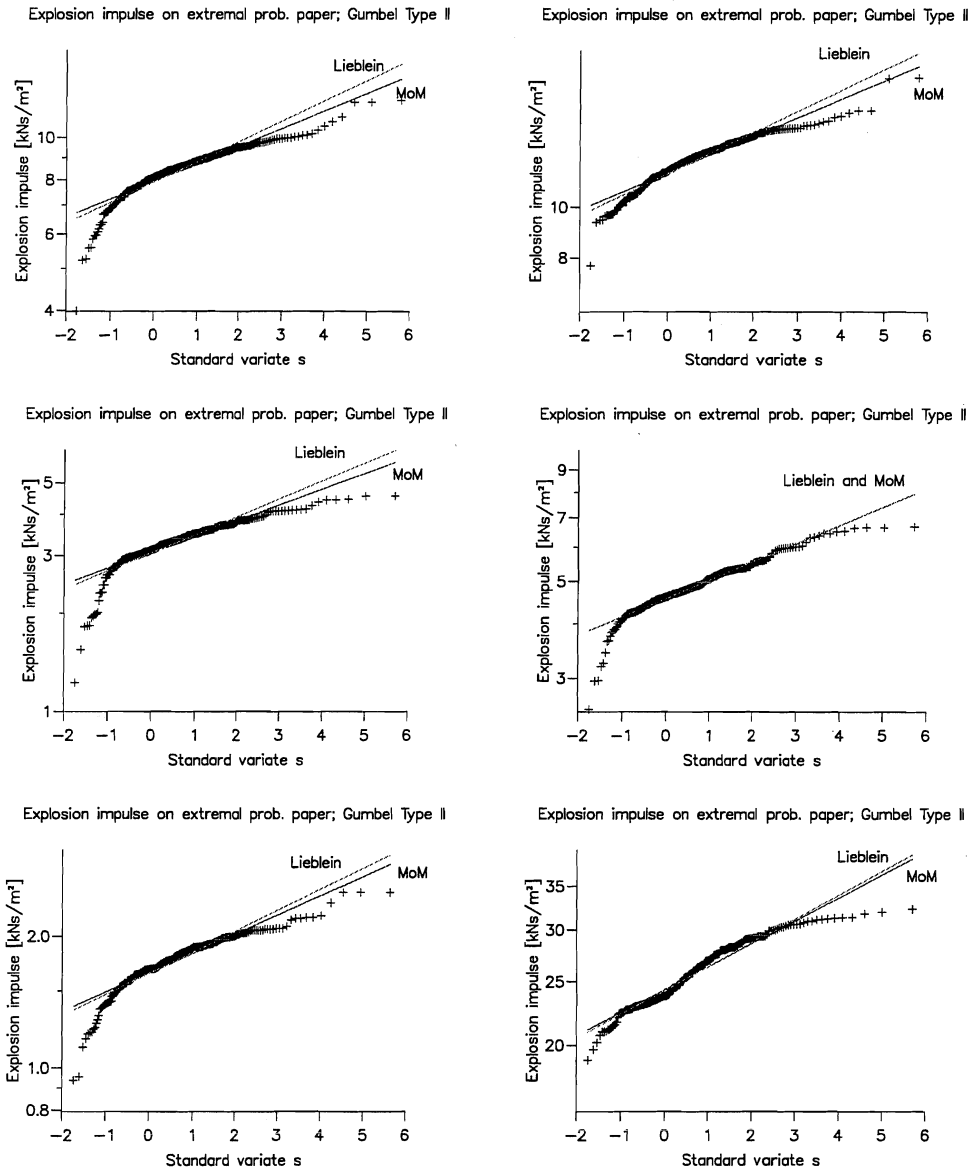

Figure A.24: CMR M25 Module. Test of explosion impulse versus Gumbel Type II distribution. Left column methane as gas, right column propane as gas. Upper row: gas in whole module, middle row: gas in lower half of module, lower row: gas in low quart of module. Straight lines are drawn by exponential interpolation between the points $(S_{0.50}, X_{0.50})$ and $(S_{0.84}, X_{0.84})$ calculated by Method of Moments (MoM) and Lieblein order statistics.

Appendix B

Weight factors for Lieblein's Order Statistics Estimators

Table B.1: Weight factors for Lieblein's Order Statistics Estimators, reproduced from Lieblein [31], ($p \geq 0.90$).

		Weights a_i and b_i for $x_1 \leq x_2 \leq \ldots \leq x_n$					
n	$i =$	1	2	3	4	5	6
2	a_i	0.91637	0.08363				
	b_i	-0.72135	-0.72135				
3	a_i	0.65632	0.25571	0.08797			
	b_i	-0.63054	0.25582	0.37473			
4	a_i	0.51100	0.26394	0.15368	0.07138		
	b_i	-0.55862	0.08590	0.22392	0.24880		
5	a_i	0.41893	0.24628	0.16761	0.10882	0.05835	
	b_i	-0.50313	0.00653	0.13045	0.18166	0.18448	
6	a_i	0.35545	0.22549	0.16562	0.12105	0.08352	0.04887
	b_i	-0.50313	0.00653	0.13045	0.18166	0.18448	0.14581

Appendix C

Colour plots from a simulation of the Piper Alpha C Module explosion

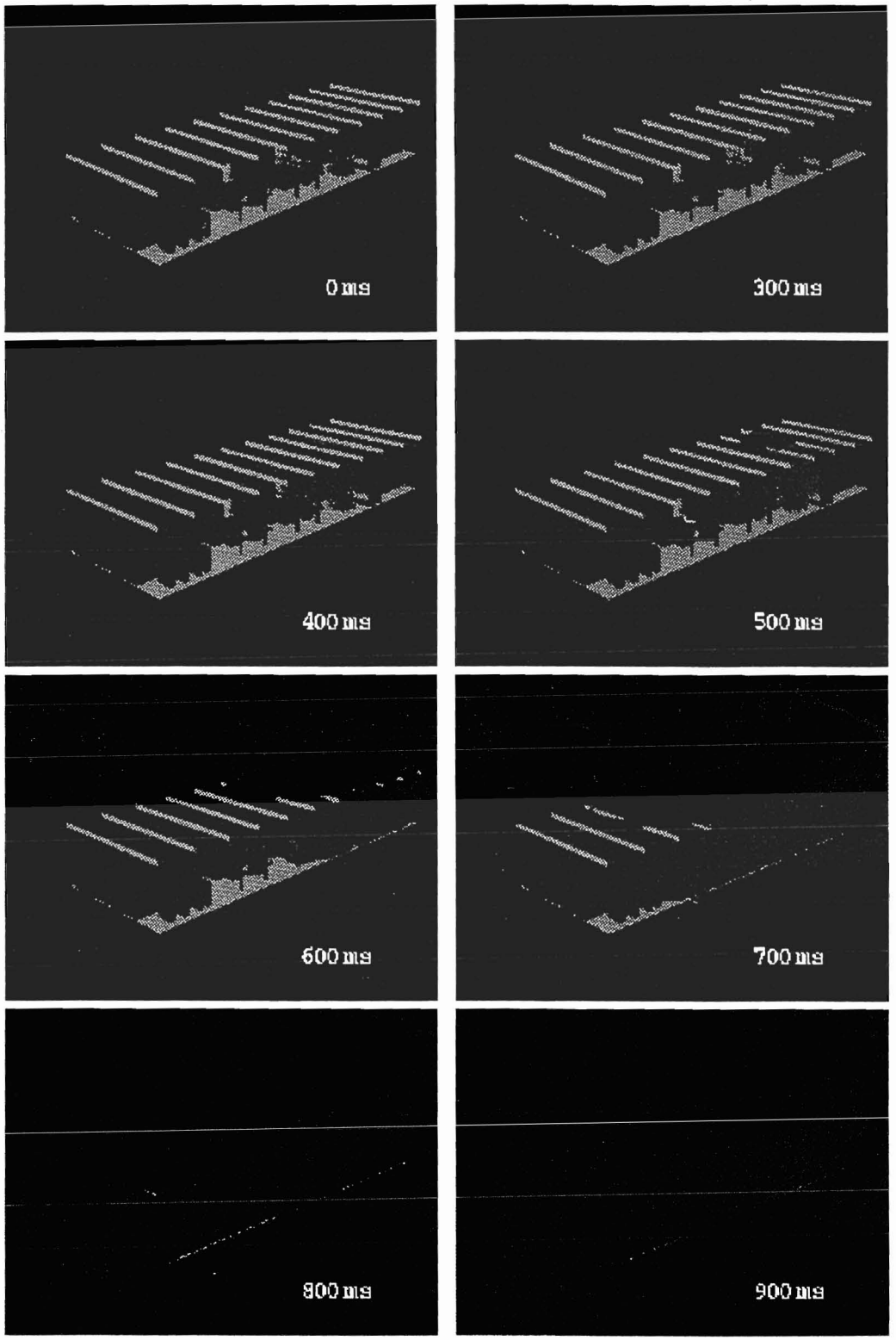

Figure C.1: Plots from a simulation of the Piper Alpha C module explosion. Methane gas in lower, eastern quadrant of module. Central ignition within gas cloud. Ceiling and walls are removed for the illustration.

Bibliography

[1] H. O. Madsen, S. Krenk, and N. C. Lind. *Methods of Structural Safety.* Prentice-Hall International Series in Civil Engineering and Engineering Mechanics. Prentice-Hall, Inc., Englewood Cliffs, New Jersey, 1986.

[2] A. M. Freudentahl. The safety of structures. *Trans. ASCE*, 112, 1947.

[3] A. I. Johnson. Strength, safety and economical dimensions of structures. Meddelande 22, Statens Kommitté för Byggnasdforskning, Stockholm, 1953.

[4] A. Pugsley. *The Safety of Structures.* Edward Arnold, London, 1966.

[5] J. Ferry Borges and M. Castanheta. *Structural Safety.* Laboratorio Nacional de Engenharta Civil, Lisbon, 1971.

[6] P. Thoft-Christensen and M. J. Baker. *Structural Reliability Theory and Its Applications.* Springer-Verlag, Berlin, 1982. ISBN 3-540-11731-8.

[7] O. Ditlefsen and H. O. Madsen. *Bærende konstruktioners sikkerhed (Safety of Structures, in Danish).* SBI-Rapport. Statens Byggeforskningsintitut, Pb. 119, Hørsholm, Denmark, 1990. ISBN 87-563-0768-3.

[8] European Committee for Standardization. *Eurocode 1 — Basis of Design and Actions on Structures — Part 1: Basis of Design (ENV 1991-1).* CEN, Central Secretariat, Brussels, September 1994. Ref. No. ENV 1991-1:1994 E.

[9] J. Ferry Borges. Implementation of probabilistic safety concepts in international codes. In H. Kupfer, M. Shinozuka, and G. I. Schuëller, editors, *Proceedings to the 2nd International Conference on Structure Safety and Reliability*, pages 121–133, Düsseldorf, Germany, September 1977. Werner-Verlag.

[10] U.S. Department of Commerce/National Bureau of Standards, Washington, D.C. *Development of a Probability Based Load Criterion for American National Standard A58*, June 1980. NBS Special Publication 577.

[11] P. Aune og P. Kr. Larsen. *Konstruksjonslære for bygningsigniører (Structural Theory for Civil Engineers, in Norwegian).* Tapir, Trondheim, Norway, third edition, 1988.

[12] D. Bjerketvedt, J. R. Bakke, and K. van Wingerden. Gas explosion handbook. *Journal of Hazardous Materials (Special Issue)*, 52(1):1–150, 1997.

[13] European Committee for Standardization. *Eurocode 1 — Basis of Design and Actions on Structures — Part 2-7: Actions on Structures — Accidental Actions Due to Impact and Explosions.* CEN, Central Secretariat, Brussels, September 1996. Ref. No. prENV 1991-2-7:1996 E.

[14] S. Høiset, B. H. Hjertager, T. Solberg, and K. A. Malo. Statistical estimation of loads from gas explosions. *Journal of Loss Prevention in the Process Industries*, 10(4):271–283, 1997.

[15] Norges Byggstandardiseringsråd, editor. *NS 3479. Prosjektering av bygningskonstruksjoner. Dimensjonerende laster. (Design of Structures. Design Loads. (In Norwegian)).* Norges Standardiseringsforbund, Oslo, Norway, third edition, October 1990.

[16] American Petroleum Institute, Washington DC. *Recommended Practice for Planning, Design and Constructing Fixed Offshore Platforms—Load and Resistance Factor Design*, first edition, July 1993. API Recommended Practice 2A—LRFD.

[17] O. Ditlefsen. Model uncertainty in structural reliability. *Structural Safety*, 1:73–86, 1982.

[18] European Committee for Standardization. *Eurocode 1 — Basis of Design and Actions — Background Documentation; Part 1 of EC1, Basis of Design.* CEN, Central Secretariat, Brussels, January 1995. First Draft.

[19] B. H. Hjertager. EXSIM: A numerical method in detail. Paper prepared for short course on "explosion prediction and mitigation: Congested volumes and complex geometries" at University of Leeds, Telemark Institute of Technology (HIT/ATF) and Telemark Technological R & D Centre (Tel-Tek), Kjølnes, 3914 Porsgrunn, Norway, 1994.

[20] K. van Wingerden, I. Storvik, B. Storvik, J. R. Bakke, I. Ø. Sand, and H. R. Sørheim. FLACS–93 — a new explosion simulator. In *Proceedings to the 2nd International Conference on Offshore Structural Design against Extreme Loads*, London, November 1993.

[21] A. C. van den Berg. REAGAS — a code for numerical simulations of 2-D reactive gas dynamics in gas explosions. PML-TNO report PML 1989-IN48, Prins Maurits Laboratory TNO, P.O. Box 45, 2280 AA Rijswijk, The Netherlands, 1989.

[22] S. V. Patankar. *Numerical Heat Transfer and Fluid Flow.* Computational Methods in Mechanics and Thermal Sciences. Taylor & Francis, 1980.

[23] B. H. Hjertager. Numerical analysis of fluid flow processes. Lecture Notes at Telemark Institute of Technology, August 1994.

[24] O. Sæter, T. Solberg, and B. H. Hjertager. Validation of the EXSIM-94 gas explosion simulator. In *Proceedings to the 4th International Conference and Exhibition: 'Offshore Structures—Hazards, Safety and Engineering'*, London, December 1995. ERA Technology Ltd.

[25] T. Solberg and B. H. Hjertager. Modelling of explosions in obstructed fields and vented enclosures — phase III. Report 500197–1, Telemark Technological R & D Centre, Kjølnes ring, 3914 Porsgrunn, Norway, 1997. Confidential.

[26] K. van Wingerden, O. R. Hansen, and I. Storvik. On the validation of a numerical tool used for explosion and dispersion predictions in the offshore industry. *BHR Group Conf. Ser. Publ.*, 15:201–219, 1995.

[27] A. H. S. Ang and W. H. Tang. *Probability Concepts in Engineering Planning and Design*, volume 1. John Wiley & Sons, Inc, Singapore, 1975.

[28] E. J. Gumbel. *Statistical Theory of Extreme Values and Some Practical Applications.* Number 33 in Applied Mathematical Series. National Bureau of Standards, Washington, D.C., February 1954.

[29] E. Gumbel. *Statistics of Extremes.* Columbia Univ. Press, 1958.

[30] A. H. S. Ang and W. H. Tang. *Probability Concepts in Engineering Planning and Design*, volume 2. John Wiley & Sons, Inc, Singapore, 1984.

[31] J. Lieblein. A new method of analysing extrem-value data. Tech. Note 3053, NACA, 1954.

[32] H. Bowerman, G. W. Owens, J. H. Rumley, and J. J. A. Tolloczko, editors. *Interim Guidance Notes for the Design and Protection of Topside Structures against Explosion and Fire.* The Steel Construction Institute, Silwood Park Ascot Berks SL5 7QN, UK, January 1992. Document No 287.

[33] The Steel Construction Institute, Silwood Park Ascot Berks SL5 7QN, UK. *Blast and Fire Engineering Project for Topside Structures — Blast Loading Series*, 1991.

[34] B. H. Hjertager. Gas explosions in obstructed vessels. In *Explosion Prediction and Mitigation: Congested Volumes and Complex Geometries.* University of Leeds, Telemark Institute of Technology and Telemark Technological R & D Centre (Tel-Tek), Kjølnes, 3914 Porsgrunn, Norway, 1993.

[35] W. P. M. Mercx, editor. *Extended Modelling and Experimental Research into Gas Explosions — EMERGE.* Commission of the European Communities, 1997. Final Summary Report, Contract EV5V–CT93–0274.

[36] J. A. Pappas. Venting of large-scale volumes. In *Proceedings from the Control and Prevention of Gas Explosions.* Oyez/IBC, December 1983.

[37] Lord W. D. Cullen. *The Public Inquiry into the Piper Alpha Disaster.* Department of Energy (DEn). HMSO (Her Majesty's Stationary Office), London, 1990.

[38] Report of the Court of Inquiry. *The Flixborough Disaster.* Department of Employment, HMSO, London, 1975.

[39] J. E. Førrisdahl. Scenario analyse av gasseksplosjonsulykker *(Scenario Analysis of Gas Explosion Accidents, in Norwegian).* Msc dissertation, Telemark Institute of Technology, Kjølnes, 3914 Porsgrunn, Norway, 1990.

[40] B. H. Hjertager, K. Fuhre, and M. Bjørkhaug. Gas explosion experiments in 1:33 and 1:5 scale offshore separator and compressor modules using stoichiometric homogenous fuel/air clouds. *Journal of Loss Prevention in the Process Industries*, 1:197–205, 1988.

[41] Health & Safety Executive. Photos and drawings from the Flixborough plant before and after the explosion. Research and Laboratory Services Division, Sheffield, England.

[42] Statens bygningsteknisk etat, editor. *Ren veiledning til teknisk forskrift til plan- og bygningsloven 1997. (Guides to the Norwegian Construction Regulations).* Norsk Byggtjenestes Forlag, 1997.

[43] Norwegian National Office of Building Technology and Administration. Technical regulations under the planning and building act 1997. On-line information at <URL:http://www.bebygg.no/beweb/english/techreg97.html>, January 1997.

[44] Norges Byggstandardiseringsråd, editor. *Forslag. NS-ENV 1991-1. Grunnlag for prosjektering av konstruksjoner — krav til pålitelighet. (Proposal. NS-ENV 1991-1. Basis of Design of Structures. Demands on Reliability. (In Norwegian)).* Norges Standardiseringsforbund, Oslo, Norway, third edition, October 1997.

[45] C. Ramsay. Scope and strategies for risk assessment offshore. IBC Workshop; Risk Analysis in the Offshore Industry, October 1990. Aberdeen.

[46] C. A. Cornell. A probability-based structural code. *ACI-Journal*, 66:974–985, 1969.

[47] R. A. Fisher and L. H. C. Tippett. Limiting forms of the frequency distributions of the largest or smallest number of a sample. In *Proc. Cambridge Philosophical Society, XXIV*, volume II, 1928.

[48] The Nordic Committee on Building Regulations. *Recommendation for Loading- and Safety Regulations for Structural Design*, November 1978. NKB-Report No 36.

[49] Per Kr. Larsen. *Dimensjonering av stålkonstruksjoner.* Tapir, Trondheim, Norway, 1990.

[50] K. Gugan. *Unconfined Vapor Cloud Explosions.* Gulf Publishing Company, Houston, USA, 1979.

[51] B. H. Hjertager and T. Solberg ans O. Sæter. *EXSIM-94. User's Manual.* Telemark Technological R & D Centre (Tel-Tek), Kjølnes, N-3914 Porsgrunn, Norway, December 1994. Confidential.

[52] R. W. Clough and J. Penzien. *Dynamics of Structures.* McGraw-Hill, second edition, 1993.

[53] E. Kreyszig. *Advanced Engineering Mathematics.* Wiley, New York, seventh edition, 1993.

[54] The Steel Construction Institute, Silwood Park Ascot Berks SL5 7QN, UK. *Blast and Fire Engineering Project for Topside Structures — Blast Response Series*, 1991.

[55] E. E. Dougherty. *Probability and Statistics for the Engineering, Computing and Physical Sciences.* Prentice-Hall, Englewood Cliffs, N.J., USA, 1990.

[56] H. Kortner, K. Emblem, and B. Rør, editors. *Prosessikkerhet og risikoanalyse— notater til forelesninger (Lecture Notes in Process Safety and Risk Analysis (partly Norwegian, partly English)).* Lecture Notes at Telemark Institute of Technology. Hydro Forskning, Porsgrunn, Norway, 1990.

[57] J. Dickinson Gibbons. *Nonparametric Statistical Inference*, volume 65 of *STATISTICS: Textbooks and Monographs.* Marcel Deccer, Inc, New York, second edition, 1985.

[58] C. Sadee, D. E. Samuels, and T. P. O'Brien. The characteristics of the explosion of cyclohexane at the Nypro (UK) Flixborough plant on 1st June 1974. *Journal of Occupational Accidents*, 1:203–235, 1976/1977.

[59] V. C. Marshall. *Major Chemical Hazards.* Chemical Engineering. Ellis Horwood Limited, Chichester, England, 1987.

[60] K. Gugan. Flixborough — a combustion specialists view. *The Chemical Engineer*, pages 341–352, 1976.

[61] A. F. Roberts and D. K. Pritchard. Blast effect from unconfined vapour cloud explosions. *Journal of Occupational Accidents*, 3:231–247, 1982.

[62] B. Efron. *The Jackknife, the Bootstrap and Other Resampling Methods.* Regional Conference Series in Applied Mathematics. Society for Industrial and Applied Mathematics, Philadelphia, second edition, 1982.

[63] B. Efron and R. J. Tibshirani. *An Introduction to the Bootstrap.* Chapman & Hall, New York, 1993.

[64] L. Lamport. *LaTeX : A Document Preparation System.* Addison-Wesley Publishing Company, Inc., second edition, 1994.

[65] H. Kopka and P. W. Daly. *A Guide to LaTeX 2ε.* Addison-Wesley Publishing Company, Inc., second edition, 1995.

[66] M. Goossens, F. Mittelbach, and A. Samarin. *The LaTeX Companion.* Addison-Wesley Publishing Company, Inc., second edition, 1994.

[67] J. Penny and G. Lindfield. *Numerical Methods Using* MATLAB. Ellis Horwood Limited, 1995.

[68] American Mathematical Society. *AMS*-LaTeX version 1.2. Documentation with the `amsmath` Package to LaTeX, January 1995.